Statistical Models for Prediction of Mechanical Property and Manufacturing Process Parameters for Gas Pipeline Steels

by

Sonam Dahire

A Dissertation Presented in Partial Fulfillment
of the Requirements for the Degree
Doctor of Philosophy

Approved November 2018 by the
Graduate Supervisory Committee:

Yongming Liu, Chair
Yang Jiao
Yi Ren

ARIZONA STATE UNIVERSITY

December 2018

ABSTRACT

Pipeline infrastructure forms a vital aspect of the United States economy and standard of living. A majority of the current pipeline systems were installed in the early 1900's and often lack a reliable database reporting the mechanical properties, and information about manufacturing and installation, thereby raising a concern for their safety and integrity. Testing for the aging pipe strength and toughness estimation without interrupting the transmission and operations thus becomes important. The state-of-the-art techniques tend to focus on the single modality deterministic estimation of pipe strength and do not account for inhomogeneity and uncertainties, many others appear to rely on destructive means. These gaps provide an impetus for novel methods to better characterize the pipe material properties. The focus of this study is the design of a Bayesian Network information fusion model for the prediction of accurate probabilistic pipe strength and consequently the maximum allowable operating pressure. A multimodal diagnosis is performed by assessing the mechanical property variation within the pipe in terms of material property measurements, such as microstructure, composition, hardness and other mechanical properties through experimental analysis, which are then integrated with the Bayesian network model that uses a Markov chain Monte Carlo (MCMC) algorithm. Prototype testing is carried out for model verification, validation and demonstration and data training of the model is employed to obtain a more accurate measure of the probabilistic pipe strength. With a view of providing a holistic measure of material performance in service, the fatigue properties of the pipe steel are investigated. The variation in the fatigue crack growth rate (da/dN) along the direction of the pipe wall thickness is studied in relation to

the microstructure and the material constants for the crack growth have been reported. A combination of imaging and composition analysis is incorporated to study the fracture surface of the fatigue specimen. Finally, some well-known statistical inference models are employed for prediction of manufacturing process parameters for steel pipelines. The adaptability of the small datasets for the accuracy of the prediction outcomes is discussed and the models are compared for their performance.

ACKNOWLEDGMENTS

I would like to express my sincere gratitude towards my advisor, Dr Yongming Liu for his constant guidance and support throughout the duration of my study. I would like to thank him for his great mentorship and valuable insights which helped me achieve excel in achieving the research objectives. I would also like to thank the members of my Supervisory Committee, Prof. Yang Jiao and Prof. Yi Ren for volunteering their time and support towards my research work.

The work is sponsored by DOT-PHMSA CAAP program (Program Officer: Joshua Arnold, James Prothro, and James Merritt) and the financial support is greatly appreciated. Technical inputs from GTI research experts, Ernest Lever and Daniel Ersoy, is highly appreciated as well.

I am grateful to my fellow group members, current and former, for their willingness to help and their strong work ethic which motivated me in my own research. Special thanks to Fraaz Tahir for providing insightful suggestions about my research and for helping me with the experimental testing. Finally, I would like to thank my family and friends for their support and blessings.

TABLE OF CONTENTS

Page

CHAPTER Page

CHAPTER Page

CHAPTER Page

LIST OF TABLES

Table Page

LIST OF FIGURES

Figure Page

Figure Page

Figure Page

Figure Page

Figure Page

Figure Page

Figure Page

1 BACKGROUND AND MOTIVATION

The present system of natural gas pipelines in the United States comprises of a network of gathering and transmission lines with more than 210 pipeline systems laid across 305000 miles ("US Energy Information Administration Website" 2017). The pipeline systems which have been laid down for decades such as those installed in the early 1900's are still in use, however, these do not have a widely available database on manufacturing & installation, inspection as well as for the mechanical properties. An accurate estimation of the pipe material properties is, thus, crucial for the integrity and risk assessment of such aging pipeline infrastructure systems. The existing techniques for measurement of pipe strength such as the hardness testers rely on surface based measurements of the entities, and do not incorporate the impact of inhomogeneity in the material properties from surface to the bulk of the pipe wall thickness. Many other non-destructive evaluation (NDE) techniques such as acoustic(Vary 1980) , micro-magnetic (G. Dobmann, Meyendorf, and Schneider 1997), etc. predict the mechanical properties based on single modality measurements (Gerd Dobmann et al. 1995) which can be limited by pipe geometries and hence these do not account for uncertainties in the system. These form the key gaps existing methods of mechanical properties estimation. A reliable estimate of the strength and remaining life of the pipelines is therefore often difficult to obtain. It is critical to develop a novel methodology based on mutli-modalistic approach to bridge the gaps from the existing methods for accurate prediction of pipe strength and ensure a safe operation of these structures.

In order to fully characterize the condition of the pipelines in service, it is required to analyze the responsiveness of such pipe systems to the defects in the form of mechanical dents, corrosion, cracks etc. Conventionally, smart PIGs (Pipeline Inspection Gauge) are employed that use non-destructive evaluation methods such as magnetic, ultrasonic etc. [2] for assessing the condition of a pipeline to identify such defects. In the present day, however, about 63 percent of these systems cannot be inspected via conventional PIGs due to them being either too old, or with turns and twists not allowing PIGs to operate in them (US news | NBC News 2010). Fatigue is a common phenomenon that can occur in the pipelines due to cyclic loadings during transportation (transit fatigue) and during service life, and are more common in the pipelines used to transport hydrogen. The fatigue cracks may initiate at the mechanical dents or anomalies, which if not enough to lead to a fracture, may severely affect the structural integrity of these entities(Mohtadi-Bonab et al. 2016). The effect of hydrogen gas on the fatigue properties of pipeline steels is not as well documented as tensile properties, however, because fatigue is not an uncommon contributor to failures observed in the operation of pipelines, fatigue properties may provide a better metric of the performance of a material in service. A detailed understanding of the fatigue crack propagation through the pipe wall thickness is, therefore, necessary.

Although, constant efforts are made to establish the integrity of the aging pipe systems, the increasing demand for higher transportation efficiency of the gas pipelines requires a continuous evolution in the development of pipe steel grades with superior material properties(Rosado, Waele, and Vanderschueren 2013). The higher strength and

ductility are governed by a combination of alloy design and parameters of thermomechanical controlled processing (TMCP) and, therefore, optimization of the process parameters of the TMCP is vital in order to achieve the desired mechanical properties. In the present day, exhaustive production control and diverse simulation techniques are used to optimize the processing parameters for producing a desired microstructure, which tend to use a lot of resources and only achieve good results in an a posteriori fashion (Santos et al. 2009). This generates a need for a simplified and cost saving means that adds value to the prediction of TMCP process parameters. Figure 1.1 shows the evolution of pipeline technology with time, and the modification in material properties and processing routes.

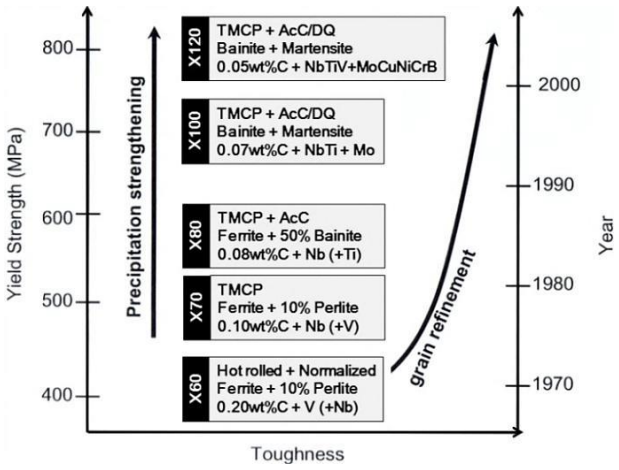

Fig 1.1. Development of pipeline steels

Based on the review, the goals of the study are:

1. Development of a novel Bayesian network tool for information fusion from multimodality diagnosis results for the probabilistic pipe strength and toughness estimation

- Experimental testing and data analysis of material mechanical property variation with respect to basic chemical and metallurgical properties.
- Development of an information fusion methodology based on Bayesian network inference using multimodality diagnosis and demonstration study using representative pipe specimens.

2. Investigation of variation in the fatigue behavior of the steels through the pipe wall thickness
   - Estimation of crack growth characteristics of the pipe samples in relation to the microstructure.
   - Investigation of variation in fatigue crack growth parameters through the pipe thickness.
3. Comparative study of statistical models for manufacturing properties prediction
   - Prediction using individual models of multivariate linear regression, ML-KNN (multi-label k-nearest neighbor) and GP (Gaussian Process) model.
   - Analyzing the effect of model parameter variation on the prediction efficiency.
   - Demonstration of a model selection procedure depending on the length and quality of the dataset.

2 BAYESIAN NETWORK TOOL FOR INFORMATION FUSION FROM MULTIMODALITY DIAGNOSIS RESULTS FOR THE PROBABILISTIC PIPE STRENGTH ESTIMATION

2.1 INTRODUCTION

The United States comprises of a large network of aging natural gas pipeline infrastructure. Many pipelines may contain defects such as mechanical dents, corrosion damage and cracks due to aging, and thereby significantly affect the integrity of the gas pipeline systems. Some NDE techniques are currently in place to identify such defects, however, in order to ensure correct responsiveness of the pipe to these defects, to be able to characterize the pipeline for the remaining life and the pressure rating, it is necessary to have a good estimate of the mechanical properties such as yield and tensile strength. As per the American Petroleum Institute (API) standards, the maximum allowable operating pressure (MAOP) can be directly related to the minimum yield strength, and the ratio specification of yield to tensile strength (Support et al., n.d.), whereas, many studies can correlate the shape and size of the defects to the remaining useful life of the pipelines Although several techniques are in place for estimation of such mechanical properties, a reliable estimate of accurate pipe strength is still not available. The techniques for estimation of pipe strength and toughness, such as the hardness testers, Automated Ball Indenter, (Haggag 2007) and others, rely on surface-based measurement of hardness and stress-strain measurements etc. Unlike the hardness-based strength estimation method, no ASME (American Society of Mechanical Engineers) standards exist for the ABI measurement method for pipe strength and toughness estimation (Amend, n.d.). Moreover, the Nondestructive evaluation (NDE) techniques such as acoustic (Vary 1980), micro-

magnetic (G. Dobmann, Meyendorf, and Schneider 1997), acoustic emission (Merson et al. 2012) etc. predict the mechanical properties based on single modality measurements(Gerd Dobmann et al. 1995). The magnetic flux leakage technique, eddy current inspection, and ultrasound inspection are all based on analysis of the distorted signal pattern around the defect and are limited by the pipe wall thickness and the flaw size (Bickerstaff et al. 2002). Although some NDE techniques like Magnetic Flux Leakage have shown the capability to be able to correlate with hardness, and correspondingly with strengths, there is a large uncertainty in such type of estimation which, on one hand, may work well for some systems and not for others (Smart and Bond 2016). The above-listed techniques predict the strength based on the assumption that the material is homogenous, and do not provide a holistic measure of the properties. For the pipeline systems, a number of factors could contribute to the presence of material inhomogeneities, such as the manufacturing process or structure changes due to strain aging may due to the long-term operation of pipelines (Nykyforchyn et al. 2009). This may initiate a phenomenon such as decarburization, resulting in a varied chemical composition and deterioration in mechanical properties that would finally cause surface properties to be different from the bulk ones (Amend, n.d.). Uncertainties in the system are another gap in the prediction of the mechanical properties(Kamtornkiat Musiket; Mitchell Rosendahl; and Yunping Xi 2016). These can manifest in terms of material properties, pipe geometries, manufacturing process, operational conditions, etc. Therefore, it is well understood that single modality analysis, not accounting for material inhomogeneity and the various uncertainties are the

major gaps in the estimation of mechanical properties from the existing methods (Amend, n.d.) (Ersoy 2015).

In a view of the above brief review, the focus of this work is to develop a methodology to aid in the accurate prediction of pipe strength. This study uses a probabilistic approach with rigorous uncertainty quantification, based on multimodal diagnosis to infer the strength of aging pipeline materials. The methodology involves using Bayesian network as a general information fusion framework, to derive the statistical inference and incorporate the multimodal measurements such as microstructure, chemical composition, and other material properties. Several analytical and characterization techniques such as SEM, EDS, EBSD, Hardness and Servo-Hydraulic Testers were adopted to capture the through-thickness multimodal measurements, each of them adding value when integrated through the Bayesian network model. Different pipe grades form industry collaborators and literature database have been utilized in prototype testing for model validation and demonstration.

This model will be based on an updating principle based on Bayes' theorem. This provides a statistical rigorous way to infer posterior distribution (i.e., fused or updated information) using prior distribution (i.e., existing information or experiences) and likelihood function (i.e., new measurements). Let M be a Bayesian model class and $p(\theta, M)$ denote the prior distribution of the parameter θ in the model. Then, for a new observed evidence or system response x' , the posterior distribution, $q(\theta, M)$ is given as:

$$q(\theta, M) \propto p(x' | \theta, \mathrm{M})\, \mathrm{p}(\theta, \mathrm{M}) \tag{1}$$

Here, $p(x' | \theta, \mathrm{M})$ is referred to as likelihood function of θ. The updated probability of each model in M is given by the posterior PDF when the new information x' is incorporated(Peng et al. 2013). The present model also includes an error term e which is a variable with 0 mean normal distribution which can be denoted as $e \sim N(0, \sigma_e)$ and is used to define the relationship between the model M and the updating variable x' for updating the parameter, θ, giving us with the following relation:

$$x' = \mathrm{M} + e \tag{2}$$

The above shown information fusion is for a single modality/source of information. One major task in the study is to extend this idea to a generalized Bayesian network for multimodality diagnosis information fusion. A Bayesian network is a probability-based graphic tool to infer systems with stochastic parameters. A schematic of the network is illustrated in Figure 1.2 for the pipe strength and toughness estimation.

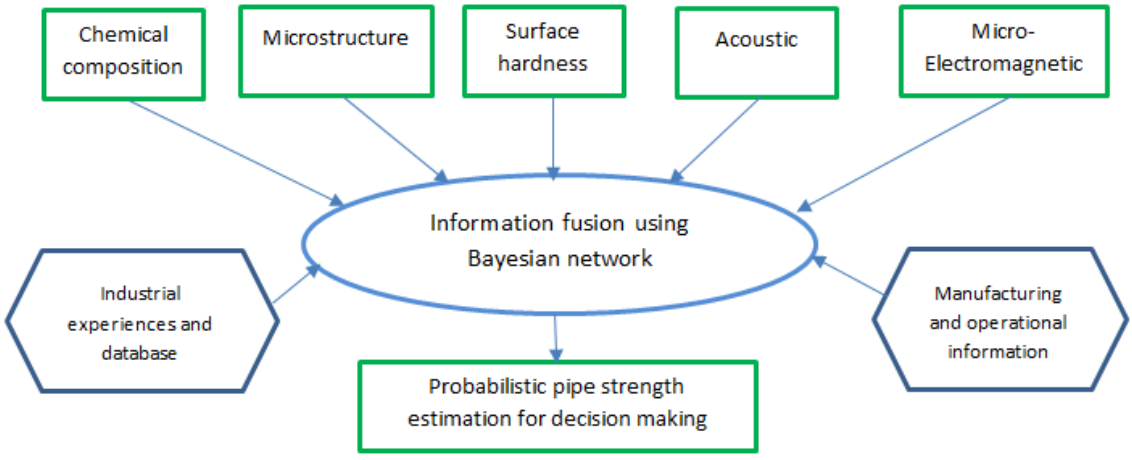

Fig 1.2. Schematic of the proposed Bayesian Network model

2.2 INVESTIGATION AND ANALYSIS OF BASIC MATERIAL PROPERTIES

Three samples from transmission pipelines were used in the present study belonging to the year of installation ranging from 1949 to1961. The pipe samples arrived with the installation year and Pipe grade information as listed in Table 1. The suspected grade and microstructure were deduced from the image analysis and year of installation information.

Table 1. Pipe grades information

Pipe Number	Installation year	Pipe grade	Suspected grade	Microstructural constituents
45 (1)	1949	1525	X50	Ferrite-Pearlite
47 (2)	1964	1025	X60	Ferrite-Pearlite
44 (3)	-	1513	-	Ferrite-Pearlite

2.2.1 Setup and Procedure

2.2.1.1 Microstructure Characterization

For the experimental analysis, a few samples were carved out along the thickness direction 10 um^2 cross-section units and polished as per the guidelines for metallographic inspection. Etching was done using 2% Nital solution, holding the samples for 10-20 seconds to reveal the grain and phase structures. The samples were viewed under Optical/Scanning Electron Microscope (SEM). Grain size of ferrite was studied along with

the volume fraction of the constituent phases with the use of a commercially available software ImageJ.

2.2.1.2 Chemical composition analysis

The chemical composition of the specimen was studied through semi-quantitative Energy Dispersive Spectroscopy (EDS) in an Electron probe micro analyzer (EPMA). Both point analysis and area analysis was carried out to determine the average composition across the phases. Polished and etched samples from microstructure analysis were used for composition testing. Figure 2 shows the spot analysis SEM image and spectrum.

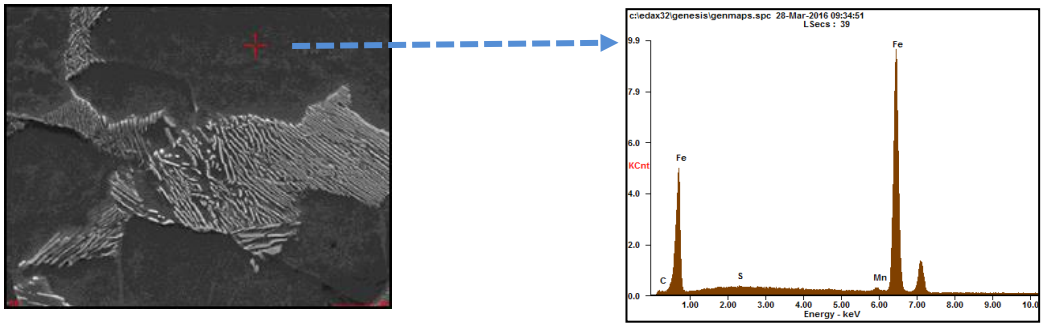

a) b)

Fig 2. Images of the EDS analysis: a) SEM image b) EDS Spectrum

2.2.1.3 Hardness Test

Hardness of the samples were examined with the Vickers Hardness tester, a tester for small area measurements [9]. 1kg small load was used for the purpose of testing as the samples were only 1mm thick. Blocks of 10mm X 10mm X 1mm were used.

2.2.1.4 Tensile Test

The stress-strain characteristics were studied through tensile tests of flat strip test samples carved out from the pipe in the hoop orientation (Figure 3 a, b) (Hashemi 2011). The samples were tested both with the use of a Tensile Stage machine (along layers) and Servo-Hydraulic MTS machine (Figure 3 c), (bulk analysis), and were custom made in as per the dimensions allowed by the machines.

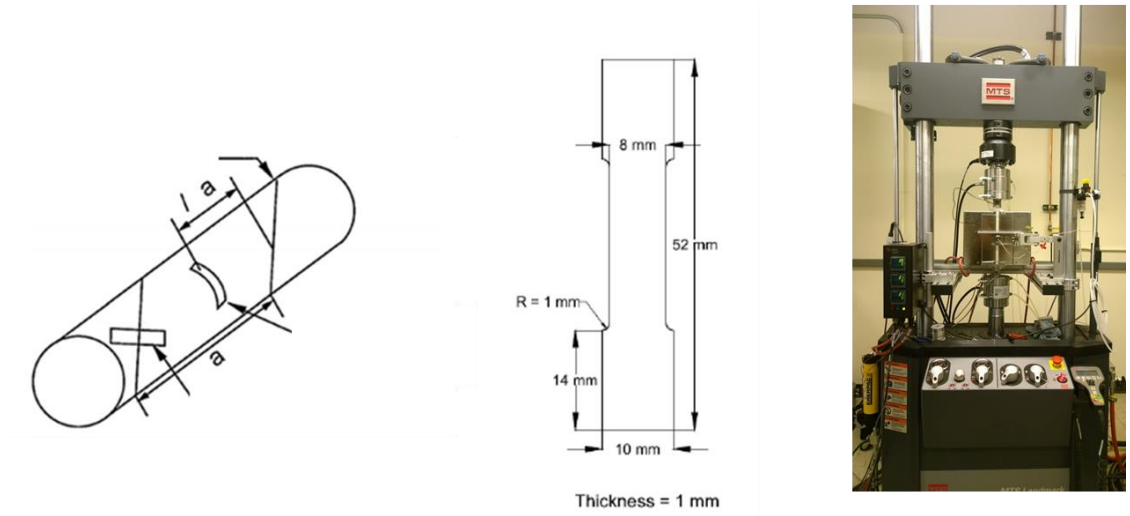

a) b) c)

Fig 3. a) Orientation of flat strip tensile specimen within the pipe sample (Hashemi 2011), b) Dimensions of flat strip tensile specimen c) Servo Hydraulic MTS machine

The experiments were repeated for different depths along the pipe wall thickness in order to examine their variation along the thickness. The thickness at different depths was measured using an Ultrasonic thickness gauge.

2.2.2 Results from the experimental analysis

2.2.2.1 Microstructure

The microstructure of the two pipe samples was studied through Secondary Electron Microscope and is reported in Figure 4. The microstructure was seen to be comprised to two phases, ferrite and pearlite, hence the likelihood model in the network takes into account effect of dual phase strength.

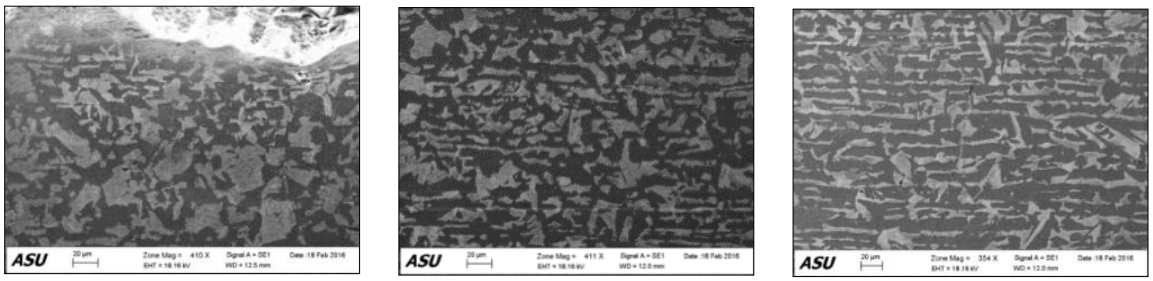

a) b) c)

Fig. 4.1 SEM images showing the microstructure of Pipe 45; a) Outer pipe wall surface b) Middle surface c) Inner pipe wall surface

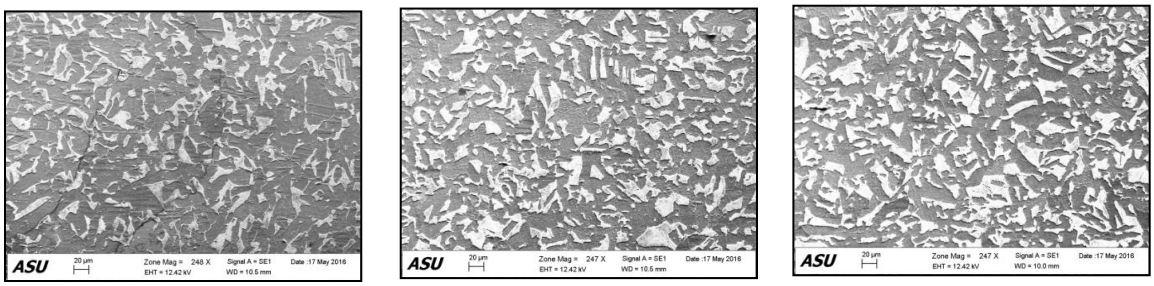

a) b) c)

Fig. 4.2 SEM images showing the microstructure of Pipe 47; a) Outer pipe wall surface b) Middle surface c) Inner pipe wall surface

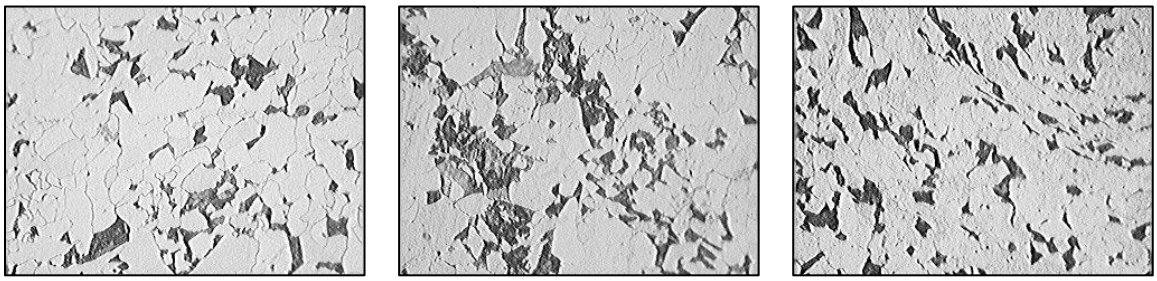

a) b) c)

Fig.4.3 Optical images showing the microstructure of Pipe 44; a) Outer pipe wall surface b) Middle surface c) Inner pipe wall surface

The figures from left to right correspond to the different depths (along the pipe wall direction) within a sample; and are only shown for three consecutive depths.

The pipe images pipe depict a prominent texture, potentially related to the manufacturing process parameters. Fine grains can also be observed from both the pipe samples that would aid in studying the grain size and volume fraction. These are used to derive the volume fraction of the constituent phases as well as the grain size, as stated in the next section.

2.2.2.2 Volume fraction of the phases:

The complete analysis was done for the distribution of phases in terms of the volume fraction with use of image analysis software Image J, as stated previously. The result is shown below in Figure 5.1; overlapped for comparison.

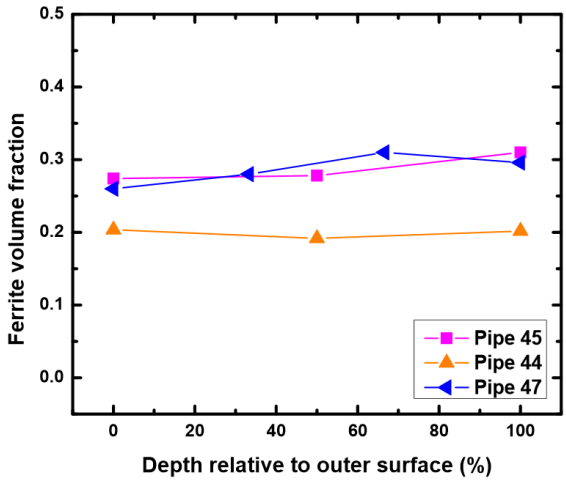

Fig 5.1. Plot showing change in the ferrite content across the pipe wall thickness

The number of measurements for each pipe specimen are limited by the thickness of the specific pipes. Therefore, the depth is listed as a function of overall thickness in Fig. 4, considering pipe sample 45 was about 8mm thick while pipe sample 2 was only 5.5mm in thickness. A total of 7-8 measurements were taken per sample. The figure shows the variation in the phase volume fraction with increasing depth from the surface. Pipe 45 shows a decrease in the pearlite content in the middle region, whereas Pipe 47 shows a slight opposite behavior where the pearlite content being higher in the middle region and lower towards the surface. Pipe 44 shows a constant higher percentage of pearlite though the entire thickness. The predicted trend and the cause of variation is out of the scope of the study and hence not presented in detail here, instead the quantitative values along the thickness are used as input in the Bayesian Model.

2.2.2.3 Ferrite Grain Size

Grain size analysis was done for the samples using the lineal intercept procedure as per the ASTM standards (Hashemi 2011). The measurements were done for each layer from outside to inside surface. The average grain size for both samples was observed to be 24um for the first two samples, and 19 um for the Pipe 44. The observed values are listed in Table 2.

Table 2. Grain size details for pipes a) Pipe 45 and 47, b) Pipe 44

a)

S.No	Pipe 45		Pipe 47	
	Layers	Grain Size (um)	Layers	Grain size (um)
1	Outer region	22.86	Outer region	24.13
2	Middle region-1	21.8	Middle region-1	20.5
3	Middle region-2	25.59	Middle region-2	27.44
4	Inner region	27.69	Inner region	25.4

b)

S.No	Pipe 44	
	Layers	Grain Size (um)
1	Outer region	17.35
2	Middle region-1	22.14
3	Middle region-2	25.13
4	Inner region	12.39

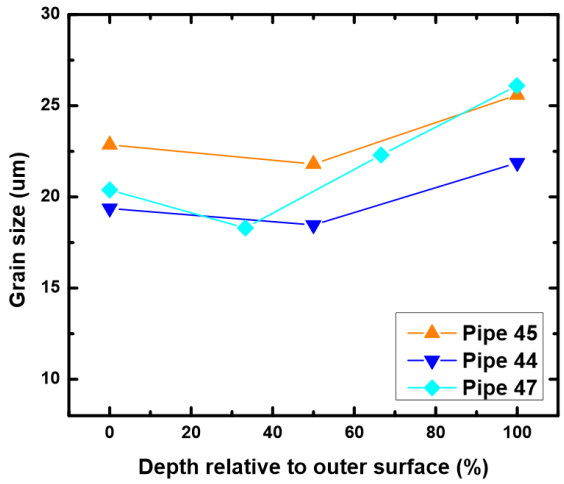

Fig 5.2. Plot showing change in the grain size across the pipe wall thickness

The grain size variation through the thickness is shown in Figure 5.2. The grain sizes for Pipe 45 and 47 seem to show a little increase towards the inner region, probably due to differential cooling during the manufacturing process. Pipe 44 appears to have smaller grain size at both surface zones and higher grain size in the middle regions, again asserting to the TMCP process and cooling process afterwards. The values are used for model training and prediction.

2.2.2.4 Chemical composition

The chemical constituent of the phases was analyzed using EDS, and was observed to be Ferrite + Pearlite system for all the specimens. The elements of interest were chosen based on their direct or indirect correlation to the Yield and Ultimate Tensile strengths, obtained from literature (Bramfitt and Corporation 1998). The primary elements of interest

were found to be Fe, Mn, Si, and N. Table 3 lists the values of composition of the pipe samples.

Table 3. Composition (weight percentage) of the pipes a) Pipe 45 b) Pipe 47 c) Pipe 44
a)

Region	Elements					
	C	N	Si	Mn	Fe	Ni
Outer region	0.09	0.23	0.26	1.29	97.92	0.31
Middle region-1	0.06	0.12	0.04	1.19	98.29	0.17
Middle region-2	0.2	0.01	0.03	1.28	97.97	0.15
Inner region	0.15	-	0.06	1.23	98.13	0.16

b)

Region	Elements					
	C	N	Si	Mn	Fe	Ni
Outer region	0.05	0.11	0.02	1.18	98.25	0.2
Middle region-1	0.21	-	0.01	0.89	98.69	0.05
Middle region-2	0.07	-	0.04	1.26	98.34	0.19
Inner region	0.08	0.02	0.02	0.93	98.66	0.23

c)

Region	Elements						
	C	N	Si	Cr	Mn	Fe	Ni
Top Layer	-	-	0.23	0.04	1.77	95.42	-
Middle region-1	0.06	-	0.25	-	1.7	97.76	0.1
Middle region-2	-	-	0.27	0.05	1.8	97.41	0.11
Inner region	-	-	0.26	-	1.73	97.33	0.19

The composition for the elements of interest did not seem to vary too much along the thickness and therefore only the average values are listed here.

2.2.2.5 Hardness

Hardness was determined using the Vickers Hardness Tester for three pipe samples. The following tables show the results for the same for the two pipe samples; Outer region

represents the outermost surface exposed to the surrounding going towards the thickness being represented by middle region 1 and 2, and inner region being the one towards the inner surface of the pipe. The results are reported for reference in Table 4 and are plotted in Figure 5.3.

Table 4. Hardness of the pipe samples a) Pipe 45 b) Pipe 47 c) Pipe 44

a)

Samples	Mean Hardness (HV)
Outer region	220.2
Middle region-1	178
Middle region-2	203.06
Inner region	219.3

b)

Samples	Mean Hardness (HV)
Outer region	208.17
Middle region-1	217.27
Middle region-2	221.73
Inner region	226.03

c)

Samples	Mean Hardness (HV)
Outer region	188
Middle region-1	188.2
Middle region-2	206.5
Inner region	200

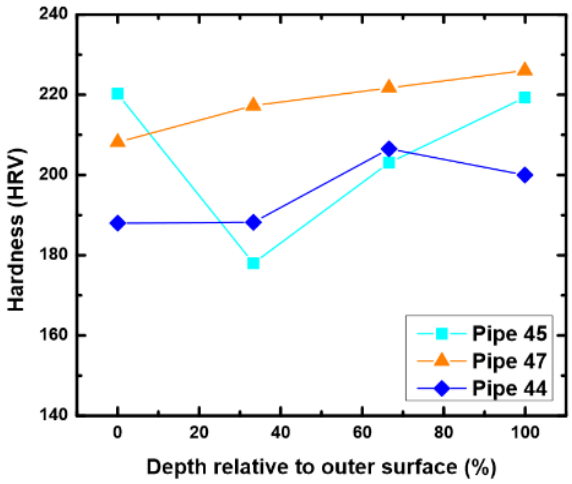

Fig 5.3. Plot showing change in Hardness across the pipe wall thickness

These values show that for pipe sample 45, the Hardness of the pipe walls, inside and outside is more than the middle regions. For pipe sample 47, the inside pipe wall appeared to have the highest hardness that correspondingly decreased towards the outer pipe wall surface. Pipe 44 appears to be stronger towards the inner regions. Although the trends observed are reported here, but they were not investigated being out of the scope of the paper, and only quantitative measures were used as input for the model.

2.2.2.6 Tensile Properties

The pipe specimen were tested using the Tensile-stage along the thickness, and the corresponding stress-strain curves were analyzed. The stress-strain plots are shown in Figure 6 and the values of yield strengths and tensile strengths through the pipe thickness are listed in Table 5.

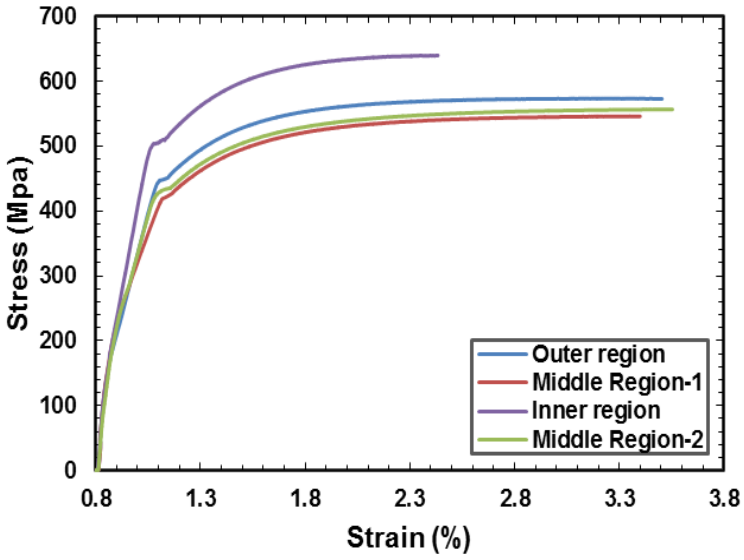

a)

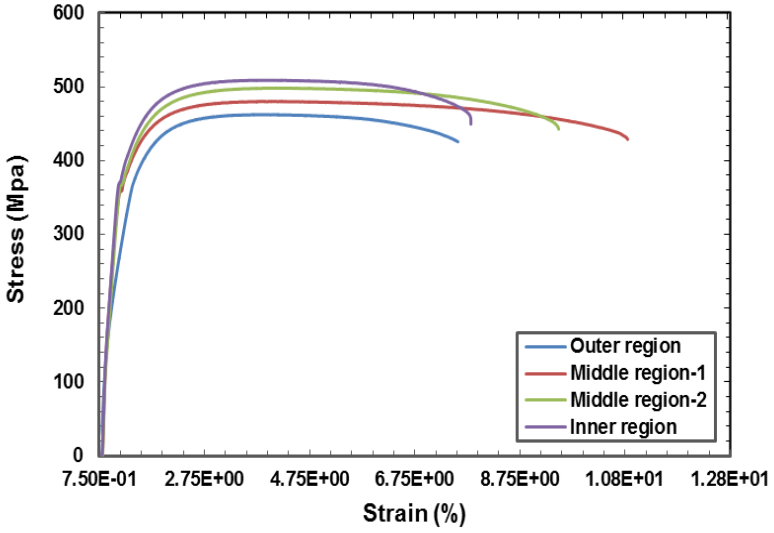

b)

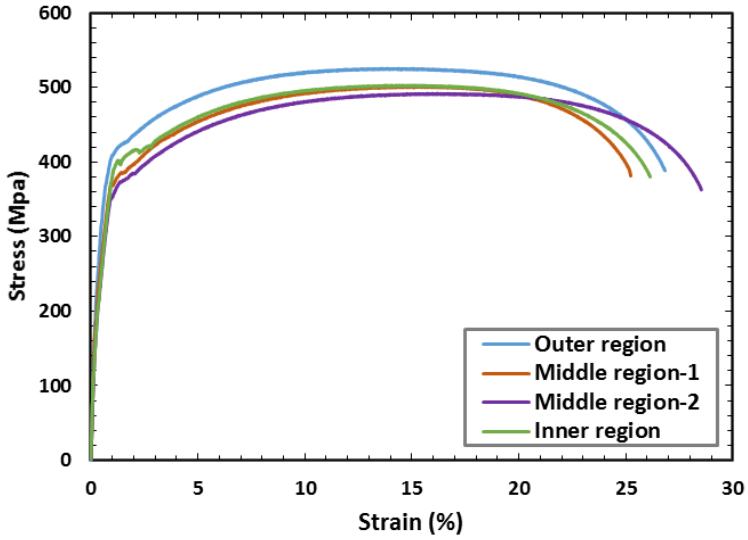

c)

Fig 6.1 Plot showing stress-strain behavior a) Pipe 45 b) Pipe 47 c) Pipe 44

Table 5. Stress-Strain data for the pipe samples a) Pipe 45 b) Pipe 47 c) Pipe 44

a) b)

Samples	YS (MPa)	UTS (MPa)	Samples	YS (MPa)	UTS (MPa)
S1(Top Layer)	450	572.99	S1(Top Layer)	355.5	462.2
S2(Layer 2)	425	538.4	S2(Layer 2)	358.4	479.4
S3(Layer 3)	435	555.6	S3(Layer 3)	366.2	497.8
S4(Layer 4)	506	637.5	S4(Layer 4)	371.08	508.4

c)

Samples	YS (MPa)	UTS (MPa)
S1(Top Layer)	406	524.2
S2(Layer 2)	373	500.4
S3(Layer 3)	367	489.6
S4(Layer 4)	397	501.5

Following the trend from the hardness study, the tensile properties of the two pipe specimens also showed similar behavior, appearing to be stronger on the pipe walls for pipe sample 1 and weaker on the inside. Also, for pipe sample 2, inside pipe wall seemed to be the strongest with middle regions being little weaker and the outermost pipe wall surface being the weakest. Once again, the reported trends are not investigated, but the values are used for model validation.

2.2.2.7 Texture analysis

Texture of the samples was studied using Electron Back Scatter Diffraction (EBSD) technique. The EBSD analysis was only extended to a few samples of the pipe in order to further establish the change in material properties through the thickness, and to account for the texture change resulting from material deformation. Pipe samples from outer surface region and middle region of pipe 45 is used for this demonstrative study.

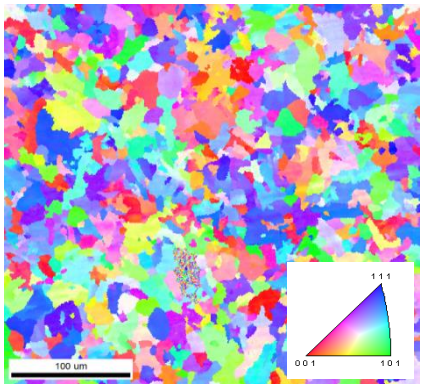

a)

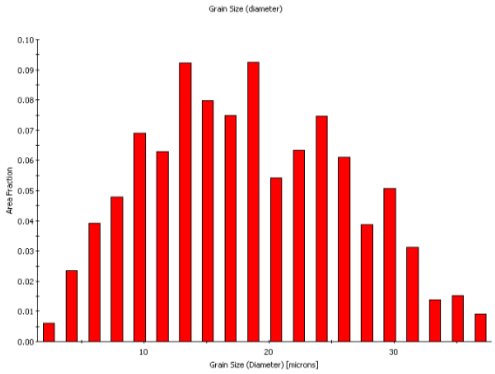

b)

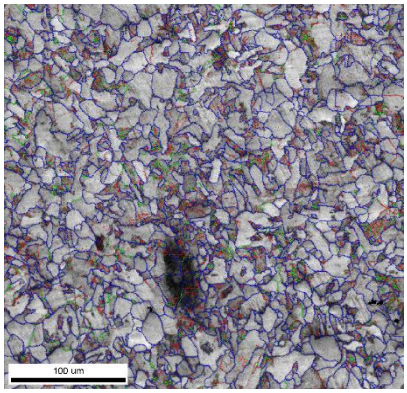

c)

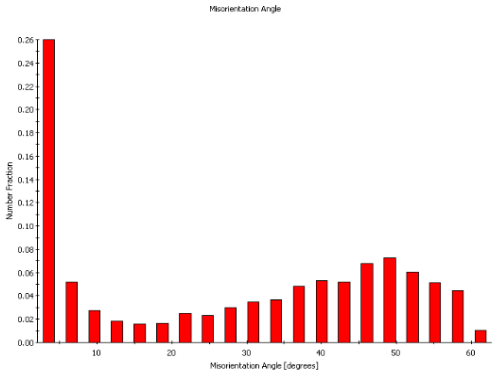

d)

Fig 6.2. EBSD maps for non-strained sample pipe 45 from the outer region a) IPF image b) Grain size distribution c) Grain boundary image d) Misorientation distribution

The EBSD maps shown in Figure 6.2 is for an undeformed area of pipe 45 from the outer surface region. The average grain size was noted to be 9.1 um, average misorientation was evaluated as 28.5 degrees and the fraction of high angle grain boundaries (>15^0) was seen to be 0.63.

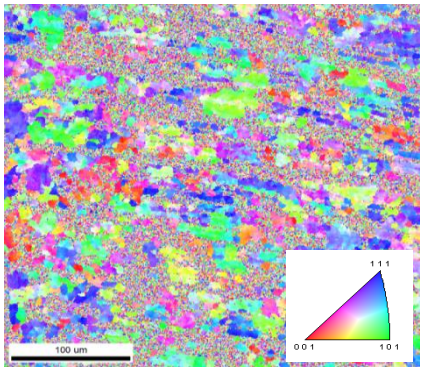

a)

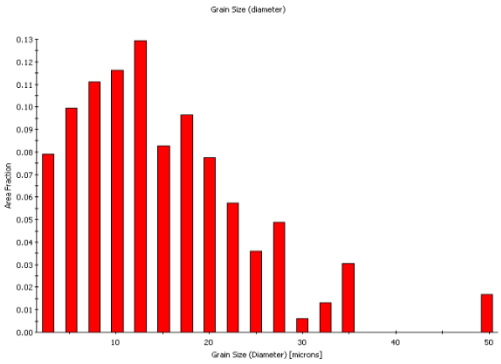

b)

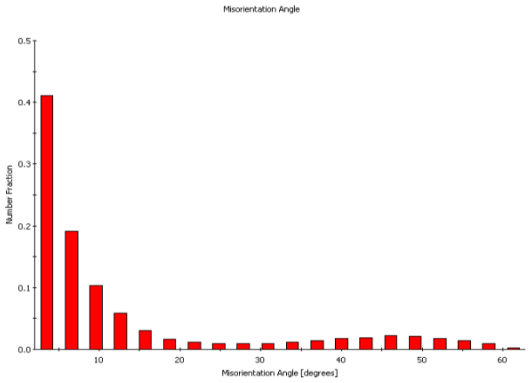

c)

Fig 6.3. EBSD maps for deformed sample pipe 45 from the outer region a) IPF image b) Grain boundary image c) Misorientation distribution

The EBSD maps shown in Figure 6.3 is for a deformed area of pipe 45 from the outer surface region. Many of the pixels could not be evaluated due to the severe plastic deformation in the region. The statistical data was obtained from the reconstructed image, however they may not be an accurate representation of the average distributions. The average grain size was noted to be 5.2 um, average misorientation was evaluated as 12.9 degrees. The fraction of low angle grain boundaries and high angle grain boundaries could not be determined at this time.

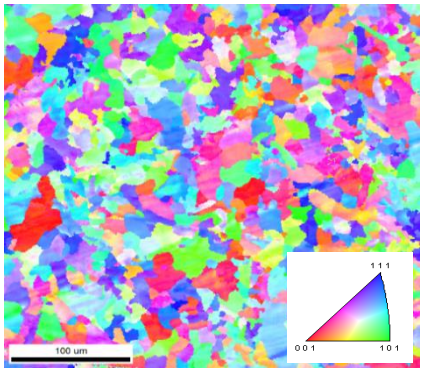

a)

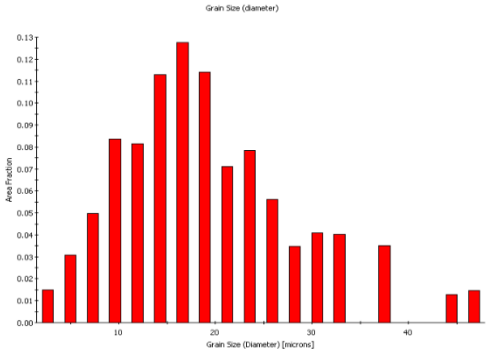

b)

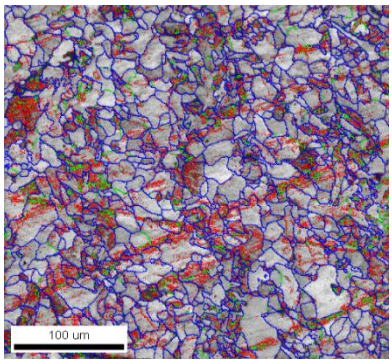

c)

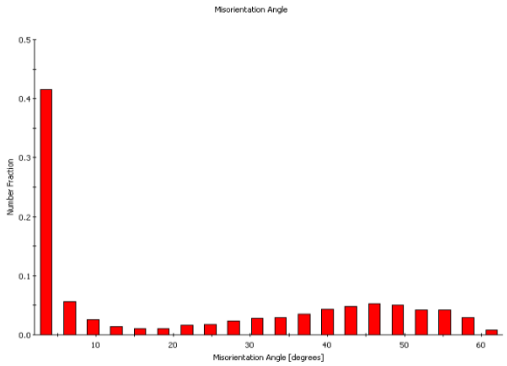

d)

Fig 6.4. EBSD maps for non-strained sample pipe 45 from the middle region a) IPF image b) Grain size distribution c) Grain boundary image d) Misorientation distribution

The EBSD maps shown in Figure 6.4 is for an undeformed area of pipe 45 from the middle region. The average grain size was noted to be 9.3 um, average misorientation was evaluated as 22.3 degrees and the fraction of high angle grain boundaries (>15^0) was seen to be 0.48.

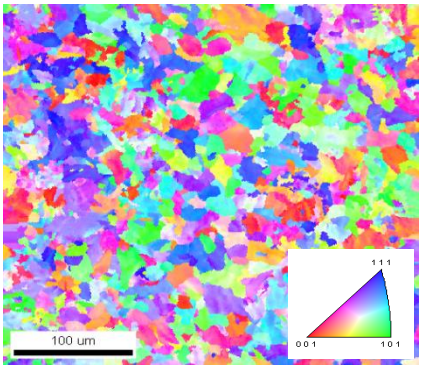

a)

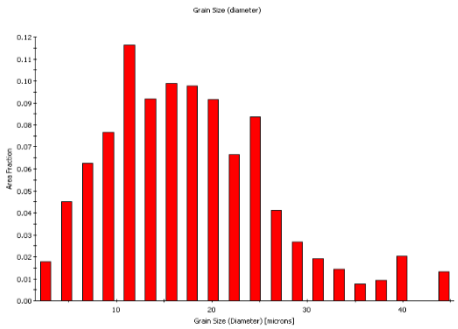

b)

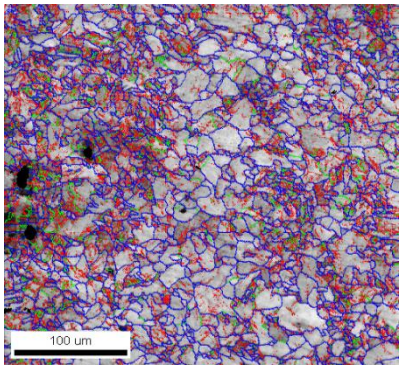

c)

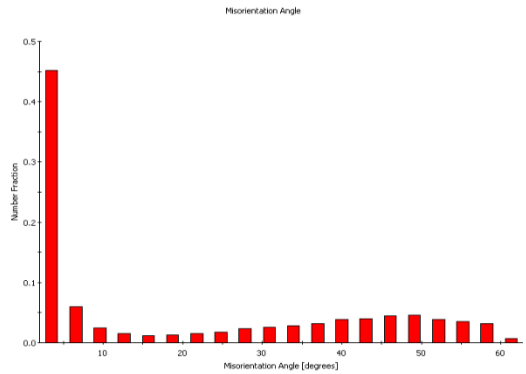

d)

Fig 6.5. EBSD maps for deformed sample pipe 45 from the middle region a) IPF image b) Grain size distribution c) Grain boundary image d) Misorientation distribution

The EBSD maps shown in Figure 6.5 is for a deformed area of pipe 45 from the middle region. The average grain size was noted to be 8.29 um, average misorientation was evaluated as 20.6 degrees and the fraction of high angle grain boundaries (>15^0) was seen to be 0.44.

It can be seen that grain size did not appear to change significantly between the outer and the middle region, and very little variation was observed upon deformation (1 um). The misorientation between the grains however, appeared to change by almost 5 degrees between the non-strained regions of outer and middle areas and less than 3 degrees

between deformed and undeformed samples. The fraction of high angle grain boundaries was seen to vary by 0.15 in the non-strained regions from outside to the middle and changed very slightly upon deformation.

2.3 BAYESIAN MODEL FORMULATION

2.3.1 Model formulation

The yield strength or ultimate tensile strength of pipeline specimen in service can be estimated in several indirect ways, through measurement of surface material properties and correlating them to strength through available literature data (Bramfitt and Corporation 1998)(Li, Schmauder, and Dong 1999)(Hashemi 2011). The material properties such as hardness and composition can be obtained experimentally without interrupting the operation of the pipeline. The current model makes use of this data and the available relationships to fuse them together and provide a more precise multimodal prediction of strength(Butz et al. 2009)(Liu, Yue, and Zhang 2009). The general model for yield strength prediction appears as follows, where YS prior is updated using data from Hardness, H, Chemical composition, C and Volume fraction, V. YS and σ_{ys} have been used interchangeably.

$$p(YS \mid H,C,V,\mathrm{M}) \propto p(H,C,V \mid YS,\mathrm{M})p(YS,\mathrm{M}) \tag{3}$$

where, $p(YS \mid H,C,V,\mathrm{M})$ is the posterior yield strength, $p(YS,\mathrm{M})$ is the prior yield strength, and $p(H,C,V \mid YS,\mathrm{M})$ is the likelihood function in the model. To start with, each of these nodes have been provided equal weightage, which can be modified later with a sensitivity analysis approach, currently outside the scope of this paper. More formally, the likelihood model of YS is given as,

$$l(\sigma_{YS}) = \mathrm{A}(\sigma_{H|YS}) + \mathrm{B}(\sigma_{C|YS}) + \mathrm{C}(\sigma_{V|YS}) \tag{4}$$

where, $l(\sigma_{YS})$ is the likelihood model with $\sigma_{H|\mathrm{YS}}$ $\sigma_{C|YS}$ and $\sigma_{V|YS}$ as the individual yield strength values derived from Hardness, chemical composition and volume fraction, as stated above. Due to the equal weightage assignment, each of the coefficients A, B and C in the likelihood model are each equal to 1/3. Figure 7 depicts the general schematic of the model.

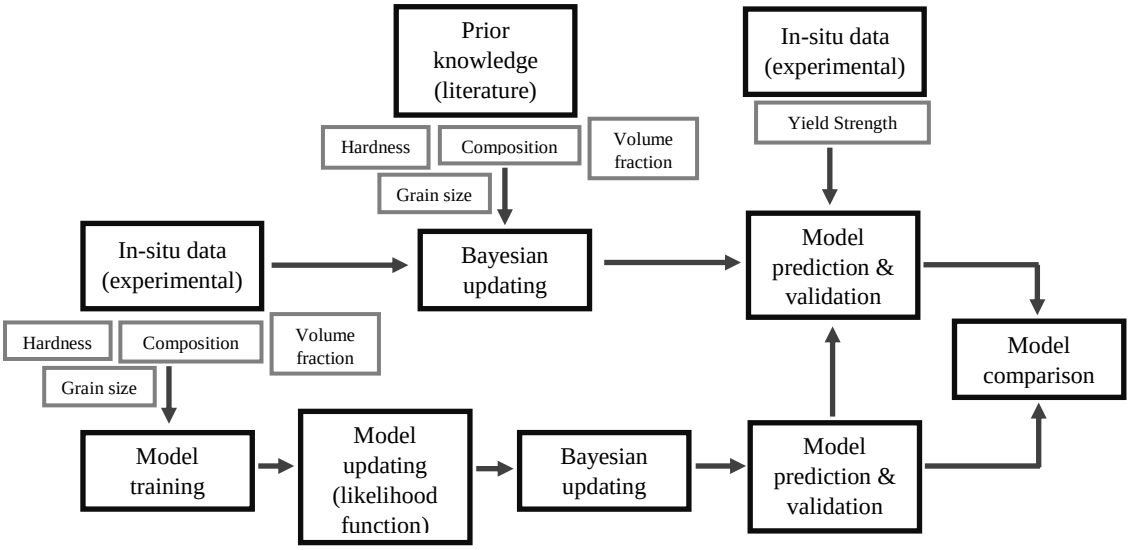

Fig 7. General flow of the model prediction and validation

Each of the individual relationships are described below.

The relationship between yield strength and material chemical composition as well as grain size is realized as follows:

$$\sigma_{YS|C} = 53.9 + 32.34(X_{Mn}) + 83.2(X_{Si}) + 354.2(X_{Nf}) + 17.4(d^{-1/2})$$ (Bramfitt and Corporation 1998) (5)

where, $\sigma_{YS|C}$ is the yield strength of the material derived from the compositional parameters, X_{Mn} is the weight percentage of Manganese, X_{Si} is the weight percentage of Silicon, X_{Nf} is the weight percentage of Nitrogen, and d is the grain size of ferrite (mm).

Similarly, for a two phase microstructure system, the overall yield strength is assumed as the weighted average of yield strength of the individual phases.

$$\sigma_{YS|V} = \sigma_{(f)}(V_f) + \sigma_{(p)}(1 - V_f)$$ (Li, Schmauder, and Dong 1999) (6)

where, $\sigma_{YS|V}$ is the yield strength of the dual phase material derived from volume fraction alone, $\sigma_{(f)}$ is the yield strength of the ferrite phase and $\sigma_{(p)}$ is the yield strength of the pearlite phase and V_f is the volume fraction of ferrite.

Next, the yield strength of the low carbon steel is related to the hardness as:

$$\sigma_{YS|H} = 2 * H + 105$$ (Hashemi 2011) (7)

where, $\sigma_{YS|H}$ is the yield strength derived from Hardness, and H is Vickers hardness.

The material ultimate tensile strength also have similar relationships. The ultimate tensile strength is related to average chemical composition, volume fraction and grain size as follows:

$$\sigma_{UTS|C,V} = 294.1 + 27.7(X_{Mn}) + 83.2(X_{Si}) + 3.9(V_p) + 7.7(d^{-1/2}) \quad \text{(Bramfitt and Corporation 1998)} \quad (8)$$

where, $\sigma_{UTS|C,V}$ is the ultimate tensile strength derived from compositional and microstructural parameters, V_p is the volume fraction of pearlite, and the other symbols have the usual meanings.

Additionally, it is related to hardness as follows:

$$\sigma_{UTS|H} = 1.3 * H + 344 \text{ (Hashemi 2011)} \quad (9)$$

where, $\sigma_{UTS|H}$ is the ultimate tensile strength derived from Hardness and H is the Vickers hardness. Known priors were used for each of these, derived from the literature knowledge of the system of API Steels with ferrite-pearlite microstructure (Bramfitt and Corporation 1998)(Li, Schmauder, and Dong 1999)(Hashemi 2011). The prior values (means) of the composition were given as; X_{Si} = 0.02 for weight percent of silicon, X_{Mn}=0.2 for weight percent manganese, X_{Nf} =0.02 as the weight percent of free nitrogen. Prior grain size, d was 10um, prior volume fraction of ferrite V_f was listed as 0.5 or 50% and prior Vickers hardness was assumed as 150 HV

The updating scheme makes use of Metropolis-Hastings algorithm to draw random samples form the probability distributions and perform updating by using the specified number of samples and allowing a margin for a burn-in period. All the priors and likelihoods follow a Gaussian distribution, for the purpose of simplicity and demonstration.

2.3.2 Strength prediction through Bayesian updating

The statistical averaging model for the yield strength being of the form as listed below:

$$YS = Ax + By + Cz + \varepsilon, \tag{10}$$

where, x, y and z are pdfs representative of the equations (5)…(9) and ε is the random error component in the system, and A, B and C are the model coefficients corresponding to the variables. The resultant model is depicted in Figure 8. YS and UTS represent the yield and ultimate tensile strength correspondingly.

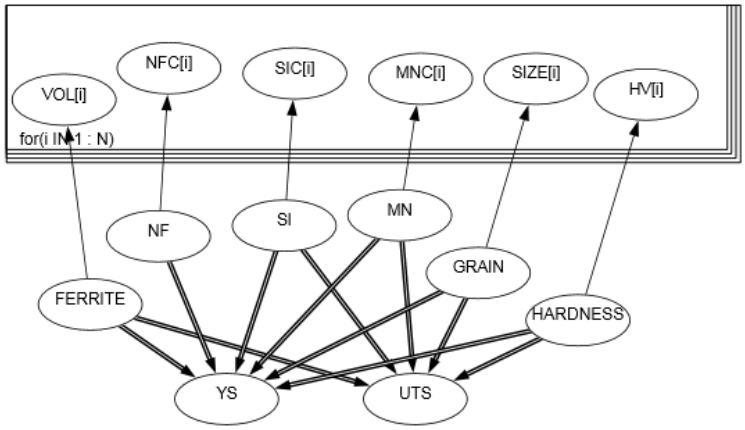

Fig 8. Schematic representation of the Bayesian Network Model for Yield and Ultimate Strength prediction

The above model for prediction of yield and ultimate strength depicts several nodes. Node FERRITE refers to volume fraction of ferrite, NF, SI and MN are the compositional parameters referring to weight percentages of free Nitrogen content, Silicon, and Manganese. Node GRAIN refers to the grain size and HARDNESS refers to Hardness of the material. The nodes VOL[i], NFC[i], SIC[i], MNC[i], SIZE[i] and HV[i] are all used for updating the corresponding primary nodes FERRITE, NF, SI, MN, GRAIN and HARDNESS, respectively, when a new observation is available. The model offers several unique features that are not available in most existing methodologies. First, continuous uncertainty reduction can be achieved if continuous observation from multimodality measurements is available for the interested material system. Another natural and important outcome from the proposed model is the node sensitivity. The predicted response could be more sensitive to one or more of the interconnected nodes, compared to the others, and this dictates the weightage assigned to the nodes. This information will be valuable for future optimization of inspection (i.e., only focusing on more sensitive node for information acquisition). Detailed the discussion on this topic is beyond the scope of the proposed study and needs further investigation.

Another feature is that all the nodes in the model are co-dependent and updating can be performed in terms of data analysis for prediction as well as for the missing values, and hence all the nodes in the system can be updated, irrespective of a direct or indirect correlation with the updating node. This helps to converge the parameter values and quantifying the uncertainty of the system as the model is updated in the view of new information from various measurements.

The next section describes the experimental procedures utilized to gather data for performing training and validation of the Bayesian Network Model. The metrics analyzed here are the ones known to have a response in the present system, based on the equations (1.6) through (1.10).

2.3.3 Model Validation for Prediction of Strength

The data from Section 3, viz microstructure, hardness and composition are used as input for the model and are integrated to predict the corresponding Yield Strength and Ultimate Tensile Strength as shown in Figure 9. The predictions are done for likelihood models with just one node for each of hardness, composition and volume fraction, as well as model with the nodes combined together as a weighted average, and are then compared to the actual experimental results from the tensile testing of the samples to measure the closeness of the predicted values with the experimental ones.

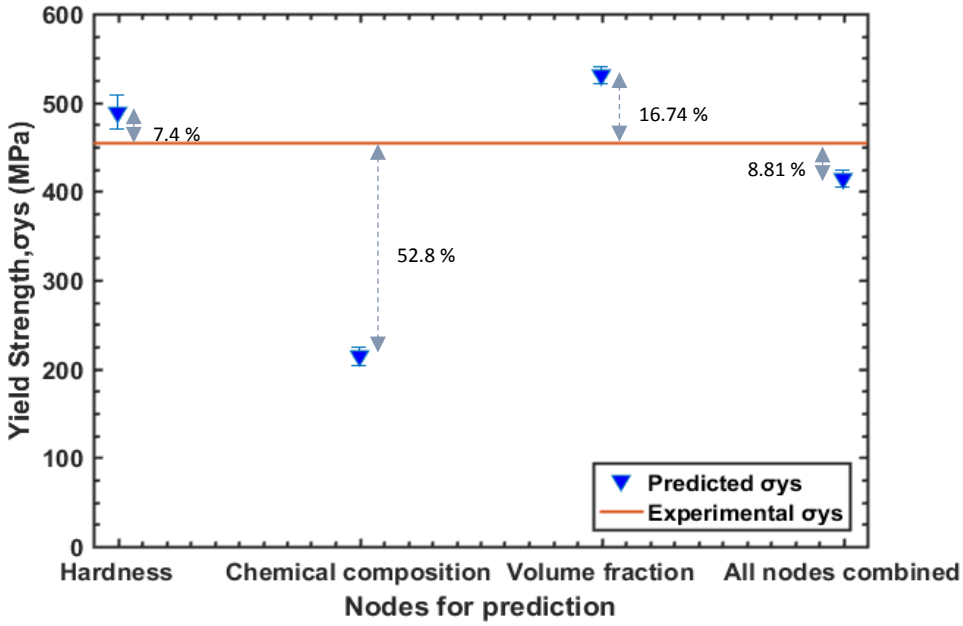

a)

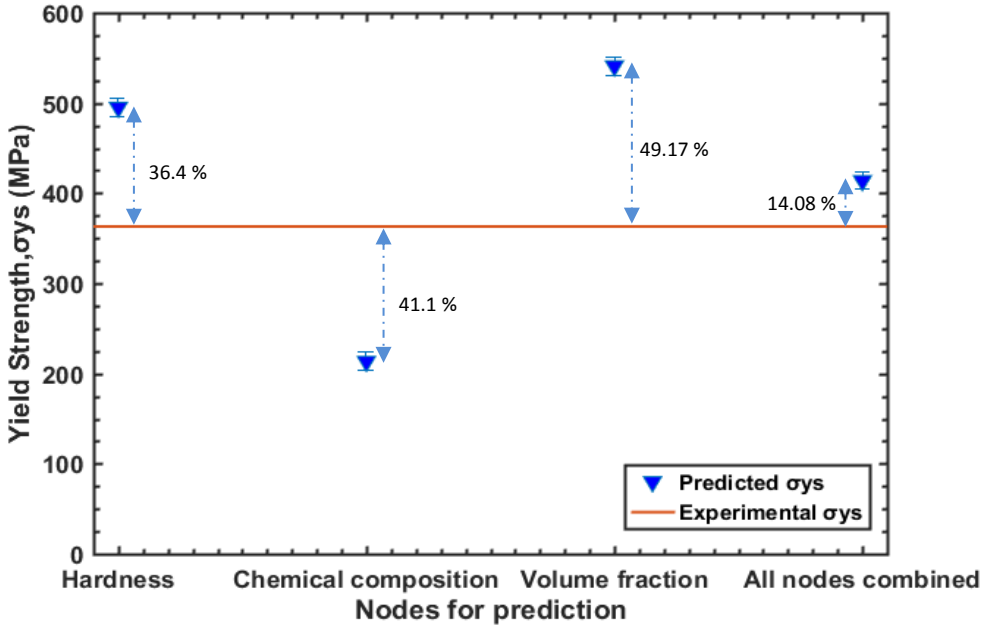
600
500
400
300
200
100
0
Yield Strength,σys (MPa)
36.4 %
41.1 %
49.17 %
14.08 %
Predicted σys
Experimental σys
Hardness
Chemical composition
Volume fraction
All nodes combined
Nodes for prediction

b)

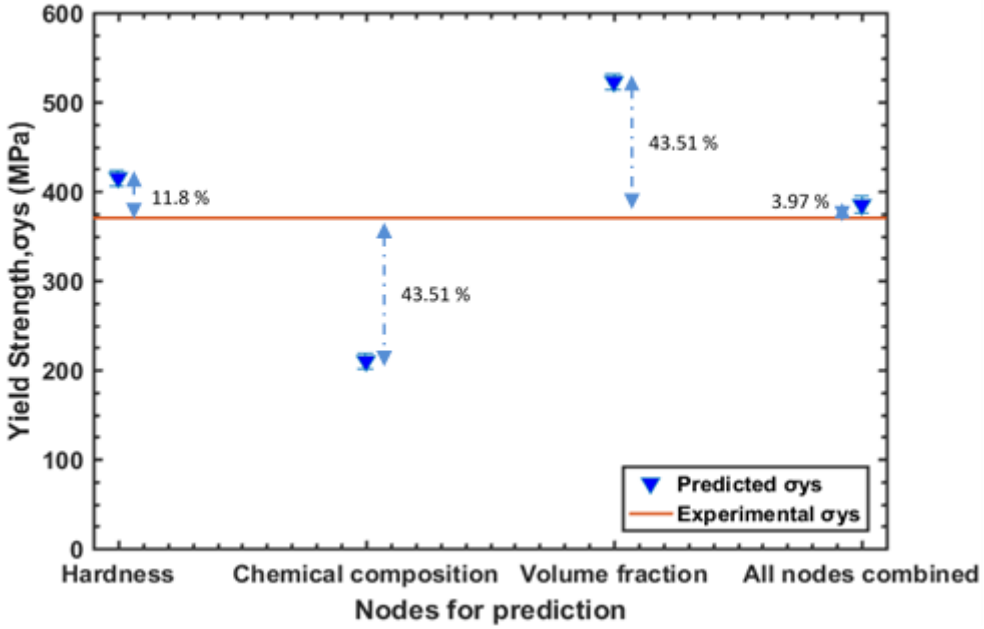
600
500
400
300
200
100
0
Yield Strength,σys (MPa)
11.8 %
43.51 %
43.51 %
3.97 %
Predicted σys
Experimental σys
Hardness
Chemical composition
Volume fraction
All nodes combined
Nodes for prediction

c)

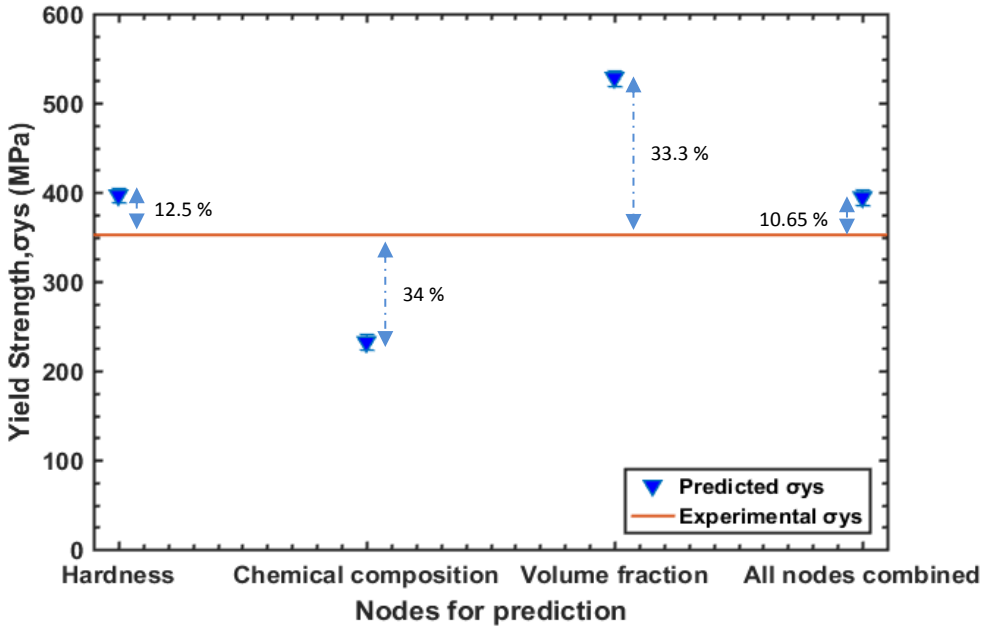
600
500
400
300
200
100
0
Yield Strength,σys (MPa)
12.5 %
34 %
33.3 %
10.65 %
Predicted σys
Experimental σys
Hardness
Chemical composition
Volume fraction
All nodes combined
Nodes for prediction

d)

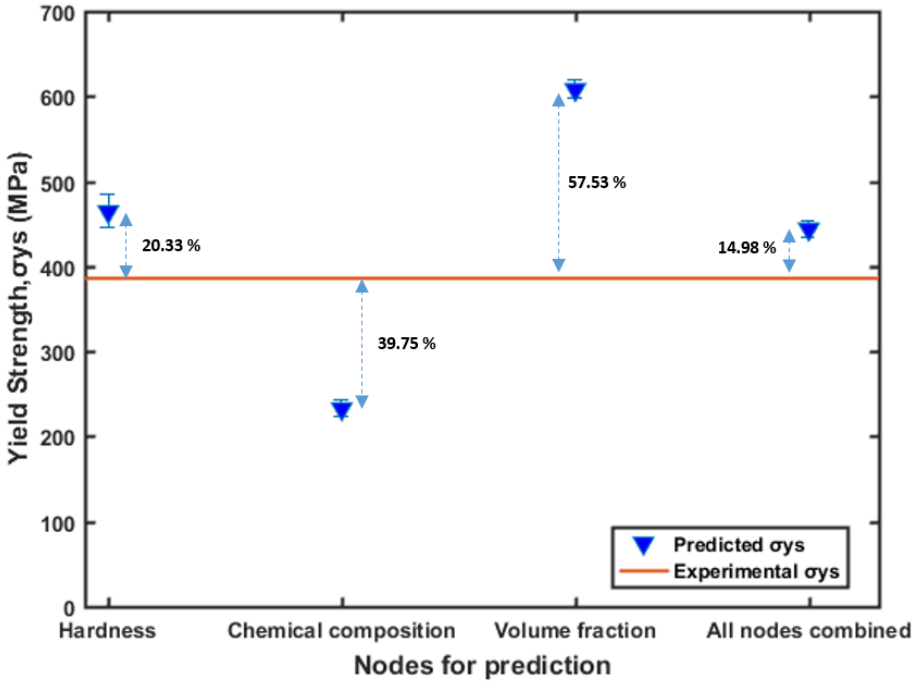
700
600
500
400
300
200
100
0
Yield Strength,σys (MPa)
20.33 %
39.75 %
57.53 %
14.98 %
Predicted σys
Experimental σys
Hardness
Chemical composition
Volume fraction
All nodes combined
Nodes for prediction

e)

Fig 9. Plot for prediction of Yield strength from individual nodes as well as put together a) Pipe 45(1) b) Pipe 47(2) c) Pipe X42R d) Pipe X42N e) Pipe 44 (3)

For the first case a), it appears that prediction with node Hardness is 488.78, showing an error of 7.4% with respect to the experimental value of 454 and the best prediction, followed by prediction from all nodes combined being 414 or 8.81% deviant from the experimental value and the prediction from chemical composition showing the largest error as 52.8%. For case b), the smallest deviation from true value was from all the nodes combined was 413.63, making it 14.08% from the true value of 362.79 and the largest one being 540.85 or 49.17% from node volume fraction.

For c), the prediction from all nodes combined was 394.3 MPa or 10.65% deviant from the experimental value of 352 MPa being the closest prediction, whereas prediction from node volume fraction was 528.38 MPa showing the largest error of 33.3%. For case d), once again, the prediction from all nodes combined was 384.69 being the closest to the true experimental value of 370 MPa in the range of 3.97% and the farthest prediction was shown by node chemical composition, resulting in a value of 209.66 MPa or 43.51% deviant from the true value.

2.3.4 Nodes codependency

The Bayesian Network features codependency of the nodes that may or may not be directly correlated. This is demonstrated by changing the input value for node Hardness and observing a change in the posterior distribution of other nodes like Silicon and Ferrite, as depicted in Figure 10.

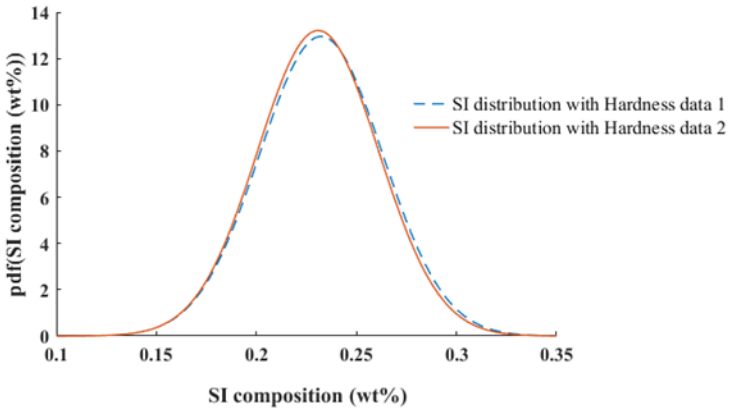

a)

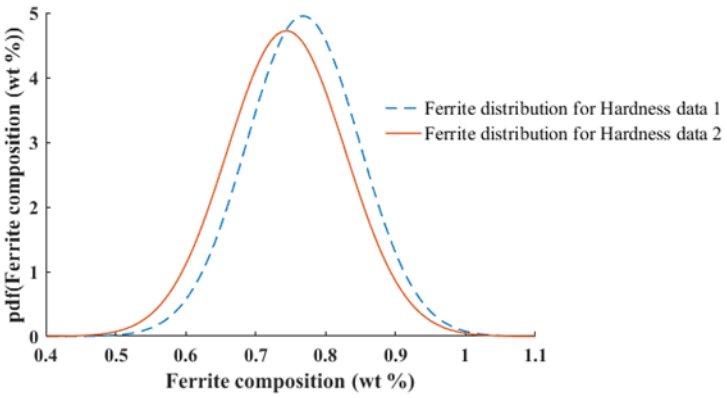

b)

Fig 10. Ilustration of nodes co-dependency a) Change in node HARDNESS followed by a change in node SILICON b) Change in the node HARDNESS followed by change in the node FERRITE

The extent of change in the posterior densities of the nodes may differ, as can be seen from the above figures. This codependency can be useful in in order to derive (predict) missing information about one or more nodes, in an event such information is hard to obtain experimentally.

2.3.5 Model Regression Coefficients Verification

The various relationship between Yield Strength and material properties listed in the equations (5) through (9) were obtained from literature for different pipe systems composed of similar microstructure. As presented in section 4.1, these system of equations combined together predict a value of yield strength that can vary from 1.34 % to 14.01 % from the actual value of yield strength derived experimentally. Therefore, in an integrated form, these relationships may not be a holistic representative of the behavior of a particular system in view. In order to improve the prediction from the present Bayesian Network model, more information in terms of both data points and new metrics would have to be added in the model. Another way to improve prediction would be to update the relationship between yield strength and material properties derived from literature. This can be done by training the individual relationships with data for a specific system of pipes and then using the updated model coefficients for prediction. In this manner, if a complete data set (including tensile properties) is available for pipeline systems in a specific area, it could be used for training the model coefficients and improving the prediction of connected pipeline systems in a different region where destructive testing may not be available. In the present study, the data from X65 steels, obtained from literature (Tovee 2014), is used for a demonstration of the same. Data training and validation is performed by training the model and obtaining updated values of the model regression coefficients, and are validated by comparing the predictions of the tensile properties from both the initial and the updated model. The procedure of this study is listed below:

This study is done for the correlation of Yield Strength to Hardness, Composition and Volume fraction of Ferrite.

Original relation from literature:

$$\sigma_{YS} = (53.9 + 32.34(X_{Mn}) + 83.2(X_{Si}) + 354.2(X_{Nf}) + 17.4(d^{-1/2}) + \sigma_{(f)}(V_f) + \sigma_{(p)}(1\text{-}V_f) + 2*H + 105)/3 \quad (11)$$

of the form $$YS = (a + b*X_{Mn} + c*X_{Si} + d*X_{Nf} + e*d^{-1/2} + f*V_f + g*H + \varepsilon)/3 \quad (12)$$

Where, $\varepsilon = N(0, \sigma^2)$, is a model error term.

In the general case, these coefficients based on the literature equation are reported as:

a = 158.9, b = 32.34,c = 83.2, d = 354.2, e = 17.4, f = , g = 2

Training of the model with the literature data for a system of X65 pipelines yielded the following results:

a =266.67, b= 28.46, c= 33.05, d= 162.33, e= 5, f= -8.67, g= 0.7

The two models were used to predict the yield strength for the other API X65 pipeline systems.

The comparative prediction with the updated coefficients for the likelihood model are listed and shown with the help of Figure 11.

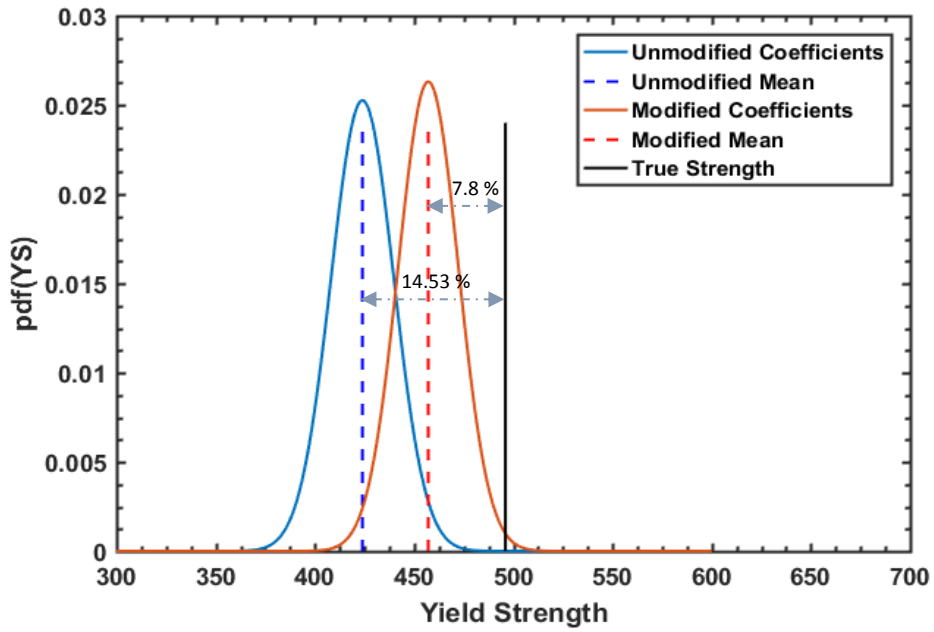

a)

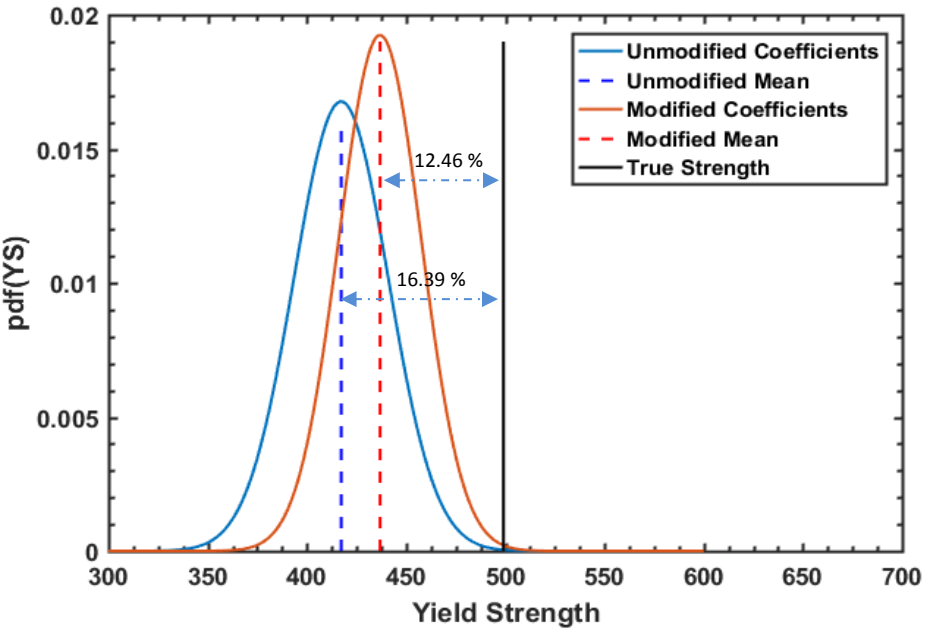

b)

Fig 11.1. Plot showing Yield Strength vs pdf values with the original and modified coefficients for the two samples a) Pipe X65 1 b) Pipe X65 2

Similar training was conducted for the pipe sample 47, as the complete data set was already available as presented before in experimental analysis section. The pipe 47 had four samples extracted from the thickness direction, as stated previously, the data points from two of which were used for training and the remaining two were used for prediction from the updated values of the coefficients. The modified coefficients were also used for prediction from Pipe 45. The original relation and the form remained the same as listed in eqn (7) and (8). The updated coefficients from the training of pipe 47 are listed below:

a =688.7, b= 83.8, c= 913.6, d= 859.4, e= 15.48, f= 72.2, g= 1.31

Fig. 10 c) shows the improved prediction from the updated coefficients.

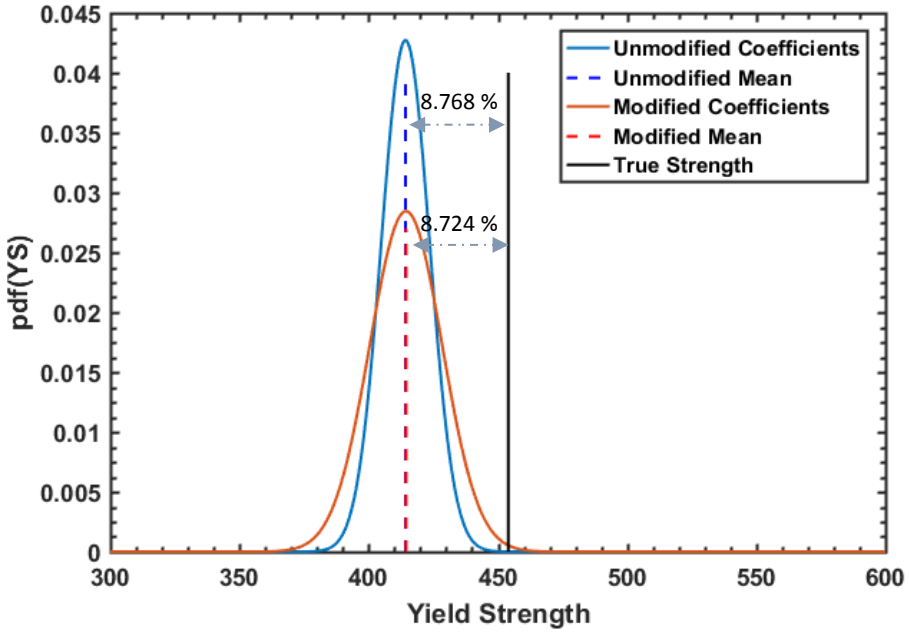

c)

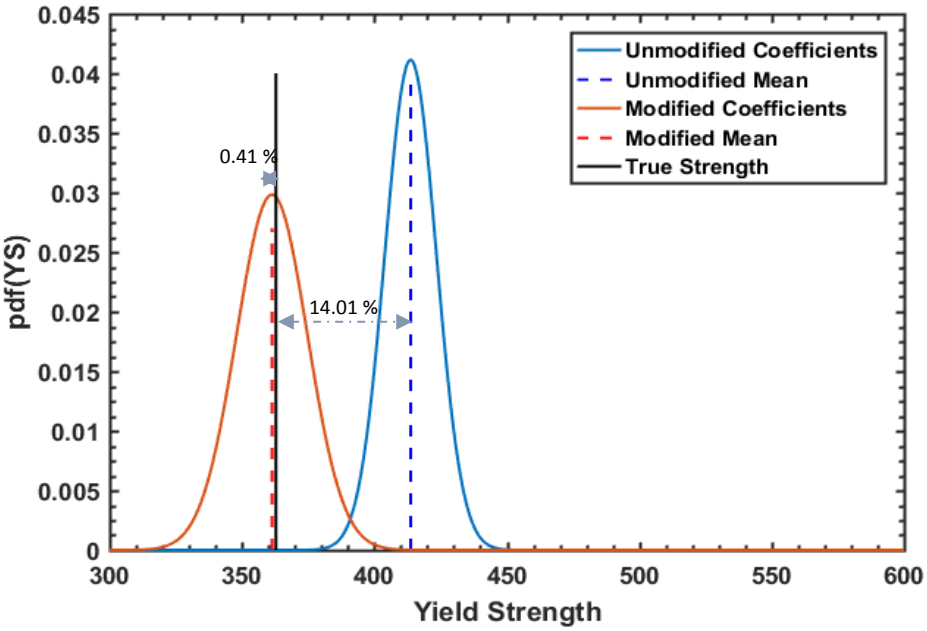

d)

Fig 11.2. Plot showing Yield Strength vs pdf values with the original and modified coefficients for the two samples c) Pipe 45 d) Pipe 47

It can be seen that in all the three cases the prediction from the updated likelihood model shows a prediction value closer to the theoretical strength, and hence data training of the model can help improve prediction. It was also tested to predict the strength of other systems such as X52, X60 etc, but it was observed that the training for a particular system of pipelines is restricted to improve the prediction of the similar systems, and specific training needs to be performed for the other grades of the pipeline systems to improve their prediction.

2.3.6 Node Sensitivity analysis

A parametric sensitivity analysis was carried out to determine the most influential factor governing the prediction of Yield Strength. Information on the nodes was varied by

+/- 30%, one at a time, and corresponding variation in the predicted results was noted. Two literature data (X65, X42) and two experimental data (Pipe 45 & 47) have been used for the demonstration of the same. The results are presented below:

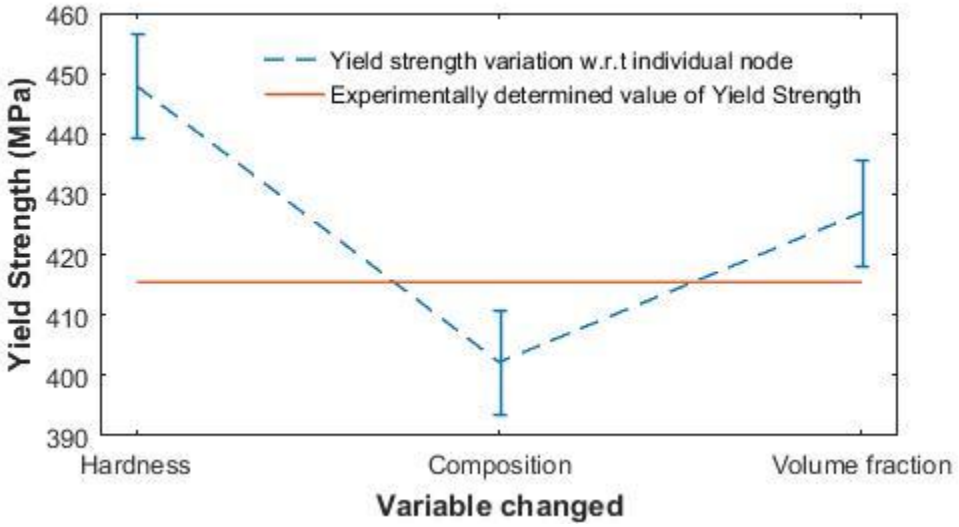

a)

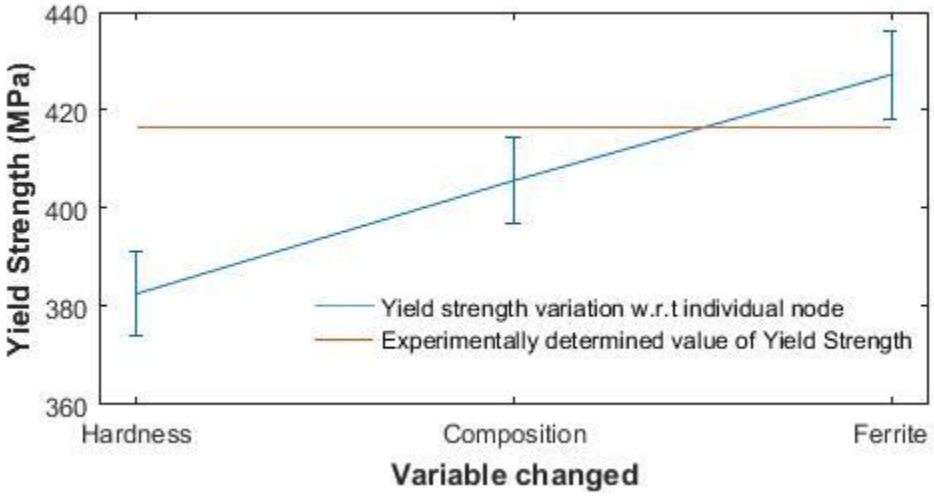

b)

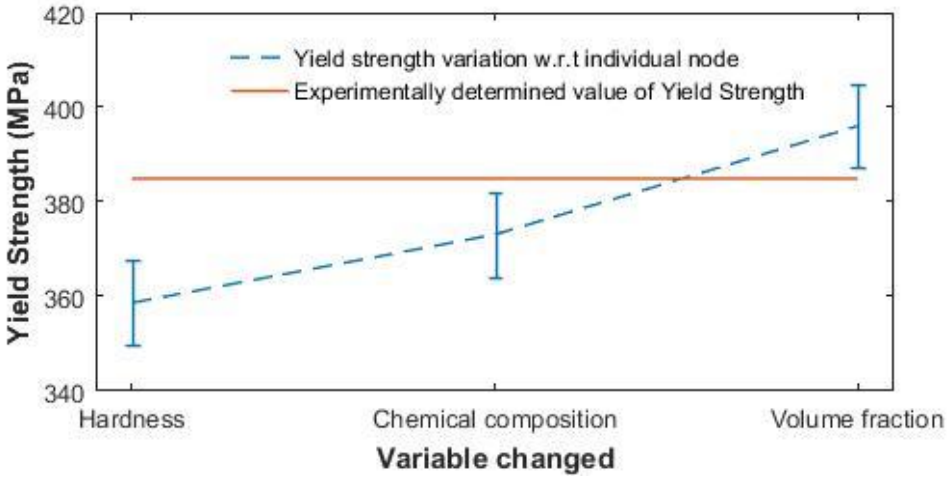
Yield strength variation w.r.t individual node
Experimentally determined value of Yield Strength
Yield Strength (MPa)
420
400
380
360
340
Hardness
Chemical composition
Volume fraction
Variable changed

c)

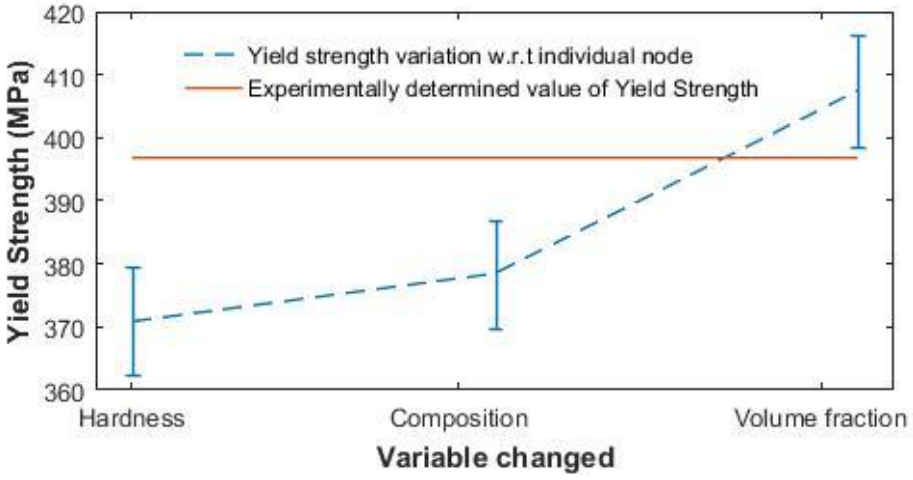
Yield strength variation w.r.t individual node
Experimentally determined value of Yield Strength
Yield Strength (MPa)
420
410
400
390
380
370
360
Hardness
Composition
Volume fraction
Variable changed

d)

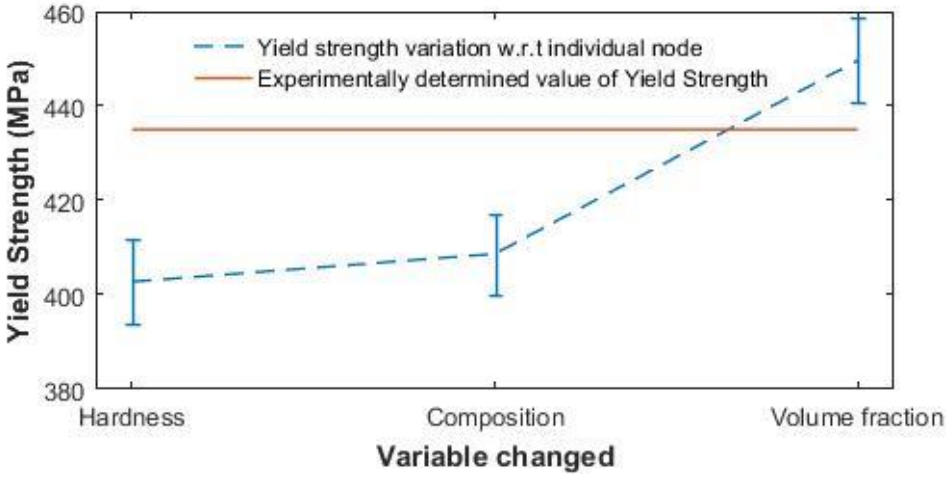
Yield strength variation w.r.t individual node
Experimentally determined value of Yield Strength
Yield Strength (MPa)
460
440
420
400
380
Hardness
Composition
Volume fraction
Variable changed

e)

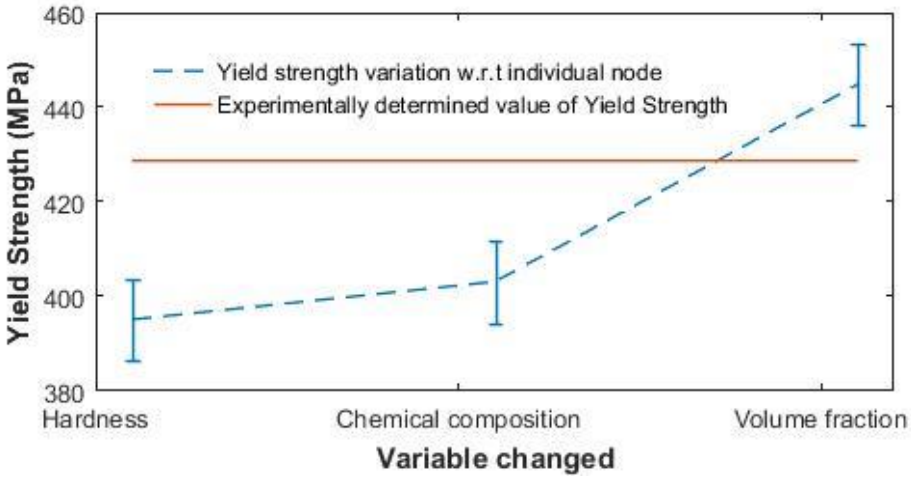

f)

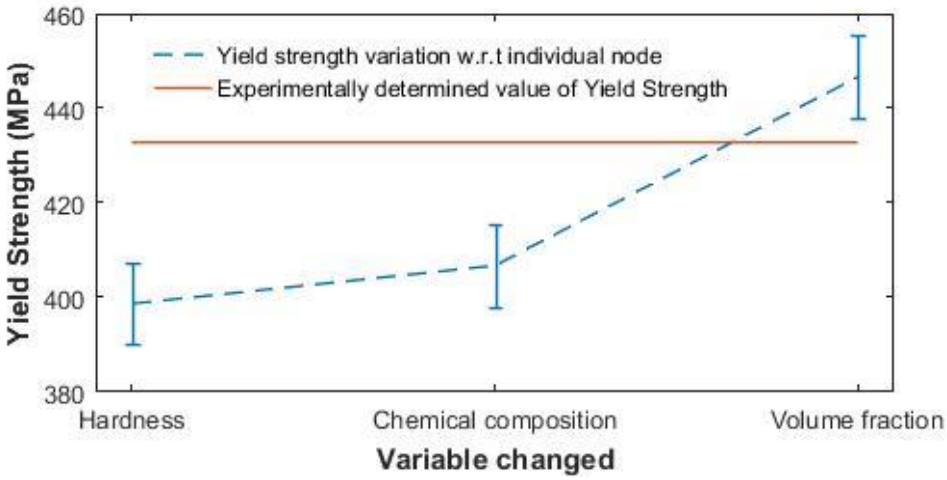

g)

Fig 12. Demonstration of variable change on the prediction capability of the different pipe systems a) X45 b) X47 c) X42R d) X42N e) X65I f) X65II g) X65III

As can be observed from Figure 12, hardness appears to be the most influential factor in prediction of Yield strength. The experimental Pipes 45 and 47 showed a variation close to 8% with hardness, and about 2.5% with both volume fraction and composition analysis. For the literature data of X42R and X42N, the change in the predicted yield

strength was about 3-4% with composition and volume fraction, and about 6.5% with Hardness. Finally with the system of X65 literature pipes, the variation in predicted yield strength was about 3% with volume fraction change, 6% with chemical composition change, and about 7.5% with Hardness change. The X65 was seen to be the only system with a high impact from the composition side. Overall hardness seemed to be the most influential parameter followed by composition and then volume fraction.

2.4 CONCLUSION

A novel approach to integrity assessment of the aging Natural gas pipeline system is proposed with the design of the Bayesian Network framework model, which integrates the different material properties derived from in-situ measurements and predicts the yield strength. The model is validated from the results of experimental measurements to show an improved accuracy of strength prediction. Several conclusions can be drawn based on the present study:

1. Model validation performed by comparing the results of yield strength prediction from individual nodes versus prediction from all nodes together, showed an improved prediction with the latter. Yield strength prediction with the individual node Hardness showed an 11.8-36.4 % variance from the true experimental value. Similarly, prediction with node Chemical composition showed a large deviance of 34-49.17%, prediction with node volume fraction showed a deviation of 27.34-49.14%, and finally, the combined prediction with all the nodes showed the smallest deviation of 1.34-14.8% from the true experimental value.

2. Another important feature extracted out of this model was the ability to update all the nodes by modifying one of the nodes (updating information on node Hardness resulted in a change in the probability distributions of nodes Silicon and Ferrite), signifying a systematic flow of information through the network. This feature can be exploited in terms of obtaining a probabilistic estimate for any missing component.

3. Next, the model was trained to modify the regression coefficients by making use of data points from the similar system and an improvement in the prediction capability of about 4-13% on an average was observed.

The present model is designed with an equal weightage of all nodes, which can be modified through extensive training with a large data set by performing sensitivity analysis to obtain a more precise prediction of the strength, or through numerical simulation approaches. The model can be further explored in terms of accommodating the acoustic and electromagnetic properties, to obtain a holistic prediction of strength from a complete set of material properties data.

3 COMPARATIVE STUDY OF STATISTICAL MODELS FOR MANUFACTURING PROPERTIES PREDICTION

3.1 INTRODUCTION

The increasing demand in the production and consumption of oil and natural gas requires continuous improvement in both the transportation efficiency and the performance of the steel pipes(Rosado, Waele, and Vanderschueren 2013). The properties at this expanse are higher strength accompanied with sufficient toughness and ductility which are determined by the proportion of multiple microstructures consisting of well-selected phases and refined grain sizes. For the currently used high-strength steels, the determining factors to achieve the above-listed superior properties relies in a combination of alloy composition design, metallurgical technology, thermomechanical processing or heat treatment(Zhao, Yang, and Shan 2002). These steels are characterized by the low Sulphur content and reduced amount of detrimental second phases such as oxides, inclusions and pearlite(Rosado, Waele, and Vanderschueren 2013). As the composition is limited to a certain value, the improvement in the mechanical properties heavily depends on the complex thermomechanical controlled processing (TMCP) routes. The optimization of the process parameters of the TMCP is vital in order to achieve the desired mechanical properties. Nowadays, exhaustive production control and diverse simulation techniques are used to optimize the processing parameters for producing a desired microstructure, both of which are extremely expensive and only achieve good results in an a posteriori fashion (Santos et al. 2009). A lot of work has been reported on analyzing the effect of the TMCP processing parameters on the microstructure and mechanical properties such as the

evolution of microstructure and precipitation state of high- level pipeline steel through TMCP process, in which the effects of processing parameters of TMCP, such as finish cooling temperature (FCT), finish rolling temperature (FRT) and coiling temperature on the microstructure and mechanical properties of low C-Mn steel were reported (Rosado, Waele, and Vanderschueren 2013).

Thus, the manufacturing process parameters play an important role in the design and synthesis of new pipe grades with improved mechanical properties. In order to simplify the extensive need of process control and simulation techniques, the present work aims to utilize the pre-existing database of the effect of manufacturing process on the material properties to make a prediction of the required process parameters to obtain the desired microstructure design. Some well-known statistical models are employed for making such predictions and compared amongst themselves viz; Multivariate Linear Regression, Gaussian Process Modeling and multi-label K-nearest neighbors (ML-KNN) model and the efficiency of these models is compared. The input for these models can be the mechanical properties such as yield strength, fracture toughness required, whereas, the output will be process parameters such as cooling rate and coiling temperature. The classical linear regression is performed for multiple datasets using the generalized least square method, by minimizing the sum of squared error. The Gaussian process models are another way to perform Bayesian supervised learning. These are provided with a mean function, covariance function, and some hyperparameters for their prediction model. The final method is specifically known as ML-KNN or multi-label K-nearest neighbor, which is an extension of the traditional KNN method. This algorithm identifies k-nearest

neighbors from the training data, based on the proximity of closeness from the given unknown samples.

3.2 MODEL FOR PREDICTION OF PROCESSING CONDITIONS

The focus of this section is on the application of the different statistical models to predict the process conditions during pipeline manufacturing process such as cooling rate, cooling temperature etc. The input can be used as the desired mechanical properties such as Yield Strength, percentage elongation etc. Table 6 shows the input and the desired output [11].

Table 6. Process parameters and mechanical properties for steel pipes

Labels				Features	
Rolling finish Temp (deg C)	Cooling start Temp (deg C)	Cooling End Temp (deg C)	Cooling rate (deg C/sec)	Elongation (%)	Yield Strength (MPa)
845	795	100	16	22	516
845	795	200	19	28	523
845	795	430	9.4	26	525
735	700	240	14.5	21	533
735	700	330	11	28	489
735	700	420	9.3	22	561

The prediction scheme used here are of three different types; Classical Linear Regression, Gaussian process model (Kocijan et al. 2004), and Multi-Label K-nearest neighbor method. The classical linear regression (Yamano, n.d.) is performed for multiple datasets using the generalized least square method, by minimizing the sum of squared error. The Gaussian process models are another way to perform Bayesian supervised learning (Kocijan et al. 2004) (Kocijan et al. 2004). These are essentially composed of mean

function, covariance function, and some hyperparameters for their prediction model. The most widely used functions in here are the meanConst mean function which has a constant mean that can be specified with a single value hyperparameter, and a covSEiso which is a Squared Exponental covariance function. It has been used for regression based problems as well(Qu Nonero-Candela et al. 2005)(Büche, Schraudolph, and Koumoutsakos 2005).

The final method is specifically known as ML-KNN or multi-label K-nearest neighbor(Zhang and Zhou 2007) (Cheng and Hüllermeier 2009), which is an extension of the traditional KNN method. This algorithm identifies k-nearest neighbors from the training data, based on the proximity of closeness from the given unknown samples. Given an unknown sample and a training set, all the distances between the unknown sample and all the samples in the training set can be computed. The distance with the smallest value corresponds to the sample in the training set closest to the unknown sample. Different types of distances can be used, Euclidean distance being most widely used. Given a training set (x1,y1) (x2,y2)….the regression model can be built.

The Euclidean distance,D is given as:

$$D(x,p) = \sqrt{(x-p)^2}$$

Where, p is the unknown test instance.

The prediction from the KNN model is the average of the outcome of the k-nearest neighbors:

$y = \frac{1}{K}\sum_i^k y_i$, where yi is the ith case of the examples sample and y is the prediction (outcome) of the query point (Imandoust and Bolandraftar 2013).

3.3 PREDICTION FROM THE DIFFERENT MODELS

Three small and different datasets were used for demonstration of prediction of the manufacturing conditions from the desired mechanical properties, and have been compared. At least 60% of the data was used for training and 40% used for prediction analysis for each dataset. For these comparison, Simple Linear regression follows the general scheme, the Gaussian process model uses meanConst as the mean function and covSEiso as the covariance function, and finally, the ML-KNN method uses the nearest neighbors value for k as 3, and a smoothing parameter, s as 1.

The results have been shown for the first dataset in Figure 13. This is a small dataset with 12 data points, 7 of which are used for training, and the remaining 5 are used for prediction:

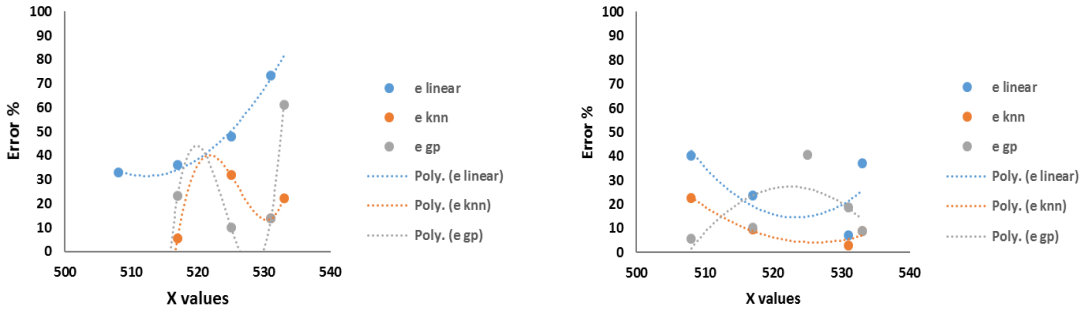

a) b)

Fig13. Plots for prediction of manufacturing process parameters for Dataset 1 a) Finish cooling temperature b) Cooling rate

It is observed that the prediction capability of Gaussian process model and ML-KNN work better than classical linear regression for this particular dataset. Some anomalies have been extracted to provide a better view of the model outcomes. This dataset

outcome shows a relatively large error for the best prediction model to be within 40% at some places which needs to be investigated.

Dataset 2:

This dataset consists of 15 points in total, 8 of which have been used for training, and the remaining 7 have been used for prediction. There are a total of four outcomes for this particular dataset, as shown in Figure 14.

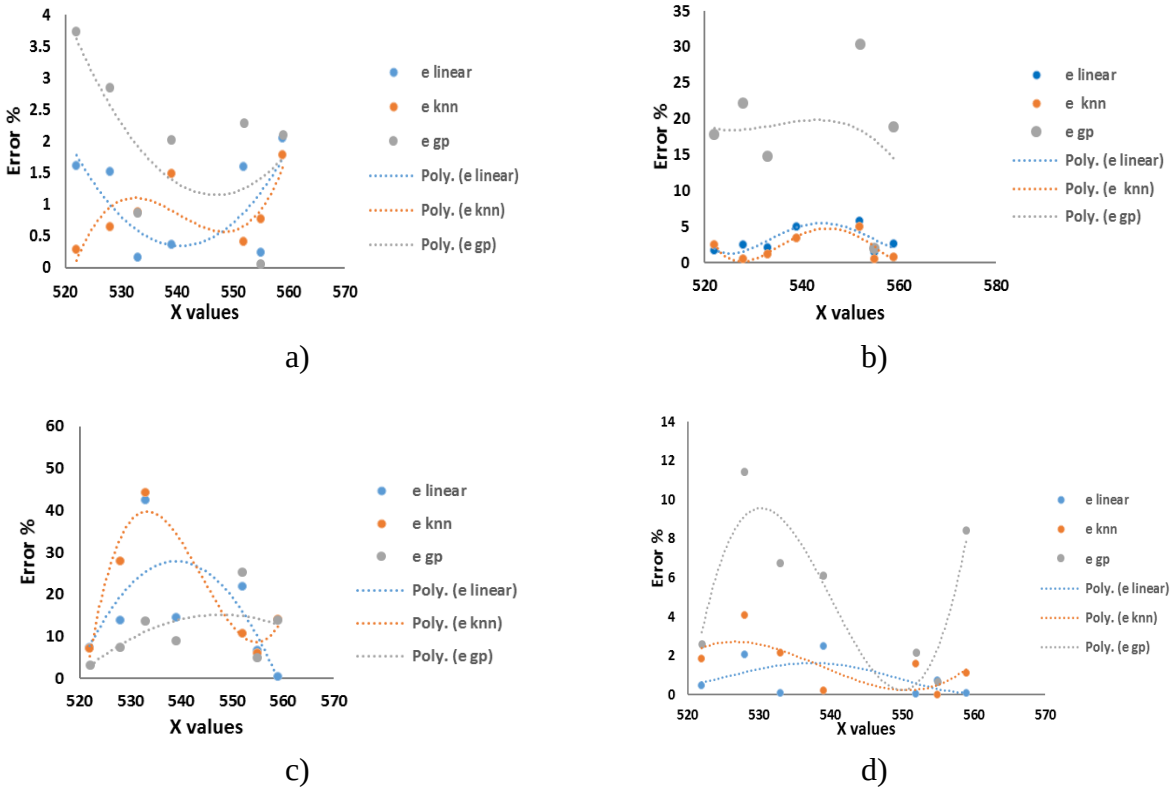

Fig 14. Plot for prediction of manufacturing process parameters for Dataset 2 a) Start Rolling Temperature b) Finish Rolling Temperature c) Cooling Rate d) Finish Cooling Temperature

It can be seen that for three of the four outcomes, the ML-KNN works either equally best or better than the classical regression (SL) model or the gaussian process (GP) model. The exception in the prediction of cooling rate may be as the data set were not normalized initially; where GP model works the best. In general, for this dataset, the error value can be kept below 15%, which is a helpful aid in the prediction of these manufacturing conditions.

Data set 3:

This is a small dataset with only 8 datapoints in total,therefore, 5 points have been used for training, and the prediction outcome is shown in Figure 15. The prediction is shown for 3 points initially, and the other graph shows the prediction for training data size 4 as well.

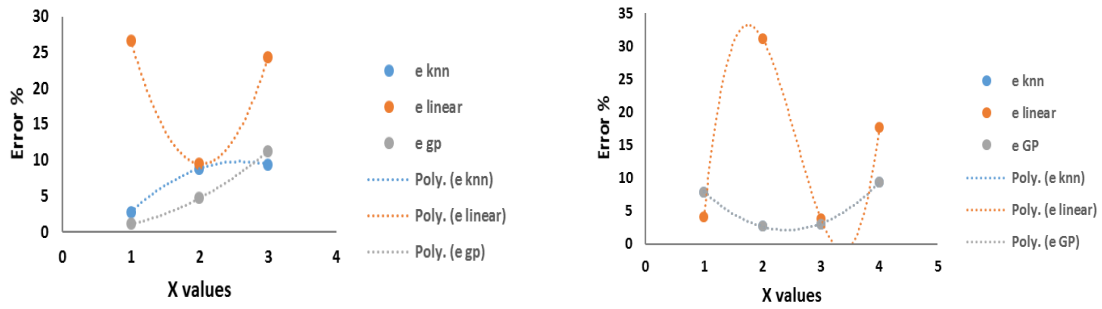

a) b)

Fig 15. Plot for prediction of Finish Rolling Temperature with two different training sizes

a) Training data size 5 b) Training data size 4

Similar to the above assessments, it can also be observed in this case that the ML-KNN and GP model work well for both training size of the data, although in this case GP

works slightly better or comparable to ML-KNN. The error for this dataset can be within 10% margin which also works well for prediction.

It can be seen from all the three datasets that these methods provide a good capability in the prediction of the manufacturing conditions for the desired mechanical properties. For the last two datasets, with the best prediction model, the error value can be controlled to be less than 10-15% at the maximum. In general ML-KNN works well for the three datasets.

3.4 MODEL PARAMETER VARIATION FOR THE DIFFERENT DATASETS

The parameters of the ML-KNN and the GP model have been varied, and the effect on the prediction has been reported.

The results in Figure 16 are for Dataset 1 for variation of k in ML-KNN method

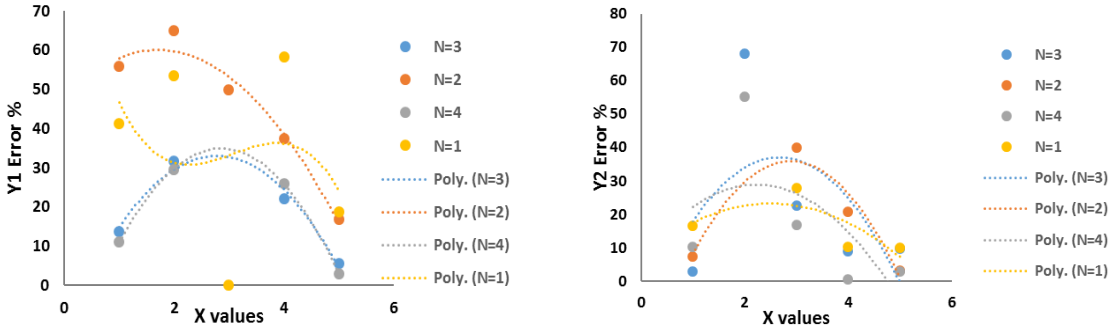

a) b)

Fig 16. Plots showing impact of N on prediction outcomes for dataset 1 a) Finish cooling temperature b) Cooling rate

The above figures represent the impact of the variation of the number of nearest neighbors, N in the prediction outcome. It appears that N value of 3, 4 work well for Y1 prediction, whereas N values of 1 & 4 work well for Y2.

Next, the results are shown in Figure 17 for Dataset 1 for GP model parameter variation.

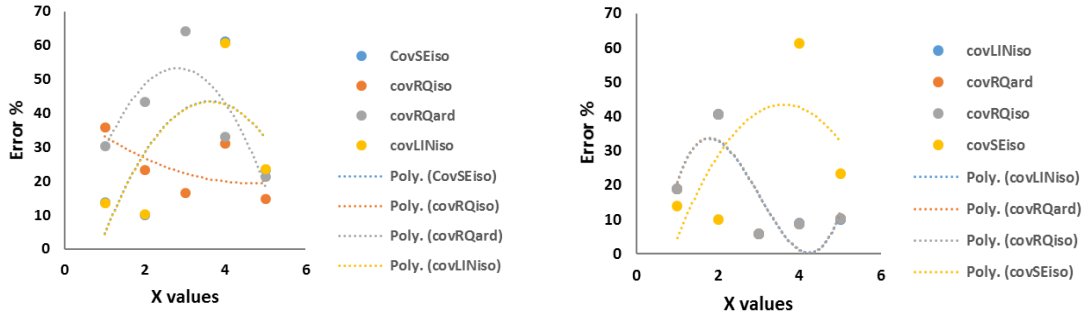

a) b)

Fig 17. Plots showing impact of variation in the covariance function on the prediction outcome for Dataset 1 a) Finish cooling Temperature prediction b) cooling rate prediction

The variation in the covariance function in Figure 18 shows that covRQiso works well for Y1, and most of the other covariance functions work well for Y2.

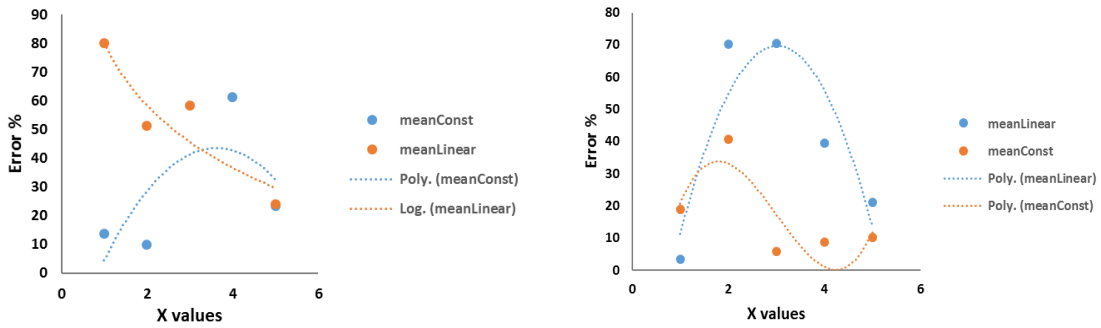

a) b)

Fig 18. Plot showing impact of mean function variation on the prediction outcome of Dataset 1 a) Finish cooling Temperature b) Cooling rate

The mean function variation shows opposite trends for both Y1 and Y2 and hence no conclusion could be drawn for better mean function.

The next results are shown for Data set 2. Figure 19 shows the ML-KNN parameter variation.

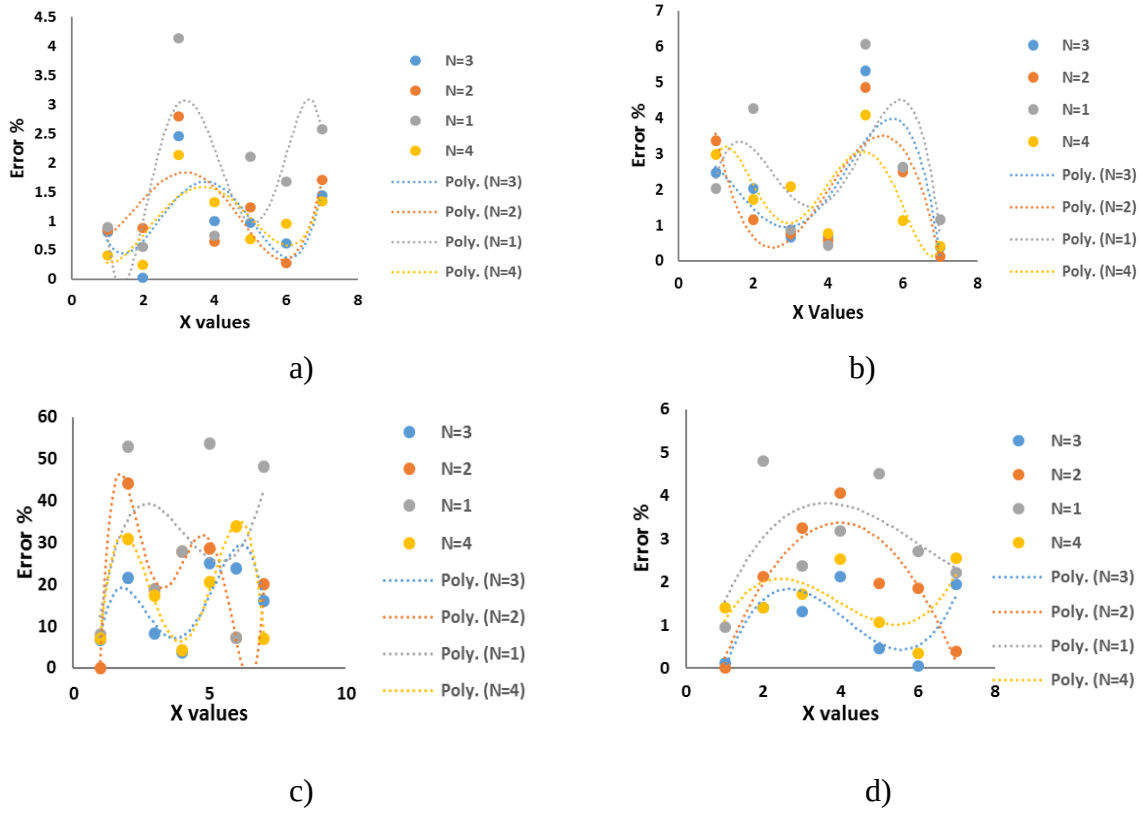

Fig 19. Plots showing impact of N on prediction outcomes for dataset 2 a) Start Rolling Temperature b) Finish Rolling Temperature c) Cooling Rate d) Finish Cooling Temperature

The N value was varied between 1 to 4. It appears that a N value of 3 and 4 works well for all the predictive outcomes.

Next, the smoothing parameter, s, was varied between 1 to 10, and no significant change was observed, as indicarted below in Table 7.

Table 7. Smoothing parameter variation for different data sets

N=3								
Y1	-0.8123	-0.0307	-2.458	0.9932	0.975	0.6184	1.4386	
Y2	-2.4664	2.0377	-0.6608	0.6696	-5.3289	2.6166	-0.3867	
Y3	6.6667	21.5686	8.3333	-3.7037	-25	23.8095	-16	
Y4	0.1287	-1.4103	1.3123	2.1164	-0.4575	-0.0647	1.9411	S=1
Y1	-0.8123	-0.0307	-2.458	0.9932	0.975	0.6184	1.4386	
Y2	-2.4664	2.0377	-0.6608	0.6696	-5.3289	2.6166	-0.3867	
Y3	6.6667	21.5686	8.3333	-3.7037	-25	23.8095	-16	
Y4	0.1287	-1.4103	1.3123	2.1164	-0.4575	-0.0647	1.9411	S=2
Y1	-0.8123	-0.0307	-2.458	0.9932	0.975	0.6184	1.4386	
Y2	-2.4664	2.0377	-0.6608	0.6696	-5.3289	2.6166	-0.3867	
Y3	6.6667	21.5686	8.3333	-3.7037	-25	23.8095	-16	
Y4	0.1287	-1.4103	1.3123	2.1164	-0.4575	-0.0647	1.9411	S=3
Y1	-0.8123	-0.0307	-2.458	0.9932	0.975	0.6184	1.4386	
Y2	-2.4664	2.0377	-0.6608	0.6696	-5.3289	2.6166	-0.3867	
Y3	6.6667	21.5686	8.3333	-3.7037	-25	23.8095	-16	
Y4	0.1287	-1.4103	1.3123	2.1164	-0.4575	-0.0647	1.9411	S=4
Y1	-0.8123	-0.0307	-2.458	0.9932	0.975	0.6184	1.4386	
Y2	-2.4664	2.0377	-0.6608	0.6696	-5.3289	2.6166	-0.3867	
Y3	6.6667	21.5686	8.3333	-3.7037	-25	23.8095	-16	
Y4	0.1287	-1.4103	1.3123	2.1164	-0.4575	-0.0647	1.9411	S=5
Y1	-0.8123	-0.0307	-2.458	0.9932	0.975	0.6184	1.4386	
Y2	-2.4664	2.0377	-0.6608	0.6696	-5.3289	2.6166	-0.3867	
Y3	6.6667	21.5686	8.3333	-3.7037	-25	23.8095	-16	
Y4	0.1287	-1.4103	1.3123	2.1164	-0.4575	-0.0647	1.9411	S=10

GP model parameter variation:

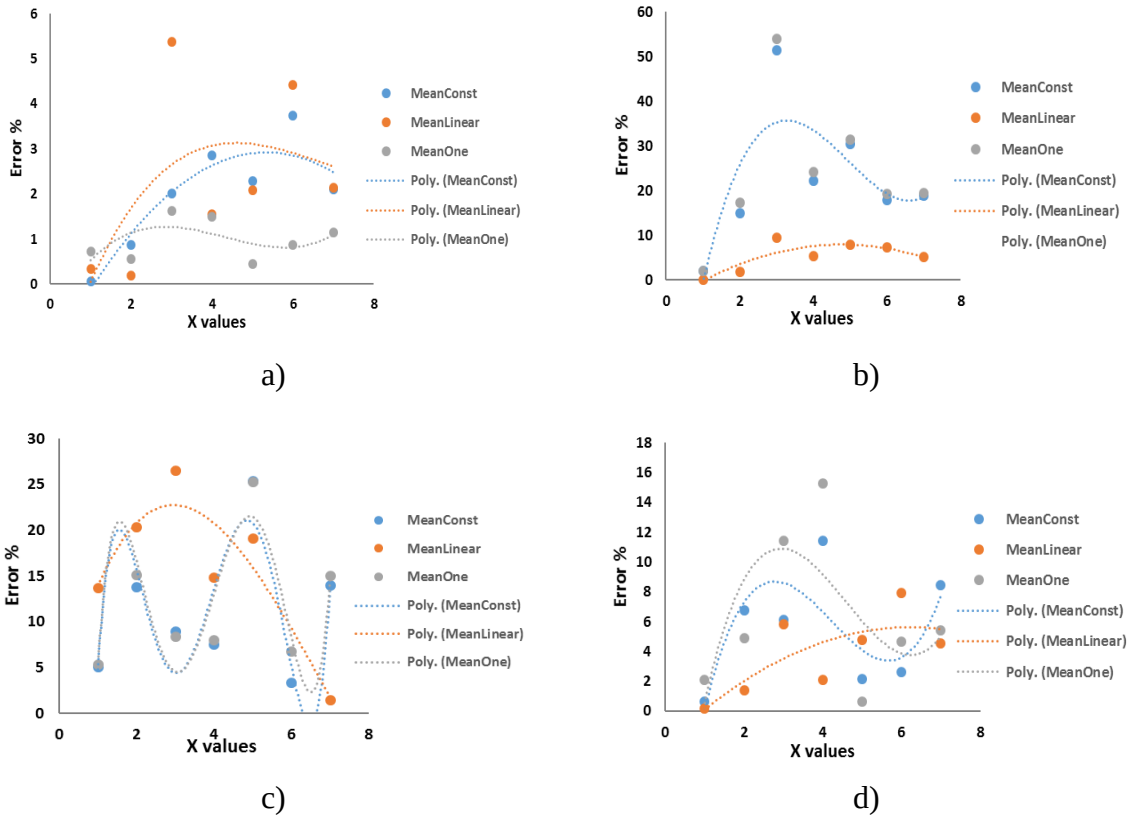

Fig 20. Plot showing the variation of mean function, and its impact on the prediction outcome of Dataset 2 a) Start Rolling Temperature b) Finish Rolling Temperature c) Cooling Rate d) Finish Cooling Temperature

It appears from Figure 20 that MeanLinear and Meanconstant both work well for most of the predictive outcomes for this data set for the mean function variation.

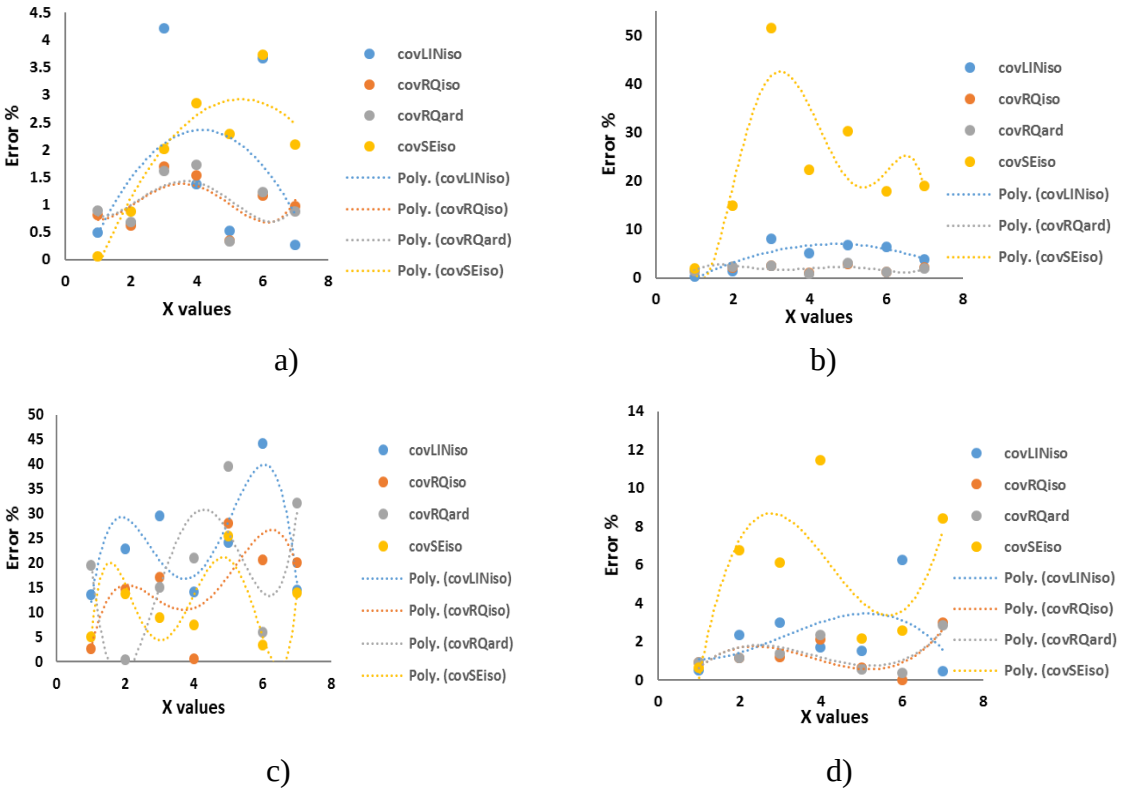

Fig 21. Plots showing impact of variation in the covariance function on the prediction outcome for Dataset 2 a) Start Rolling Temperature b) Finish Rolling Temperature c) Cooling Rate d) Finish Cooling Temperature

It can be seen from Figure 21 that for the covariance function variation, covRQard and covRQiso work well for atleast three out of four prediction outcomes.

Predictions for Dataset 3:

ML-KNN parameter variation:

The number of nearest neighbor was varied from 1 to 3 for this dataset. There is only a single outcome for this dataset as indicated earlier.

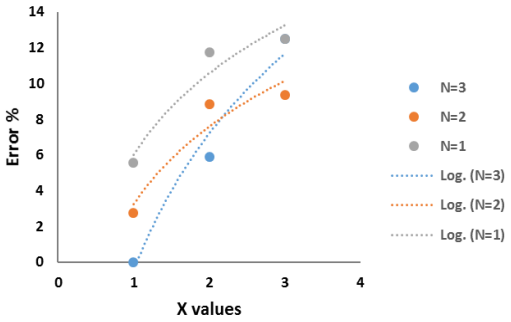

Fig 22. Plots showing impact of N on the prediction of Finish Rolling Temperature

It appears from Figure 22 that k value of 2 works best to keep the error below 10% for this particular dataset.

GP model parameter variation:

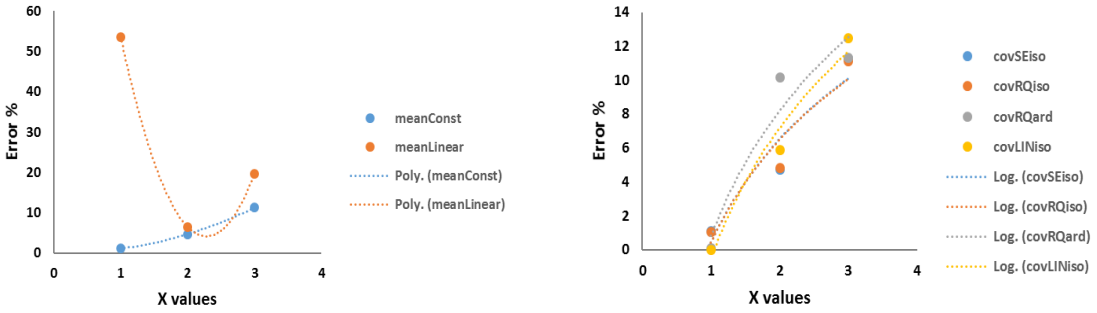

Fig 23. Impact of parameter variation on prediction of Finish rolling temperature a) Mean function variation b) Convariance function variation

It can be observed from Figure 23 that meanConst works well for meanfunction and covRQiso covariance function works well for this particular dataset to keep the error value to be about 10%.

It can be inferred from the above results that the value of number of nearest neighbor depends on the number of points in the dataset, and in general a value of N=3 would work for smaller datasets upto 15-20 points.

Also, the covariance function covRQiso works well for similar smaller datasets, whereas meanConst mean function works well for the model parameters of Gaussian process.

The indiscrepency in the prediction of cooling rate (Y3) can be noted for majority of the cases. This can be attributed to cooling rate being dependent of a number of variables such as the metallurgical phase transformation temperature, the resultant phases and the fraction of the phases.

3.5 CONCLUSION

In this work, different statistical models were employed to aid in the prediction of manufacturing process parameters to provide simplicity and cost-saving advantages to the complex methods that are currently in use and the impact of the parameter variation was studied for each model and dataset. Three different small datasets of varying length were used for demonstration. The following conclusions were drawn:

1. The model comparison for the three datasets indicated that GP and ML-KNN better than classical multivariate regression since the former can pick up the local instance based variation in the data, compared to latter that is not designed for very small datasets. In general, it was seen that ML-KNN works well

2. The individual datasets appeared to show a mixed model preference for prediction, and in general, ML-KNN seemed to be suitable.

3. The performance of KNN model depends on the number of nearest neighbors which in turn depends on the number of points in the dataset. A value of N=3 seemed to work for smaller datasets up to 15-20 points, whereas variation in the smoothing parameter didn't seem to affect the prediction outcome.

4. For the Gaussian process model, the covariance function covRQiso appears to work better for such smaller datasets, whereas mean function that works well for the same is meanConst.

The present study can be explored in terms of other datasets to obtain a more accurate measure of the generic model for best prediction. Some analysis can also be done to analyze the impact of the size of training data on the prediction outcome by adapting somewhat larger datasets up to 30-40 data points. A model selection procedure can also be explored to automatically ascertain the best prediction model for the datasets.

4 INVESTIGATION OF VARIATION IN THE FATIGUE BEHAVIOR OF THE STEELS THROUGH THE THICKNESS OF THE PIPE SAMPLE

4.1 INTRODUCTION

The pipelines used in the oil and gas exploration suffer from significant fatigue damage from cyclic loadings during transportation (transit fatigue) and during service life. The fatigue damage in the pipe may occur even before they enter in service due a mechanism called transit fatigue. During transportation, pipes are subjected cyclic stresses, related to inertial and gravitational forces which are responsible for the nucleation and growth of fatigue cracks inside them, which compromise their structural integrity. The offshore line pipes may also suffer from fatigue damage during their service life due to the structures being subjected to cyclic loading originated from: cyclic pressure and thermal expansion loads and waves movement induced loads. Another way to have fatigue failures is in the pipelines used to transport hydrogen, especially at lower frequencies(Korsunsky, Dini, and Walsh 2008). The resulting hydrogen embrittlement results in a loss of ductility and therefore the ASME codes impose the use of pipe with specified minimum yield strengths less than 360 MPa (52 ksi) for the transportation of hydrogen. This leaves steels with an API grade of X52 or lower for the same purpose, which are the steel grades associated with the present research work(Drexler and Amaro 2017). The existing NDE techniques of fatigue damage detection may be limited by the pipe geometries as stated earlier, therefore is important to quantify the fatigue crack growth properties by taking into account the inhomogeneity in the material properties across different region of the pipe. The research works therefore aims to investigate how the fatigue growth rates of cracks vary in the circumferential direction along the pipe wall thickness(Lu and Liu 2009). The

specimens are drawn from different depths and growth rates has been done through the analysis of da/dN x ΔK curves, focusing on their Region II (Figure 24.1) where the cyclic growth of the fatigue crack is linear (on a log-log plot) and can be predicted by the Paris-Erdogan Law (Korsunsky, Dini, and Walsh 2008):

$$\frac{da}{dN} = C\Delta K^m \tag{13}$$

where da/dN is the fatigue crack growth rate, C and m are scaling constants and ΔK is the stress intensity factor range. The Paris-Erdogan Law only considers the ΔK increasing for the fatigue crack growth rate evaluation, and ignores the effect of the other parameters such as the load ratio and load frequency which also may impact the values of C and m (Kim et al. 2011). Therefore, for a given material, the evaluation of crack growth rates are to be done when the environmental conditions, temperature as well the load ratio and frequency are fixed, to reduce the influence on C and m.

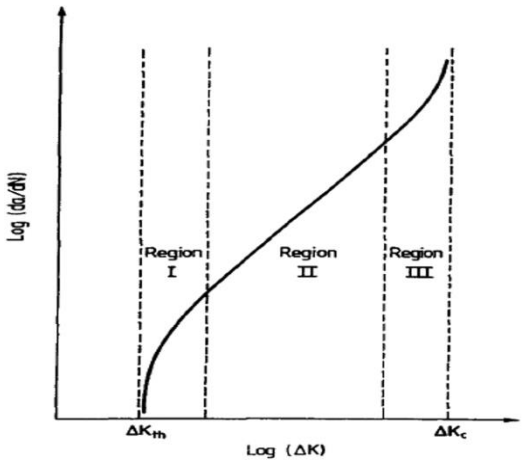

Fig 24.1. Typical fatigue crack growth curve for metals showing its Regions I, II and III(Korsunsky, Dini, and Walsh 2008)

4.2 TEST SET UP FOR FATIGUE PROPERTY ANALYSIS

The fatigue behavior of five pipe steels have been analyzed here. The experimental investigation of fatigue behavior was conducted in the Servo-hydraulic MTS machine. A single edge notch specimen SE(T) (Blatt, John, and Coker 1994) was used for the study, a schematic of the SE(T) geometry is shown in Figure 24.2. The experiment was conducted at room temperature with a pre-crack, and the load levels varied from 1000~1700N depending on the strength of the different pipes. An interrupted testing was conducted to enable the observation of crack growth with respect to the cycles. The R-ratio used was 0.1, and the frequency was 10 Hz.

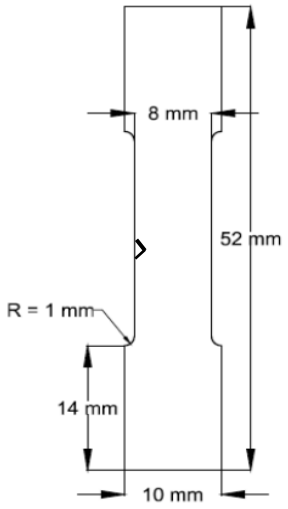

Fig 24.2. Dimension of fatigue test specimen with notch

The notch is sharpened further prior to the experiment to ease in crack initiation. The samples are extracted from different region along the pipe to capture the variation in the fatigue crack growth parameters along the thickness. The fatigue property analysis includes studying the crack growth rate of the specimen with respect to the number of cycles, and are not tested till complete failure. The images for the crack initiation are presented here:

4.3 CRACK GROWTH BEHAVIOR OF THE PIPE STEEL

The crack growth is assessed in terms of Number of cycles and crack length. The results are shown below for the five pipe specimen. Figure 25 shows the da/dN curves for Pipe 47.

Pipe 47:

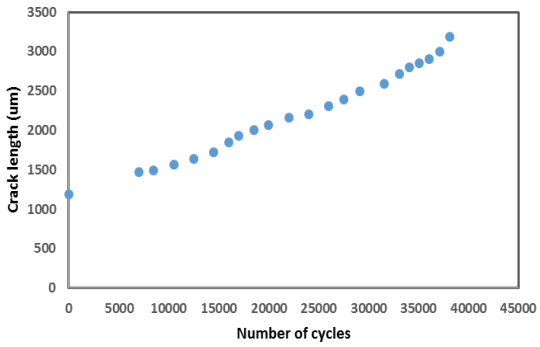

a)

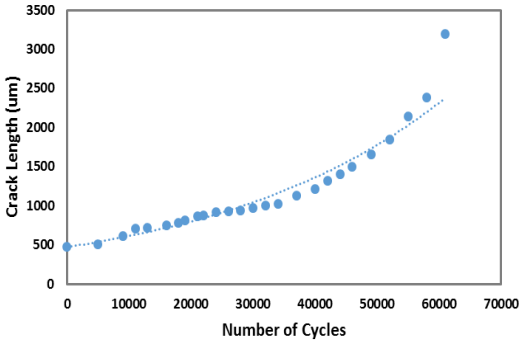

b)

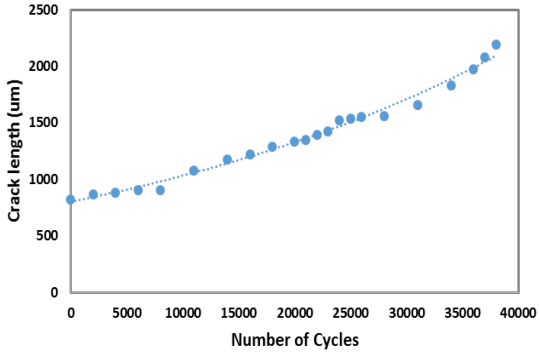

c)

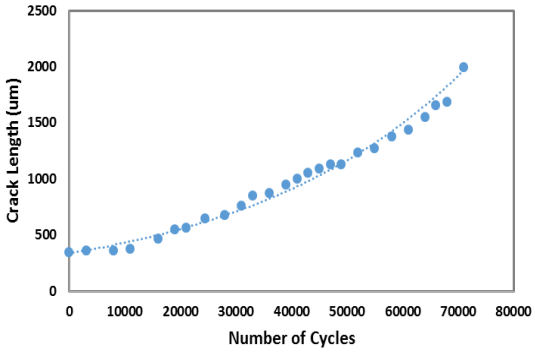

d)

Fig 25. Fatigue crack growth, da/dN curves for Pipe 47 along the depth; a) Outer surface b) Middle region-1 c) Middle region-2 d) Inner surface

The crack growth for the pipe samples showed slight variation with thickness but generally appeared to increase steadily with respect to the number of cycles across all the regions. The grain structure of the samples are presented next.

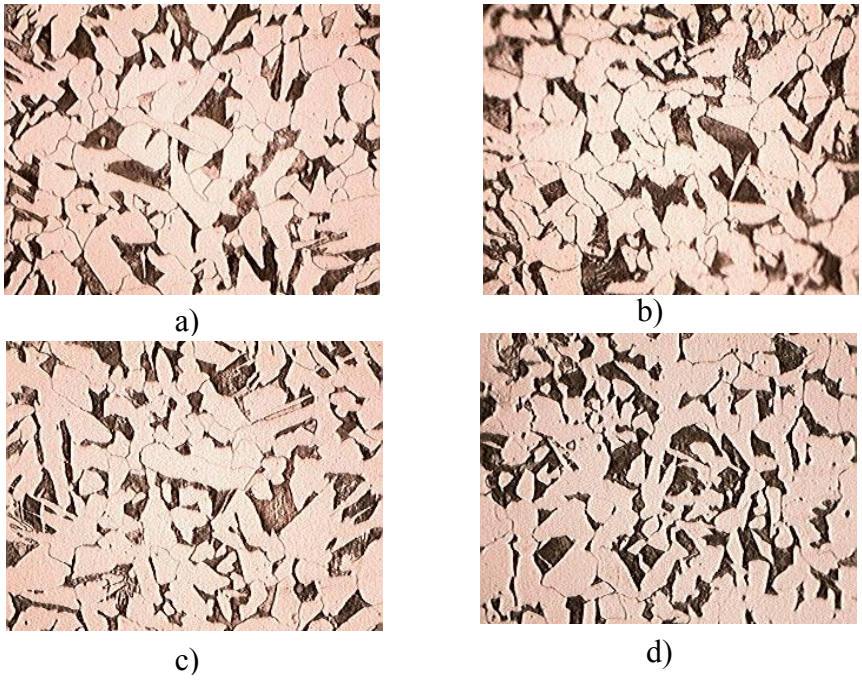

Fig 26. Grain structure after deformation of Pipe 47 a) Outer region 1 b) Middle region-2 c) Inner region-1 d) Inner region-2

The microstructure images depicted in Figure 26 are taken from 100 um radius around the crack. The grain structure appear deformed near the crack zone, and the average grain size for the deformed specimen was found to be 21.77 um, which is about 3 ASTM grain sizes lesser than the undeformed specimen with a grain size of 24.36 um.

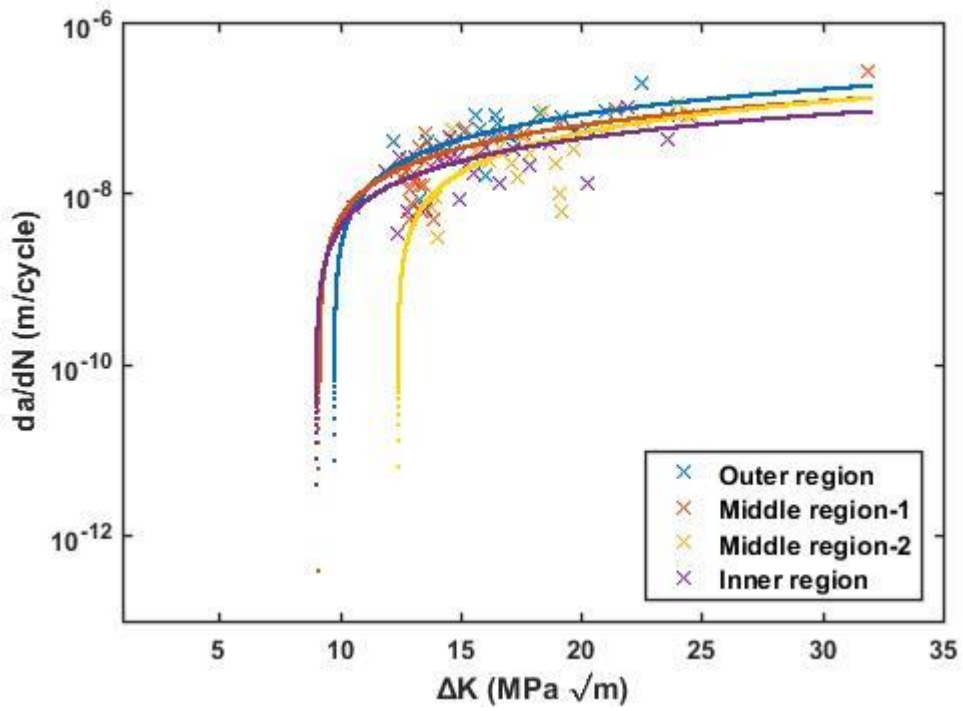

Fig 27. Fatigue crack growth rate versus stress intensity factor range (da/dN versus ΔK) for four different specimens corresponding to the different regions along the pipe thickness for Pipe 47

The da/dN vs ΔK curve for the pipe 47 is depicted in Figure 27. It appears that the curve shifts a little for the top and bottom regions, however, the middle regions tend to somewhat overlap.

In order to investigate the pattern of crack growth (intergranular or transgrannular), etching was done on the sample and the crack was viewed under SEM. The images in Figure 28 show the crack growth pattern for Pipe 47.

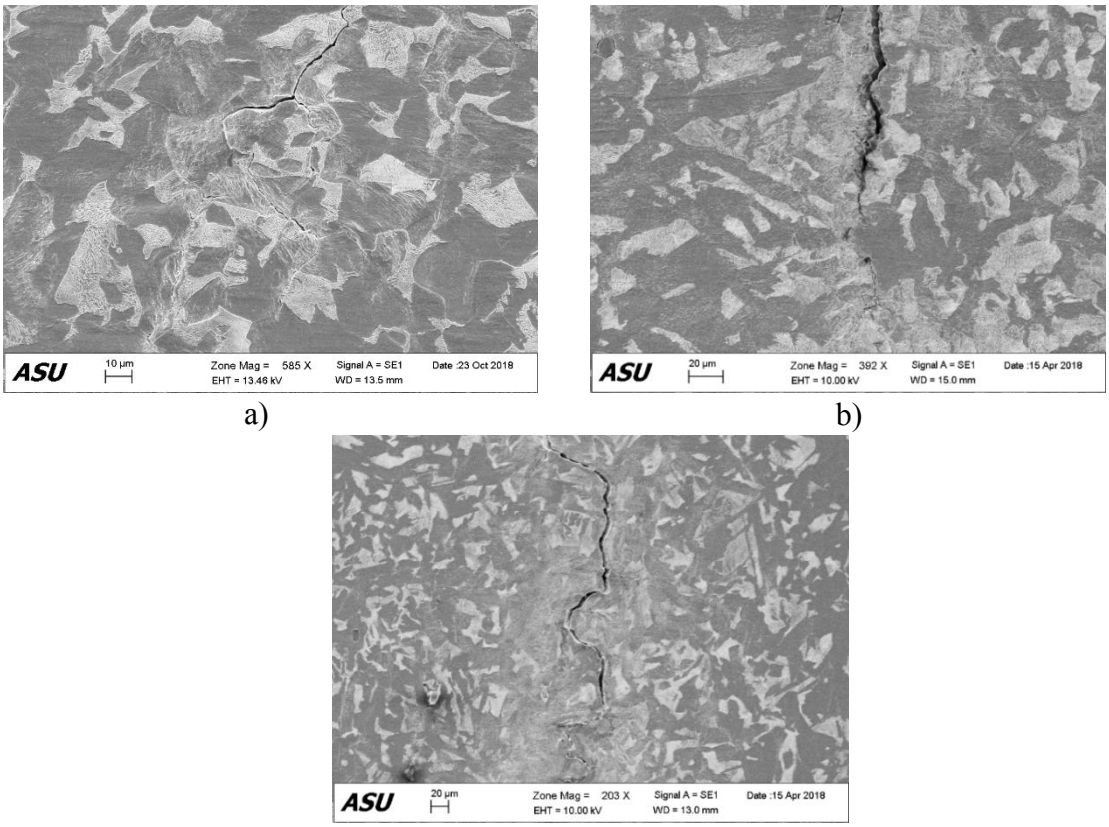

a) b)

c)

Fig 28. Crack growth pattern of Pipe 47 a) Outer region 1 b) Middle region-2 c) Inner region

It can be observed that the crack cuts directly through the phase boundaries of the pearlite zone and in general is seen to follow a transgrannular pattern.

Pipe 44:

The crack growth curves for Pipe 44 are:

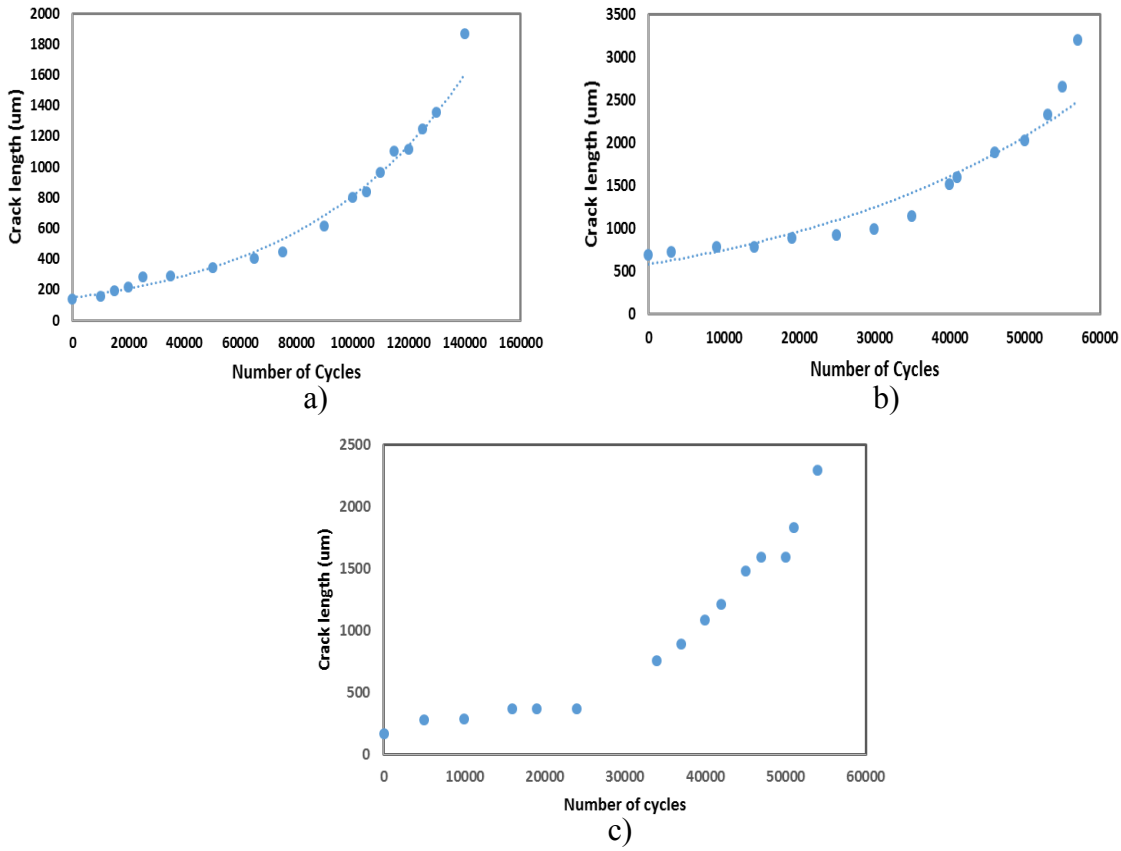

Fig 29. Fatigue crack growth, da/dN curves for Pipe 44 along the depth; a) Outer surface b) Middle region c) Inner surface

The crack growth for the pipe samples appeared steady with respect to the number of cycles across all the regions, as per Figure 29.

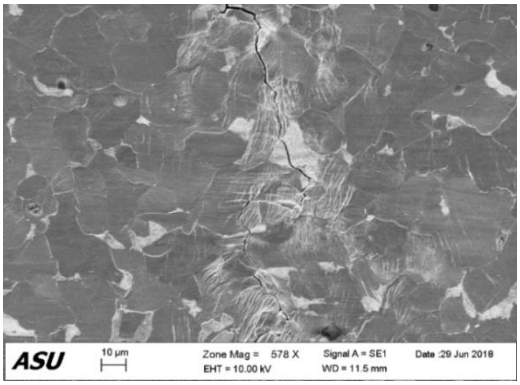

a)

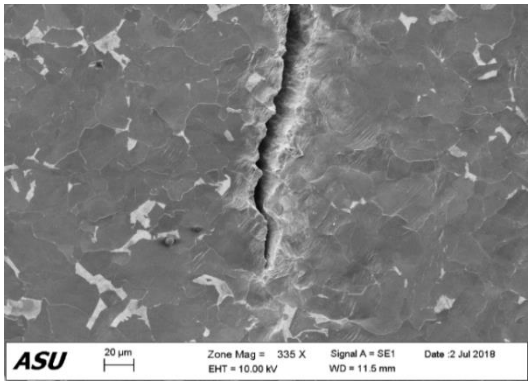

b)

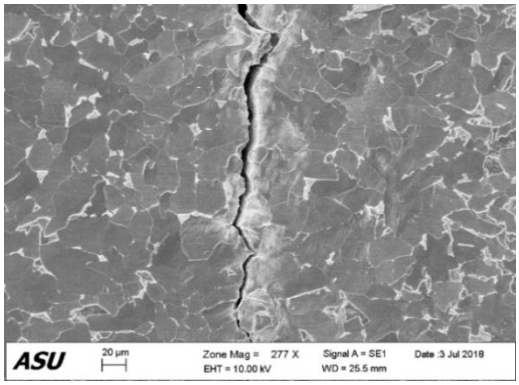

c)

Fig 30. Crack growth pattern of Pipe 44 a) Outer region 1 b) Middle region c) Inner region

It can be seen from Figure 30 for Pipe 44 that the crack follows a transgranular pattern of growth and cuts through the phases, similar to pipe 47.

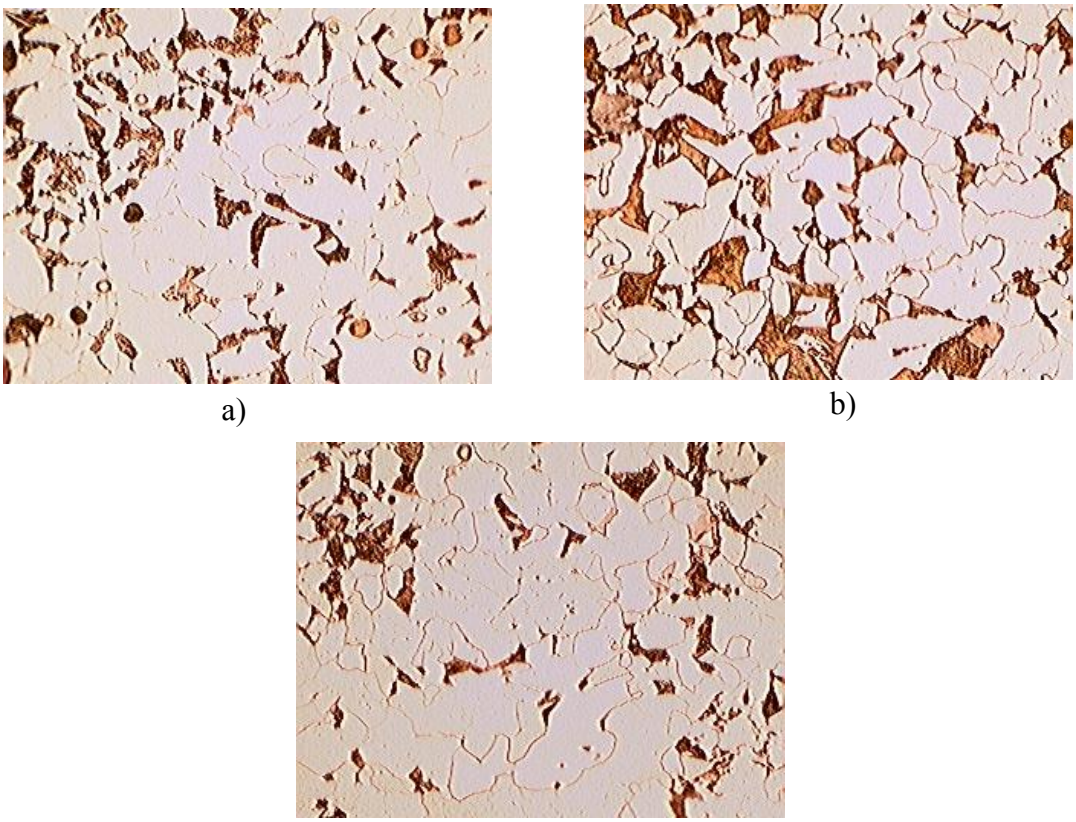

Fig 31. Grain structure after deformation of Pipe 44 a) Outer region b) Middle region c) Inner region

The images from the optical microscope are reported in Figure 31 for Pipe 44 after deformation. The images are used for measuring the grain sizes and phase volume fraction. The average grain diameter after deformation was seen to be 19.9 um, compared to the undeformed grain size of 21.5 um, thereby reflecting a change of less than 2 ASTM grain sizes.

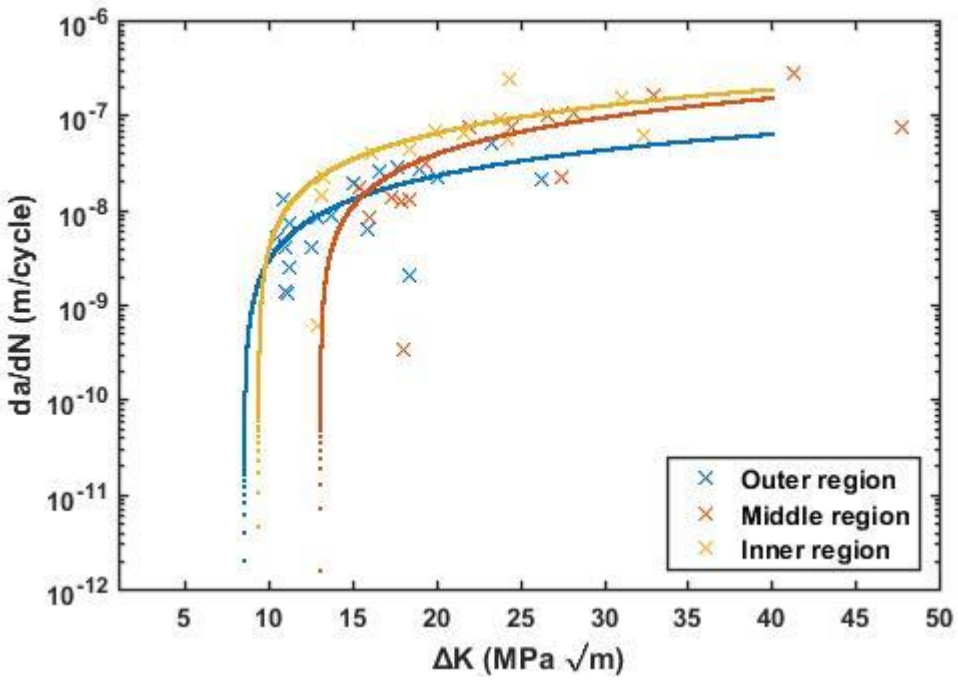

Fig 32. Fatigue crack growth rate versus stress intensity factor range (da/dN versus ΔK) for three different specimens corresponding to the different regions along the pipe thickness for Pipe 44

The da/dN versus ΔK graph for pipe 44 is depicted in Figure 32. A very significant shift can be seen in the graph for the different regions.

Pipe 35:

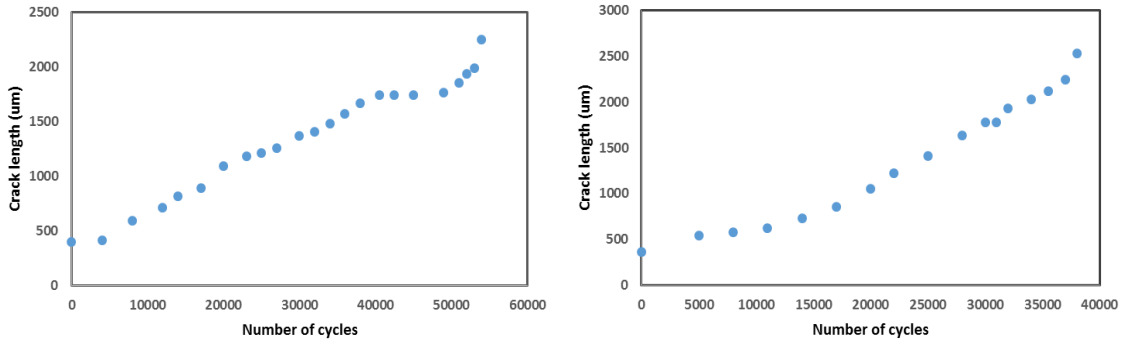

a) b)

Fig 33.1. Fatigue crack growth, da/dN curves for Pipe 35 along the depth; a) Outer surface b)Middle region-1 c) Middle region-2 d) Inner surface

A generic trend is expressed by the graph between crack length and the number of cycles for pipe 35, as shown in Figure 33.1.

The fatigue crack growth characteristics are presented in Figure:

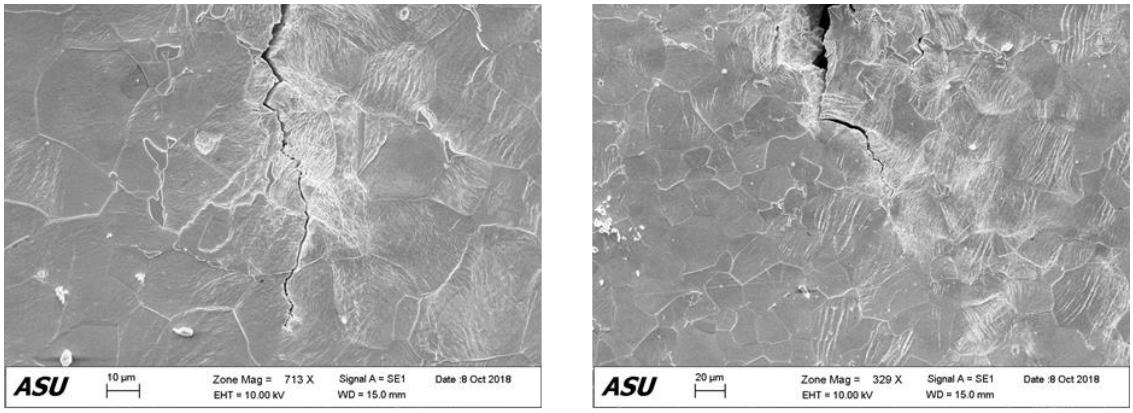

a) b)

Fig 33.2. Crack growth pattern of Pipe 35 a) Outer region b) Inner region

The crack can be seen to follow a transgranular pattern of propagation for pipe 35, as seen in Figure 33.2. It is seen to be mostly composed of ferrite grains which have lower strength.

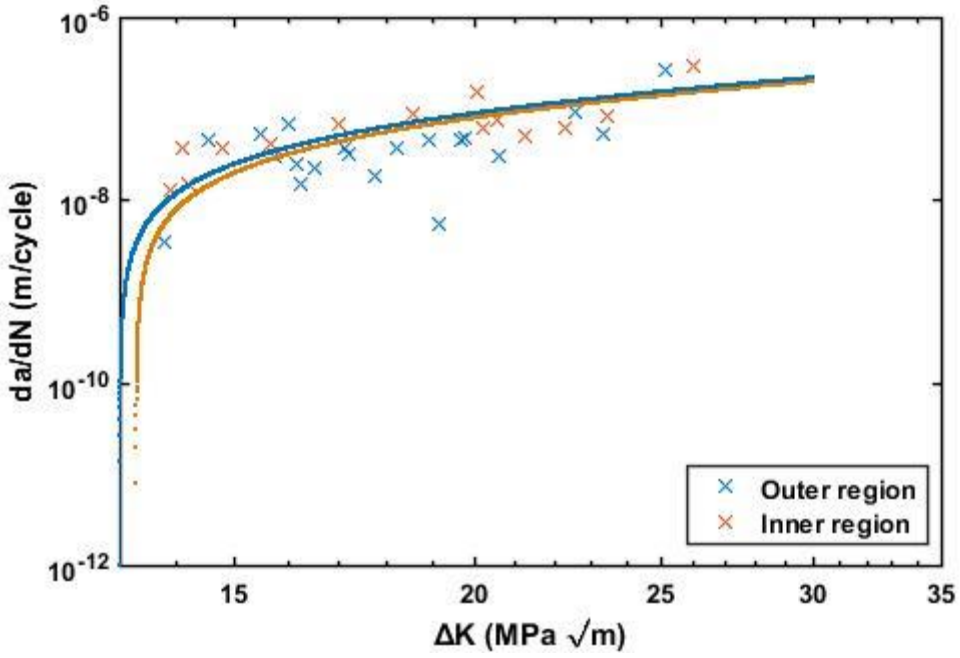

Fig 34. Fatigue crack growth rate versus stress intensity factor range (da/dN versus ΔK) for two different specimens corresponding to the different regions along the pipe thickness for pipe 35

The graph for crack growth rate versus stress intensity factor range is shown in Figure 34. The two regions of crack growth seem to be overlapping and hence not a lot of change is observed in the fatigue crack growth parameters.

Pipe 32

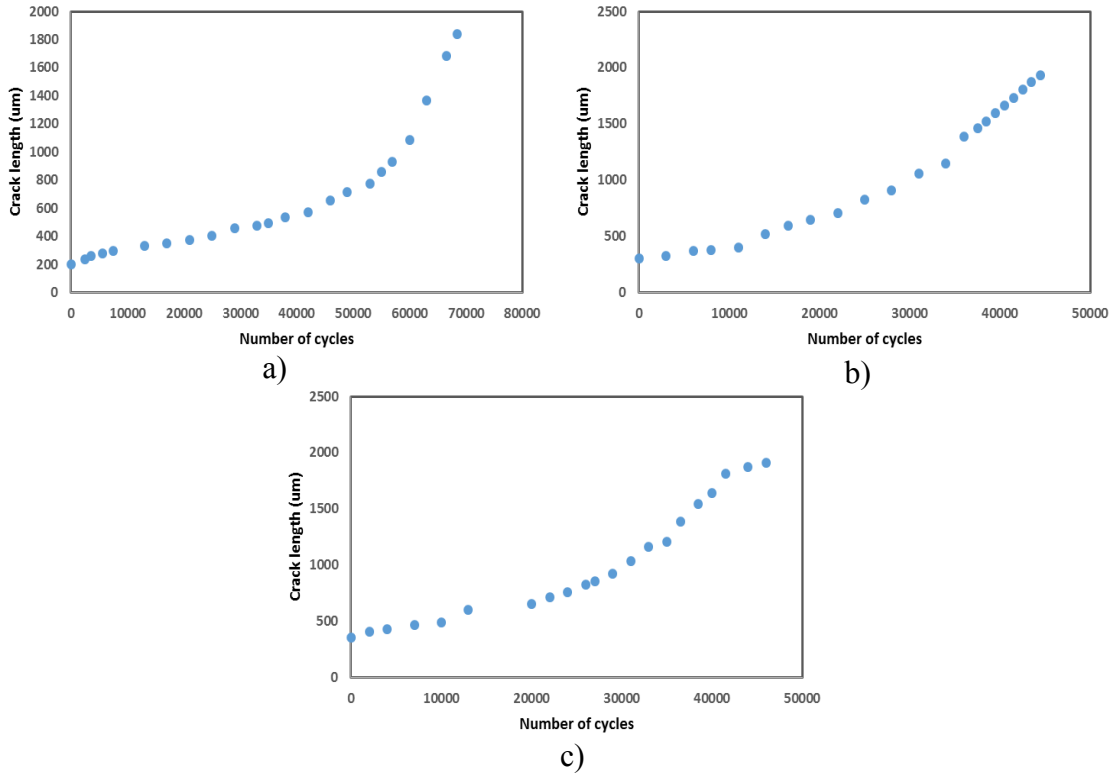

Fig 35. Fatigue crack growth, da/dN curves for Pipe 32 along the depth; a) Outer surface b) Middle region c) Inner surface

The crack growth for the pipe samples appeared to be staedy with respect to the number of cycles across all the regions for pipe 32, similar to the other pipe systems as seen from Figure 35.

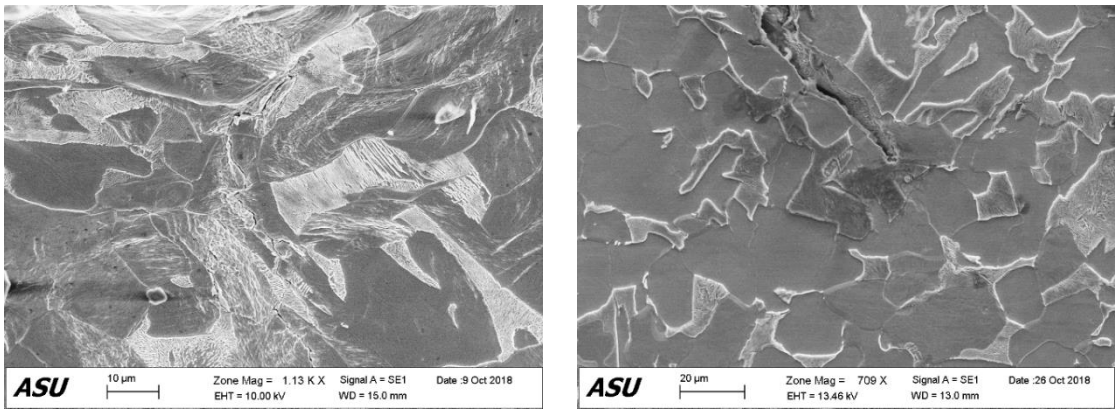

a) b)

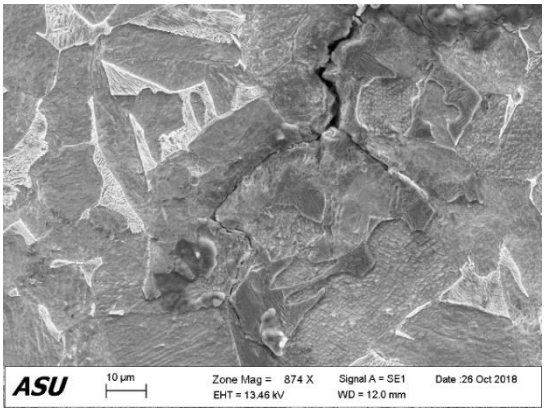

c)

Fig 36. Crack growth pattern of Pipe 32 a) Outer region 1 b) Middle region c) Inner region

Pipe 32 interestingly shows an intergranular pattern of crack growth for the top layer, whereas it tends to follow the grain and phase boundary for the bottom region. The middle region appears to pass through the pearlite phase, as seen from Figure 36.

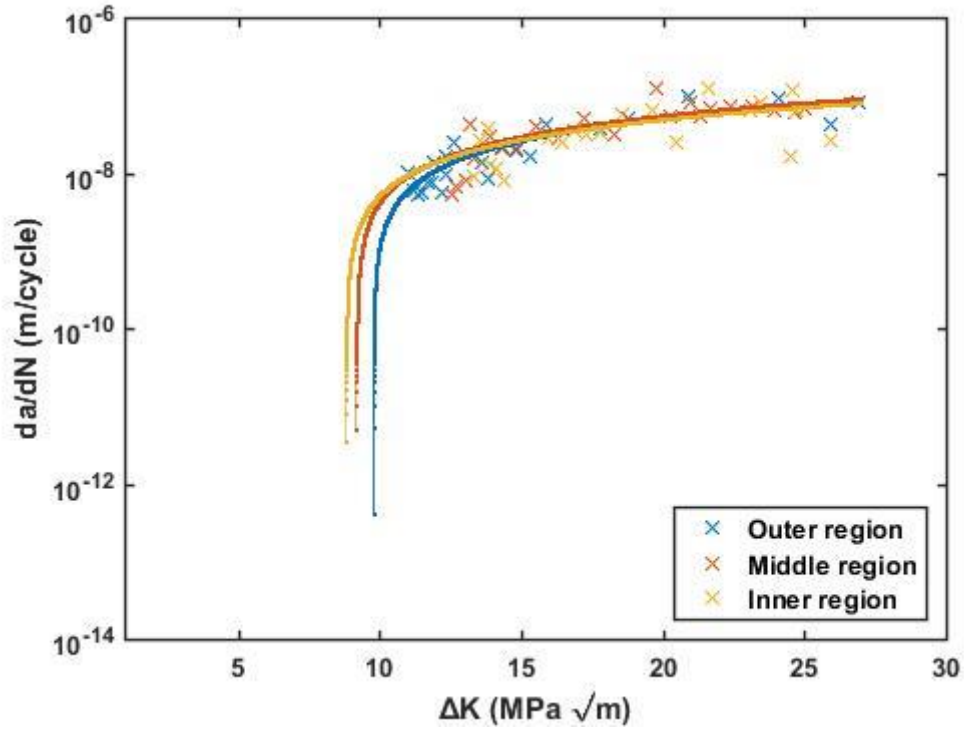

Fig 37. Fatigue crack growth rate versus stress intensity factor range (da/dN versus ΔK) for three different specimens corresponding to the different regions along the pipe thickness for pipe 32

The graph with da/dN versus ΔK for pipe 32 as shown in Figure 37 shows only a slight variation across the different regions.

Pipe 45

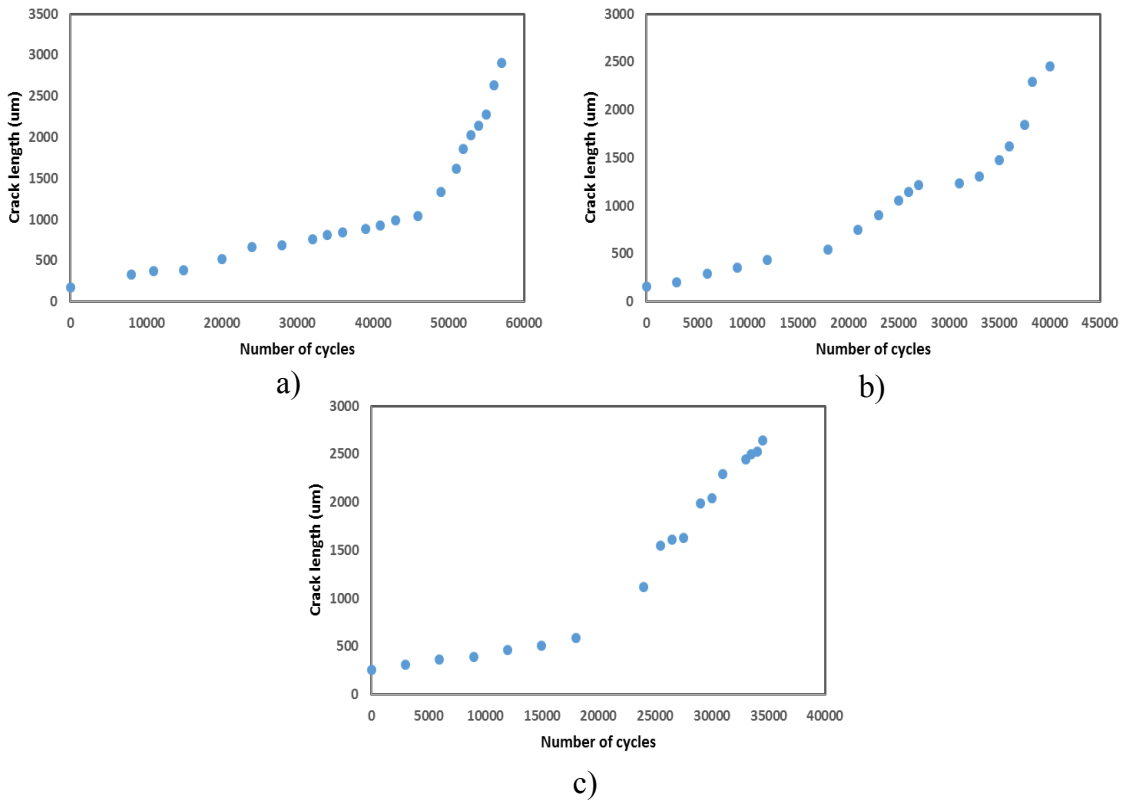

Fig 38. Fatigue crack growth, da/dN curves for Pipe 45 along the depth; a) Outer surface b) Middle region c) Inner surface

Similar to all the other pipe systems, the crack length appears to increase steadily after the initial phase for pipe 45 as well, this can be seen in Figure 38.

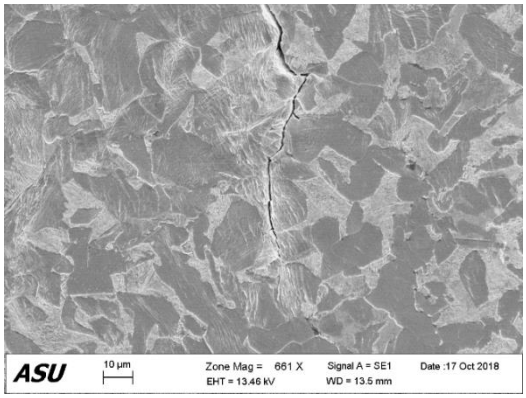

a)

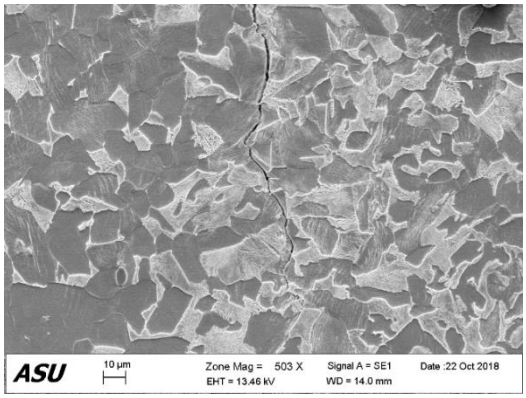

b)

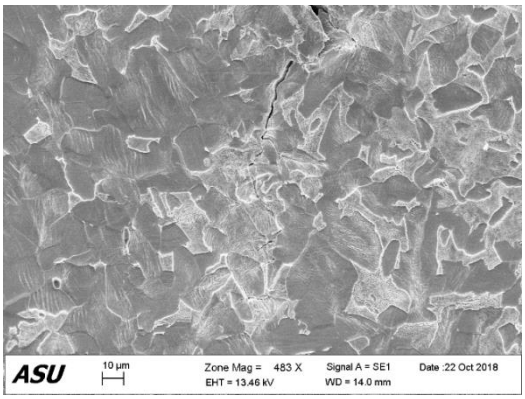

c)

Fig 39. Crack growth pattern of Pipe 32 a) Outer region 1 b) Middle region-2 c) Inner region

The crack growth pattern for pipe 45 is observed to be transgranular for all the regions from Figure 39, since this is a stronger pipe. The crack is also seen to bifurcates the pearlite phase easily.

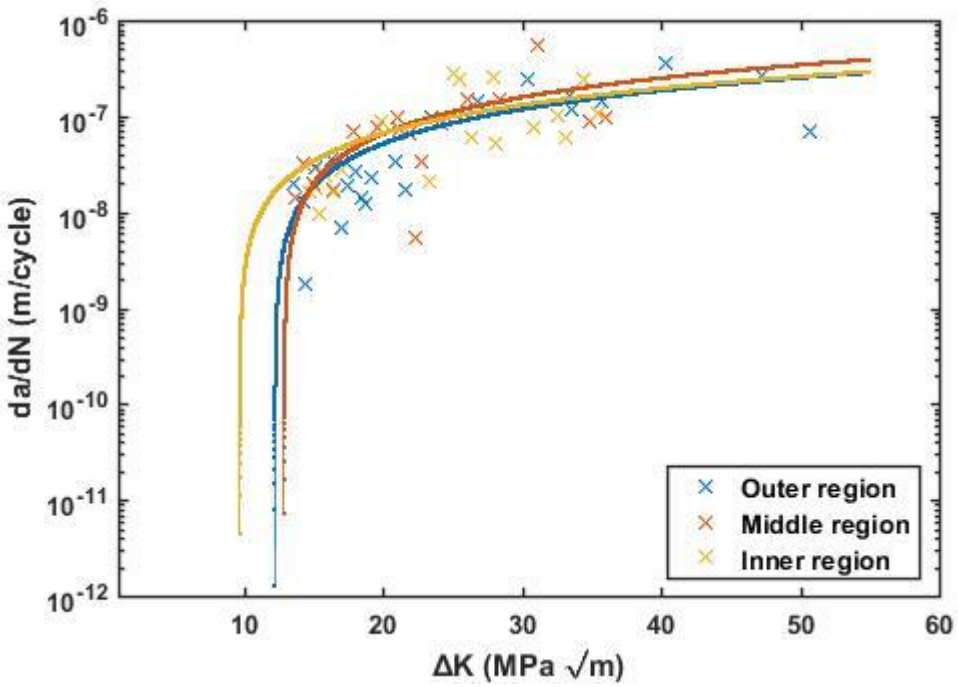

Fig 40. Fatigue crack growth rate versus stress intensity factor range (da/dN versus ΔK) for three different specimens corresponding to the different regions along the pipe thickness for pipe 45

Figure 40 shows that the crack growth rate changes between the different regions of the pipe 45. In general the behavior from the middle region shows a considerable difference from the surface regions.

The parameters of fatigue crack growth are depicted in Table 8.

Table 8. Constants m and C for the five pipe specimen

Pipe Layers	Pipe 44		Pipe 47		Pipe 35	
	m	C	m	C	m	C
Outer region	2.56	$10^{-11.07}$	2.34	$10^{-10.15}$	3.2	$10^{-11.5}$
Middle region-1	3.2	$10^{-11.91}$	2.43	$10^{-10.49}$		
Middle region-2		$10^{-13.4}$	3.52	$10^{-11.99}$		
Inner region	3.47	$10^{-11.92}$	2.38	$10^{-10.52}$	3.19	$10^{-11.29}$
Pipe Layers	Pipe 45		Pipe 32			
	m	C	m	C		
Outer region	2.71	$10^{-11.08}$	2.9	$10^{-11.2}$		
Middle region-1	2.3	$10^{-10.3}$	2.89	$10^{-11.06}$		
Inner region	2.56	$10^{-10.7}$	2.14	$10^{-10.2}$		

A mixed behavior is observed in the variation of the fatigue crack growth parameters through the thickness of the pipe sample. This is a combined function of the pipe wall thickness, composition, other material properties such as grain size, distribution of the phases, and the presence of inclusions. The variation of the fatigue constant m is studied with respect to the material properties; grain size, ferrite volume fraction and hardness.

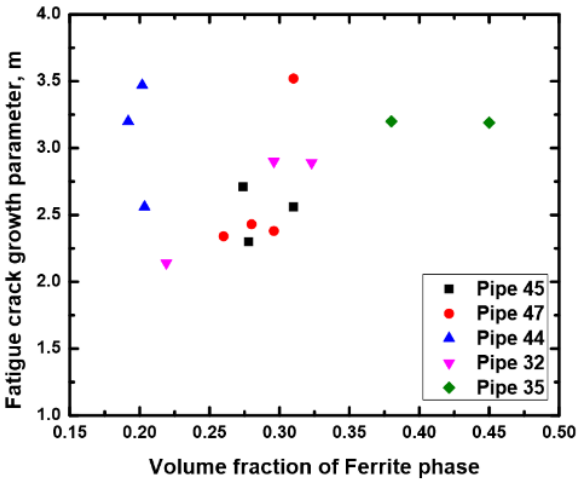

Fig 41. Variation of fatigue crack growth parameter, m, with respect to the content of the ferrite phase

The plot shown in Figure 41 shows the variation of m with respect to the ferrite content. Ideally, with the increase in the content of ferrite phase distribution, the material becomes softer and stronger at the same time which should result in reducing the rate of crack growth and the corresponding parameter of crack growth, m. However, since a number of factors are controlling the crack growth rate in here, an ideal behavior is certainly not observed; instead a scattered pattern can be observed.

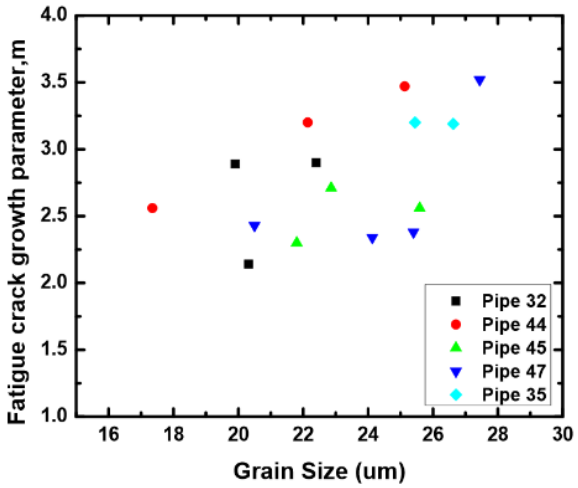

Fig 42. Variation of fatigue crack growth parameter, m, with respect to grain size

The variation in the constant m with respect to the ferrite grain size is shown in Figure 42. With the increase in grain size, the strength of the material reduces and enables crack growth, thereby increasing m. This trend can be seen from the figure.

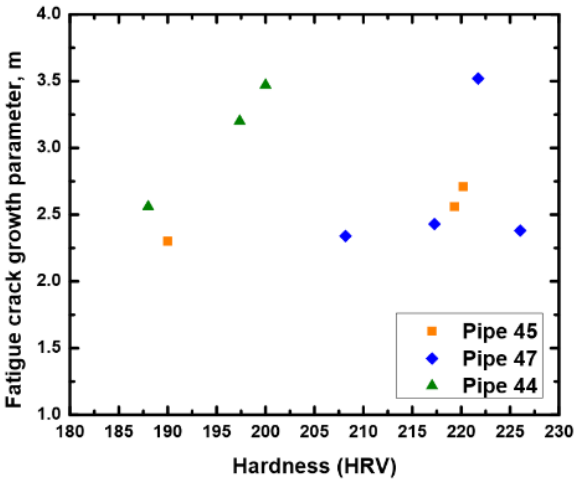

Fig 43. Variation of fatigue crack growth parameter, m, with respect to Hardness

Figure 43 depicts the variation in fatigue crack growth constant m with respect to Hardness through the pipe wall thickness. Although a scattered behavior is seen by the combined plot, individually, the pipes somewhat depict an increase in m with increasing the hardness. This is more clearly seen in Pipe 44 compared to the other two pipes.

A combination of the material properties is seen to be contributing to the crack growth rate and the corresponding parameters m and C and hence no generic trend is observed when m is plotted with respect to the material properties (Elwazri et al. 2005).

4.4 FRACTURE SURFACE INVESTIGATION OF THE BROKEN SAMPLES

The fracture surface of the specimen was studied through SEM imaging and some inclusions were seen on the surface. These were analyzed using EPMA to test for their composition. The images for the fracture surfaces and their EDS spectrums are shown

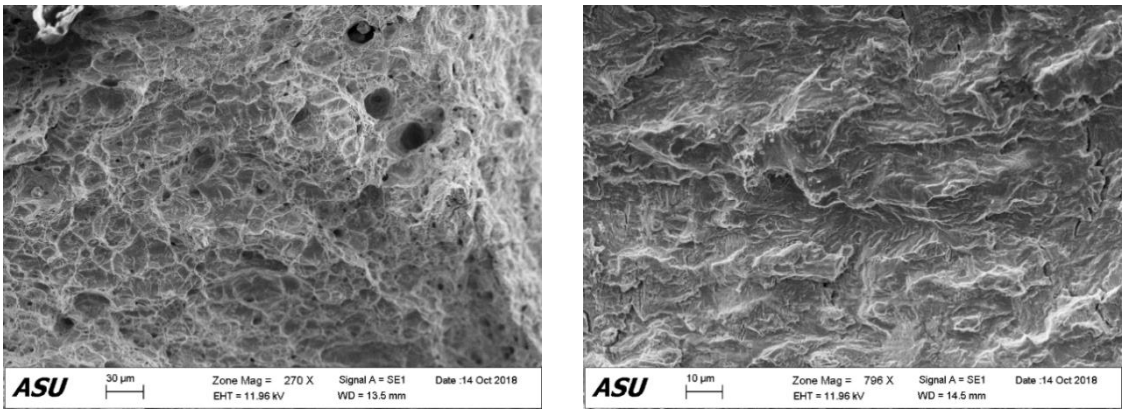
ASU
30 µm
Zone Mag = 270 X
EHT = 11.96 kV
Signal A = SE1
WD = 13.5 mm
Date :14 Oct 2018
ASU
10 µm
Zone Mag = 796 X
EHT = 11.96 kV
Signal A = SE1
WD = 14.5 mm
Date :14 Oct 2018

a)

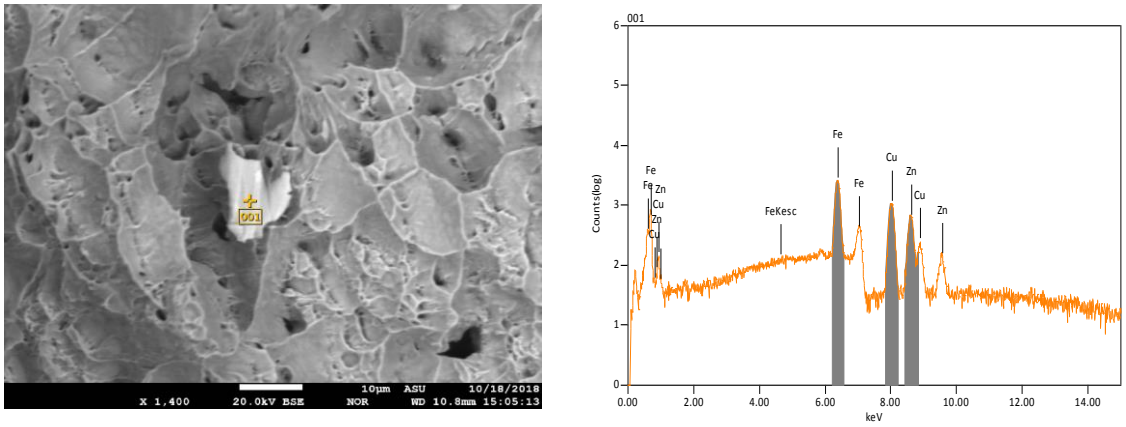
001
X 1,400
20.0kV BSE
10µm ASU
NOR
10/18/2018
WD 10.8mm 15:05:13
Counts(log)
keV
Fe
Fe
Zn
Cu
Zn
Cu
FeKesc
Fe
Cu
Zn
Cu
Zn

b)

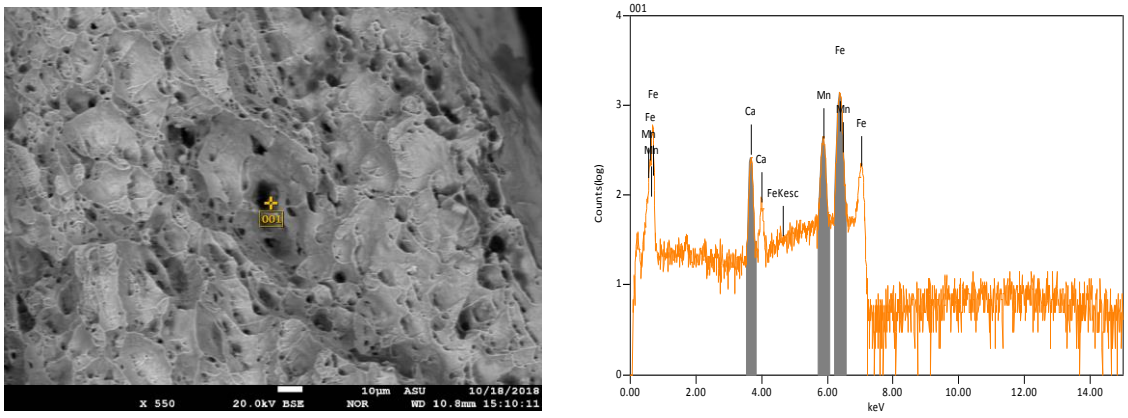
001
X 550
20.0kV BSE
10µm ASU
NOR
10/18/2018
WD 10.8mm 15:10:11
Counts(log)
keV
Fe
Fe
Mn
Mn
Ca
Ca
FeKesc
Fe
Mn
Mn
Fe

c)

Fig 44. Fracture surface images and EDS spectrum for pipe 44 a) Fracture surface b) Fe-Cu-Zn inclusion c) Ca-Mn inclsuion

The fracture surface images for pipe 44 are shown in Figure 44. The fracture region shows a typical ductile failure characterized with dimples for a majority of the fracture surface area. Some areas also show the presence of fatigue ridges.

Inclusions are also seen on the fracture surface and likely to have interacted with the crack and caused a failure. One inclusion appears to be a compound of Fe-Cu-Zn, whereas the other shows a Ca-Mn compound.

Pipe 45

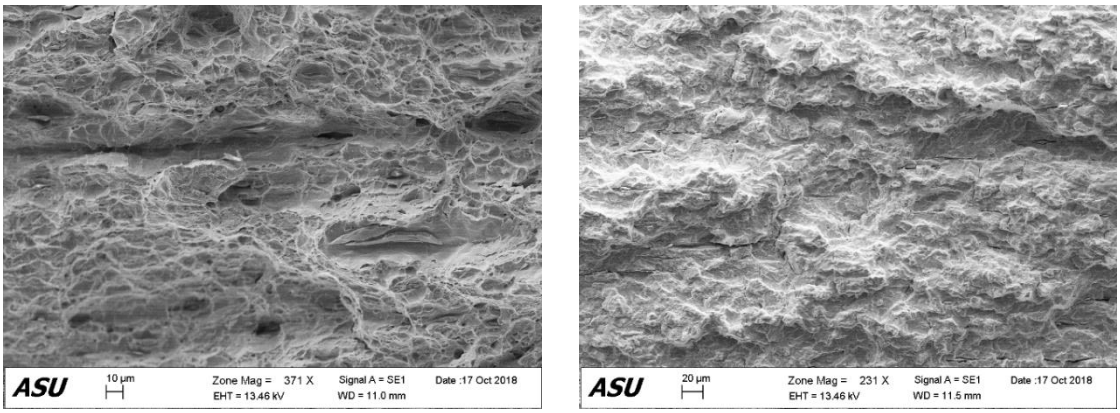

a)

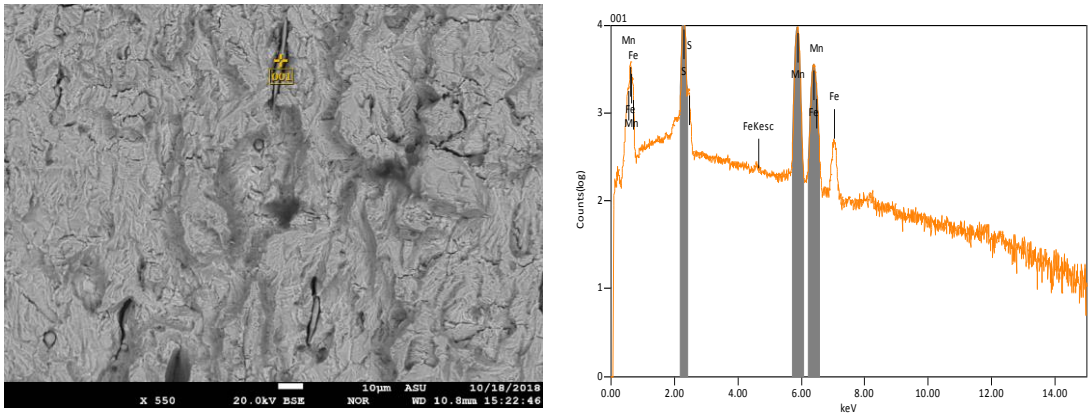

b)

Fig 45. Fracture surface and EDS spectrum images for pipe 45 a) Fracture surface b) MnS elongated inclusion

The fracture surface for pipe 45 depicted in Figure 45 is also seen to be comprised of dimples, a characteristic of ductile fracture. Some other regions show fracture ridges which are dominated by the inclusions, instead of dimples. MnS inclusions can be seen to be elongated along the crack path, signifying their interaction.

Pipe 47:

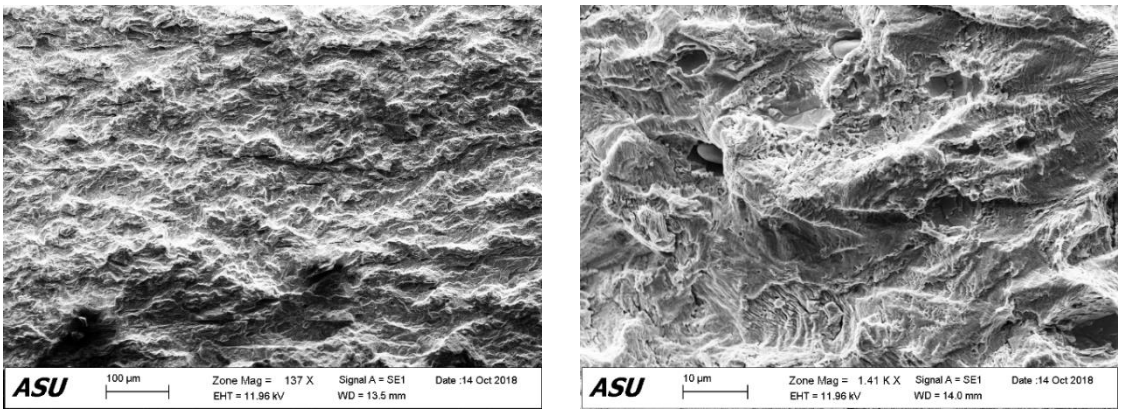

a)

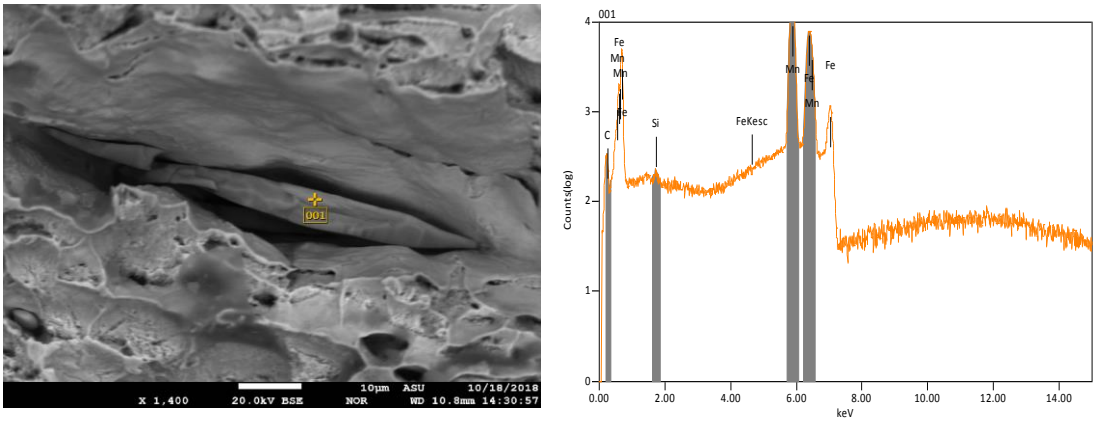

b)

Fig 46. Fracture surface and EDS spectrum fracture surface images for pipe 47 a) Fracture surface b) Elongated Mn inclusions

The fracture surface of pipe 47 as shown in Figure 46 shows the absence of dimples and presence of ridges. This is likely due to the dominance of inclusions contained within the fracture surface which are composed of Mn.

The size of the Ca-rich inclusion was seen to be about 10 um, whereas the Mn-based inclusions appeared larger as much as 80 um. It is safe to say that such a large size of inclusions resting in the voids and broken along the crack path have appeared to have an impact on the crack growth rate and in some cases completely dominated the same (Mohtadi-Bonab et al. 2016). As such, the direct impact of each material property on the rate of crack growth is hard to see and can be derived by combining a number of contributing factors, some more dominant than the others.

4.5 CONCLUSION

The fatigue crack growth analysis was done for five different steel pipe specimen, which are composed of similar microstructure (ferrite and pearlite).The values for the constants or parameters for fatigue crack growth were identified and studied for a variation along the thickness. Some major conclusions from the study are listed here:

1. The fatigue crack growth pattern was observed to be transgranular through the specimen. The microstructural features such as the grain size and volume fraction of ferrite depicted a slight change after deformation, compared to the base metal.

2. The parameters of fatigue crack growth depicted a slight change through the thickness of the pipe sample relating to the microstructure. The constant m was found in the range of 2.5~4.5, whereas the constant C was observed to be in the range of 10^{-9} ~ 10^{-13}

3. Elongated and broken inclusions were observed on the fracture surface and seen to be resting on the voids. These were composed of Mn, Mn-S, Ca-Mn and Fe-Cu-Zn and varied from 10 um diameter to 80 um. The inclusions appear to have contributed to the variation in the crack growth rate for the different pipe specimen with similar microstructure, and possibly through the bulk of their thickness.

It can be concluded that different damage mechanisms are active at different regions along the pipe wall, pertaining to the metallurgical technology used in their production. A surface-level assessment of the material properties is therefore, not a complete representative of the bulk properties. This is further backed by the differential data in hardness and tensile properties along the thickness, presented in section 2. An in-situ testing with the real time monitoring of the microstructural damages is desired as it can provide more detailed insight of the damage progression through the bulk of the pipes.

5 3-D STOCHASTIC RECONSTRUCTION MODEL

5.1 INTRODUCTION

This reduction in the data volume will be achieved through the development of a 3-D reconstruction model, of the stochastic type, from the 2-D morphological information available from the surface depths, primarily for a two phase system, to be a representative of the bulk structure of the material.

The methodology used for this is based on the stochastic reconstruction scheme developed by Yeong and Torquato (Yeong and Torquato 1998). Key structural features, known as statistical descriptors are extracted from the 2D images that can contain various correlation functions. A typical 2-point correlation function for a statistically inhomogeneous system is;

$$S_2^{(i)}(x_1, x_2) = \langle I^{(i)}(x_1) I^{(i)}(x_2) \rangle = S_2^{(i)}(|x_1 - x_2|) \tag{14}$$

where x1 and x2 are two arbitrary points and $S_2^{(i)}(x_1,x_2)$ is the probability of finding the two points in the same phase. A state of minimum "energy" is then computed from the given set of local minima, by the phase pixel interchange procedure in the digitized media.

$$E = \sum_i [f_s(r_i) - f_s(r_i)]^2 \tag{15}$$

where, $f_0(r)$ is the known two-point correlation function of the reference system, and $f_s(r)$ of the reconstructed digitized system, with r being the distance between two points in the system. The resultant energy from the phase interchange method is obtained as E',

with the energy difference as E-E'. The probability of the phase interchange given by the Metropolis method is given as:

$$P\left(E_{old} \rightarrow E_{new}\right) = \begin{cases} 1, & \Delta E < 0 \\ \exp\left(-\frac{\Delta E}{T}\right), & \Delta E \geq 0 \end{cases} \tag{16}$$

where T represents temperature, and is adjusted with the simulation annealing method to converge the energy to a global minimum, the schematic of this is shown in Figure 47.

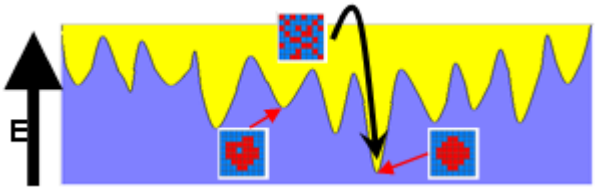

Fig 47. The local minima, with the arrow towards the global minimum

5.2 3-D STOCHASTIC RECONSTRUCTION MODEL FOR PIPE 45

The 3-D reconstruction was performed for two surface layers of Pipe 45, outer and middle region using a 2-D correlation function in perpendicular directions. The reconstructed images are presented below:

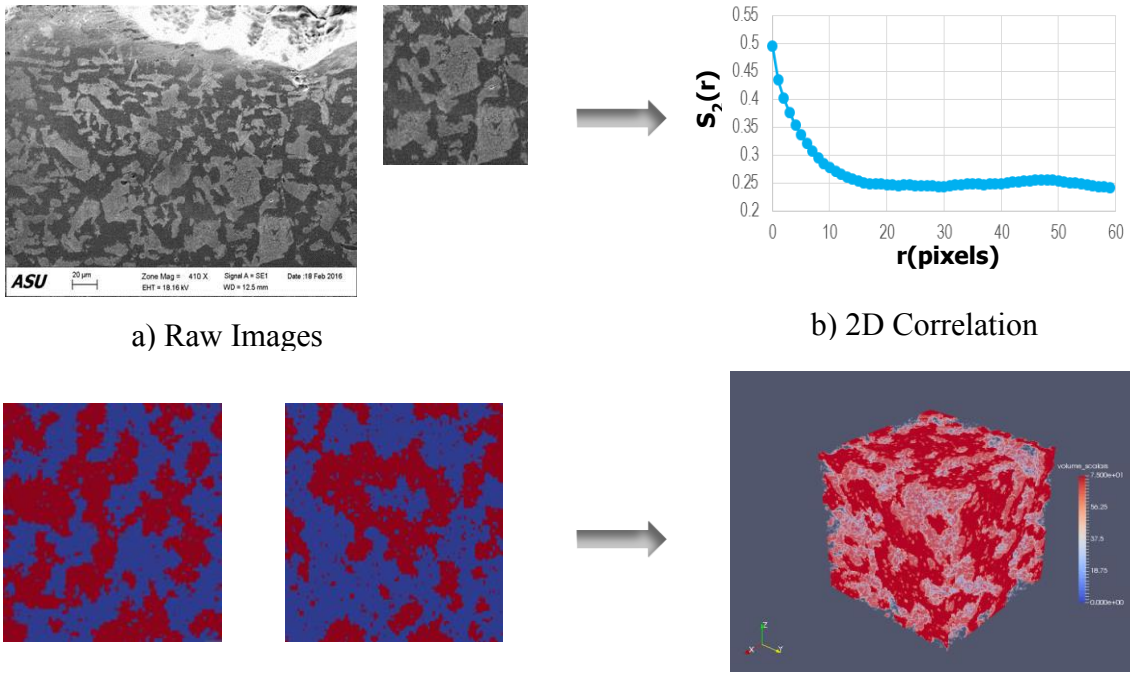

a) Raw Images

b) 2D Correlation

c) 2D slices

d) 3D Reconstruction

Fig 48. 3-D reconstruction for outer surface of Pipe 45

The reconstruction representation has the base image, followed by the cropped image fed for reconstruction. The extracted 2-D correlation function is presented and the final obtained reconstructed slices and 3-D image are presented in Figure 48.

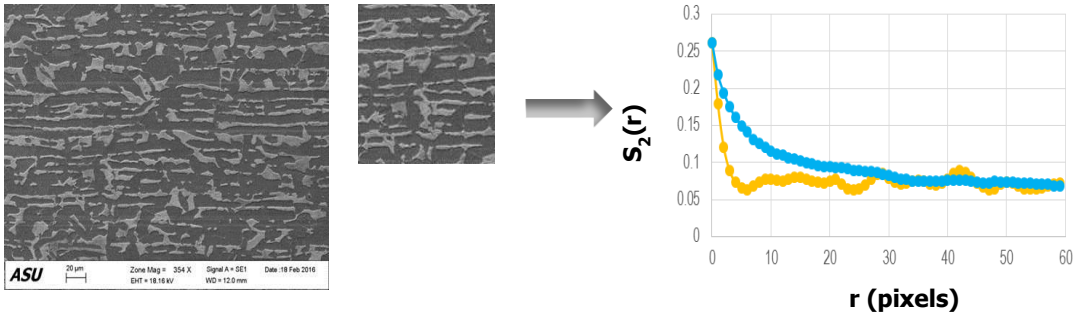

Fig.15 a): Raw Images

Fig.15 b): 2D Correlation

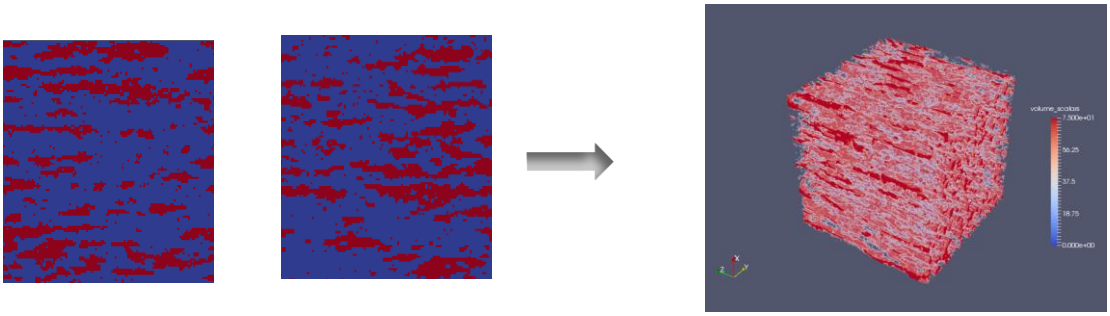

Fig.15 c): 2D slices

Fig.15 d): 3D Reconstruction

Fig 49 3-D reconstruction for middle surface region of Pipe 45

It can be seen from Figure 49 that there is a considerable difference in the features of the outer and the middle region, which can be very well picked up by the reconstruction algorithm as well. This is used to extract linear elastic properties from these reconstructed segments using techniques such as Finite Element Method and compare them against the true properties for validation. This can be followed by plastic properties depending on the performance of the elastic properties prediction.

6 CONCLUSION AND FUTURE WORK

The integrity assessment of the aging Natural gas pipeline system is proposed through the design of the Bayesian Network framework model, which integrates the different material properties derived from in-situ measurements. The model is validated from the results of experimental measurements to show an improved accuracy of strength prediction. Three field samples and a few literature databases were investigated to obtain the data for the model prediction and training. Several imaging, analytical and mechanical testing techniques were employed for macro assessment of material properties. Next, a comparative study of different statistical models were employed to aid in prediction of manufacturing process parameters and the impact of the parameter variation was studied for each dataset. Finally, fatigue behavior of five pipe specimen was investigated for variations in crack growth rate. The crack growth rate appeared to vary through the bulk for majority of the samples. The failed samples were analyzed using Scanning Electron Microscopy (SEM) and Energy Dispersive Spectroscopy (EDS), and the presence of inclusions on the fracture surface was noted. The major conclusions from the present study are depicted here:

1. The integrated Bayesian network model showed a significant improvement in accuracy compared to prediction with individual nodes, signifying the impact of multi-modal approach on strength prediction of the pipeline systems.

2. Data training for modification of the likelihood model also resulted in a significant improvement of prediction accuracy. The parametric studies for the nodes indicated a

higher impact by certain nodes compared to others, which is linked to their weight distribution.

3. The performance of the statistical models showed a preference for ML-KNN approach for the major part to obtain the best prediction for the process parameters. The parametric analysis for the individual models helped identify the best values resulting in best predictions.

4. The fatigue analysis showed a variation in the crack growth rate along the pipe thickness for the major part. The parameters of crack growth C and m appeared to differ among the different pipe specimen with similar microstructure. The pipe specimen were seen to be strong for the crack to propagate through the grains.

Several future studies are suggested based on the current investigation

1. As the current system is mainly focused on the prediction of Yield strength, the same can be replicated for the ultimate tensile strength for all the samples. This study, overall, can be extended to a larger volume of data to improve the prediction capability of the model system, and training and validation can also be performed on specific grades of interest

2. Larger datasets can be employed for the comparative assessment of the statistical models. For the present study, 60 percent of the data was used for training and the remaining was used for prediction. An interesting thing to analyze would be the performance of these models to varying sizes of training data (limited due to the small datasets).

3. Texture of the deformed samples can be studied using Electron backscatter diffraction (EBSD) analysis and compared to the base metal. The same can also be evaluated for variability along the pipe wall thickness direction.

4. The current study for fatigue analysis focuses on the macro level study of the material behavior. In order to understand the failure mechanics at the grain level, a micro-level investigation with TEM and X-ray tomography studies can be conducted.

7 REFERENCES

Amend, Bill. n.d. “In-Situ Analyses to Characterize the Properties and Metallurgical Attributes of In-Service Piping.” NACE International.

Bickerstaff, Robert., Mark. Vaughn, Gerald. Stoker, Michael . Hassard, and Mark. Garrett. 2002. “Review of Sensor Technologies for In-Line Inspection of Natural Gas Pipelines.” *Sandia National …*, no. Ili: 1–10. http://netl.doe.gov/technologies/oil-gas/publications/Status_Assessments/71702.pdf.

Blatt, Drew, Reji John, and Demirkan Coker. 1994. “Stress Intensity Factor and Compliance Solutions for a Single Edge Notched Specimen with Clamped Ends.” *Engineering Fracture Mechanics* 47 (4): 521–32. doi:https://doi.org/10.1016/0013-7944(94)90252-6.

Bramfitt, Bruce L, and Bethlehem Steel Corporation. 1998. “Structure / Property Relationships in Irons and Steels.” *Metals Handbook Desk Edition, Second Edition*, 153–73.

Büche, Dirk, Nicol N Schraudolph, and Petros Koumoutsakos. 2005. “Accelerating Evolutionary Algorithms With Gaussian Process Fitness Function Models.” *Systems, Man, and Cybernetics, Part C: Applications and Reviews, IEEE Transactions on* 35 (2): 183–94. doi:10.1109/TSMCC.2004.841917.

Butz, C. J., S. Hua, J. Chen, and H. Yao. 2009. “A Simple Graphical Approach for Understanding Probabilistic Inference in Bayesian Networks.” *Information Sciences* 179 (6): 699–716. doi:10.1016/j.ins.2008.10.036.

Cheng, Weiwei, and Eyke Hüllermeier. 2009. “Combining Instance-Based Learning and Logistic Regression for Multilabel Classification.” *Machine Learning* 76 (2–3): 211–25. doi:10.1007/s10994-009-5127-5.

Dobmann, G., N. Meyendorf, and E. Schneider. 1997. “Nondestructive Characterization of Materials A Growing Demand for Describing Damage and Service-Life-Relevant Aging Processes in Plant Components.” *Nuclear Engineering and Design* 171: 95–112. doi:10.1016/S0029-5493(96)01319-2.

Dobmann, Gerd, Michael Kröning, Werner Theiner, Herbert Willems, and Uwe Fiedler. 1995. “Nondestructive Characterization of Materials (Ultrasonic and Micromagnetic Techniques) for Strength and Toughness Prediction and the Detection of Early Creep Damage.” *Nuclear Engineering and Design* 157 (1–2): 137–58. doi:10.1016/0029-5493(95)00992-L.

Drexler, Elizabeth, and Robert Amaro. 2017. “No Title.”

Elwazri, Abdelbaset M., R. Varano, F. Siciliano, D. Bai, and S. Yue. 2005. “Effect of Cool Deformation on Mechanical Properties of a High-Strength Pipeline Steel.” *Metallurgical and Materials Transactions A: Physical Metallurgy and Materials*

Science 36 (11): 2929–36. doi:10.1007/s11661-005-0066-7.

Ersoy, D. 2015. "Existing Gaps between Current Diagnosis Techniques and True Material States for Pipe Integrity Assessment."

Haggag. 2007. "In-Situ Measurement of Pipeline Mechanical Properties Using Stress-Strain Microprobe – Validation of Data for Increased Confidence & Accuracy."

Hashemi, S. H. 2011. "Strength-Hardness Statistical Correlation in API X65 Steel." *Materials Science and Engineering A* 528 (3): 1648–55. doi:10.1016/j.msea.2010.10.089.

Imandoust, Sadegh Bafandeh, and Mohammad Bolandraftar. 2013. "Application of K-Nearest Neighbor (KNN) Approach for Predicting Economic Events : Theoretical Background." *Int. Journal of Engineering Research and Applications* 3 (5): 605–10.

Kamtornkiat Musiket; Mitchell Rosendahl; and Yunping Xi. 2016. "Fracture of Recycled Aggregate Concrete under High Loading Rates." *Journal of Materials in Civil Engineering* 25 (October): 864–70. doi:10.1061/(ASCE)MT.1943-5533.

Kim, Youngju, Jaeki Kwon, Hyunjung Lee, Wookil Jang, Jongkyo Choi, and Sangshik Kim. 2011. "Effect of Microstructure on Fatigue Crack Propagation and S-N Fatigue Behaviors of TMCP Steels with Yield Strengths of Approximately 450 MPa." *Metallurgical and Materials Transactions A: Physical Metallurgy and Materials Science* 42 (4): 986–99. doi:10.1007/s11661-010-0577-8.

Kocijan, J, R Murray-Smith, C E Rasmussen, and A Girard. 2004. "Gaussian Process Model Based Predictive Control." *Response* 3 (DP-8710): 2214–19. http://eprints.gla.ac.uk/3041/.

Korsunsky, A.M., D. Dini, and M.J. Walsh. 2008. "Fatigue Crack Growth Rate Analysis in a Titanium Alloy." *Key Engineering Materials* 385–387 (June 2017).

Li, Z, S Schmauder, and M Dong. 1999. "A Simple Mechanical Model to Predict Fracture and Yield Strengths of Particulate Two-Phase Materials." *Computational Materials Science* 15 (1): 11–21. doi:10.1016/S0927-0256(99)00014-2.

Liu, WeiYi, Kun Yue, and JiaDong Zhang. 2009. "Augmenting Learning Function to Bayesian Network Inferences with Maximum Likelihood Parameters." *Expert Systems with Applications* 36 (2 PART 2): 3497–3504. doi:10.1016/j.eswa.2008.02.018.

Lu, Zizi, and Yongming Liu. 2009. "An Incremental Crack Growth Model for Multi-Scale Fatigue Analysis," no. May: 1–9.

Merson, E. D., M. M. Krishtal, D. L. Merson, A. A. Eremichev, and A. Vinogradov. 2012. "Effect of Strain Rate on Acoustic Emission during Hydrogen Assisted Cracking in High Carbon Steel." *Materials Science and Engineering A* 550: 408–17. doi:10.1016/j.msea.2012.04.094.

Mohtadi-Bonab, M. A., M. Eskandari, H. Ghaednia, and S. Das. 2016. “Effect of Microstructural Parameters on Fatigue Crack Propagation in an API X65 Pipeline Steel.” *Journal of Materials Engineering and Performance* 25 (11). Springer US: 4933–40. doi:10.1007/s11665-016-2335-6.

Nykyforchyn, H. M., O. T. Tsyrul’Nyk, D. Yu Petryna, and M. I. Hredil’. 2009. “Degradation of Steels Used in Gas Main Pipelines during Their 40-Year Operation.” *Strength of Materials* 41 (5): 501–5. doi:10.1007/s11223-009-9158-8.

Peng, Tishun, Abhinav Saxena, Kai Goebel, Yibing Xiang, Shankar Sankararaman, and Yongming Liu. 2013. “A Novel Bayesian Imaging Method for Probabilistic Delamination Detection of Composite Materials.” *Smart Materials and Structures* 22 (12). doi:10.1088/0964-1726/22/12/125019.

Qu Nonero-Candela, Joaquin, Jqc@tuebingen Mpg De, Carl Edward Rasmussen, and Carl@tuebingen Mpg De. 2005. “A Unifying View of Sparse Approximate Gaussian Process Regression.” *Journal of Machine Learning Research* 6: 1939–59. http://www.jmlr.org/papers/volume6/quinonero-candela05a/quinonero-candela05a.pdf.

Rosado, D Belato, W De Waele, and D Vanderschueren. 2013. “Latest Developments in Mechanical Properties and Metallurgycal of High Strenght Line Pipes.” *Sustainable Construction and Design* 4 (1): 1–10. doi:http://dx.doi.org/10.21825/scad.v4i1.742.

Santos, I, J Nieves, Y K Penya, and P G Bringas. 2009. “Machine-Learning-Based Mechanical Properties Prediction in Foundry Production.” *2009 Iccas-Sice*, 3–8.

Smart, Luncinda, and Leonard J. Bond. 2016. “Material Property Relationships for Pipeline Steels and the Potential for Application of NDE.” In *AIP Conference Proceedings 1706, 160003*.

Support, Technical, E G Kirkpatrick, A D Eastman, California Gas Transmission, California Public, Utilities Commission, General Order, Technical Support, Pipeline Dimensions, and Low Pressure. n.d. “Approved by : A-34 A :,” 1–26.

Tovee, John-Paul. 2014. “Microstructural Influence on the Effects of Forward and Reverse Mechanical Deformation in HSLA X65 and X80 Line Pipe Steels,” 231. http://etheses.bham.ac.uk/5171/.

“US Energy Information Administration Website.” 2017. *June 2007*. Accessed November 7. https://www.eia.gov/naturalgas/archive/analysis_publications/ngpipeline/index.html.

US news | NBC News. 2010. “Most Gas Lines Don’t Use Latest Inspection Technology,” September 14. http://www.nbcnews.com/id/39174246/ns/us_news/#.Wgt5yFtSyUk.

Vary, Alex. 1980. “Concepts and Techniques for Ultrasonic Evaluation of Material Mechanical Properties.” In *Mechanics of Nondestructive Testing*, edited by W W Stinchcomb, J C Duke, E G Henneke, and K L Reifsnider, 123–41. Boston, MA:

Springer US. doi:10.1007/978-1-4684-3857-4_5.

Yamano, Takashi. n.d. “Lecture Notes on Advanced Econometrics Lecture 4 : Multivariate Regression Model in Matrix Form,” 1–29.

Yeong, C L Y, and S Torquato. 1998. “Reconstructing Random Media I and II.” *Physical Review E* 58 (1): 224–33.

Zhang, Min Ling, and Zhi Hua Zhou. 2007. “ML-KNN: A Lazy Learning Approach to Multi-Label Learning.” *Pattern Recognition* 40 (7): 2038–48. doi:10.1016/j.patcog.2006.12.019.

Zhao, Ming-Chun, Ke Yang, and Yiying Shan. 2002. “The Effects of Thermo-Mechanical Control Process on Microstructures and Mechanical Properties of a Commercial Pipeline Steel.” *Materials Science and Engineering: A* 335 (1–2): 14–20. doi:10.1016/S0921-5093(01)01904-9.